THE UNIVERSITY OF MICHIGAN

INDUSTRY PROGRAM OF THE COLLEGE OF ENGINEERING

DIFFUSION OF TRITIATED HYDROGEN IN DENSE GAS SYSTEMS OF HYDROGEN, HYDROGEN AND CARBON DIOXIDE, AND HYDROGEN AND ARGON

(Ben George)

Ben G. Bray

A dissertation submitted in partial fulfillment
of the requirements for the degree of
Doctor of Philosophy in The
University of Michigan
1960

September, 1960

IP-458

engm

UMR0555

Doctoral Committee:

Professor Joseph J. Martin, Co-Chairman
Professor Brymer Williams, Co-Chairman
Associate Professor Edward E. Hucke
Associate Professor Donald R. Mason
Associate Professor W. Wayne Meinke
Professor Robert R. White

ACKNOWLEDGEMENT

The author would like to express his appreciation to several individuals and organizations for assistance received during the work which is reported in this dissertation. First, I am indebted to my wife who typed the initial draft of the dissertation, and offered support and encouragement during the years required to complete this work. Thanks are also due to the members of the doctoral committee for their suggestions which have been incorporated into this work; to Professor J. J. Martin who originally suggested the problem and became committee chairman; to Professor G. B. Williams who served as chairman and advisor during the last year of the work; to Frank Drogosz, instrument maker for the Department of Chemical and Metallurgical Engineering who substantially assisted in the construction of the fine tube bundle diffusion paths; and to John Davis, graduate student, who assisted in some of the preliminary work and prepared Figures 6 and 24 included in the dissertation.

Further acknowledgment of gratitude is expressed toward the Department of Chemical and Metallurgical Engineering staff which provided services and funds for the construction of equipment used in the experimental work and which recommended that I receive personal financial aid during the work; toward the E. I. Du Pont de Nemours and Company, the Shell Oil Company, and the Sinclair Refining Company for fellowship grants received during the doctoral work; toward the staff of the Computing Center at The University of Michigan for providing computer time to simplify the data processing operations required by this work; and toward the Industry Program of the College of Engineering and its contributors for preparing and publishing the final manuscript of this dissertation.

To all these and many others, I am indebted for invaluable assistance received.

TABLE OF CONTENTS

TABLE OF CONTENTS (cont'd)

LIST OF TABLES

LIST OF TABLES (cont.'d)

LIST OF FIGURES

LIST OF FIGURES (cont'd)

LIST OF APPENDICES

I. INTRODUCTION

The molecular interactions which occur in the gas phase have long been of interest to men in many branches of science. These usually complex interactions result in a number of phenomena which are readily noted by even the scientifically untrained individual. Some effects of the interactions, such as the macroscopic state effects, are static while others are dynamic with respect to time. The phenomenon of diffusion is a physical, dynamic process and is termed a transport property because it occurs as the result of a gradient which causes the space displacement of a certain entity, in this case, of mass. In order to facilitate the quantitative discussion of diffusion, the coefficient of diffusion has been defined which provides a means for comparison or prediction of diffusion processes in systems of interest.

Attempts have been made to theoretically predict diffusion in a general manner, with varying degrees of success. Many experimental determinations of specific diffusion coefficients have been made. At the present time diffusion processes can be quantitatively described theoretically to within normal experimental accuracy for simple systems at moderate temperatures and at pressures less than or near one atmosphere. Theoretical attempts have not successfully generalized the description

of diffusion processes at elevated densities where the complexities of molecular interactions are intensified.

The investigation described in this dissertation was undertaken in order to attempt to increase the understanding of the diffusion processes occurring in dense gases through the taking of experimental data. The specific objectives realized in the investigation were:

1. The modification of the basic quasi steady-state equipment constructed by O'Hern [30,31] so that a larger range of operating densities could be investigated.
2. The design and construction of one or more diffusion paths which successfully eliminated any appreciable effects of convection and yet for which the geometry could be satisfactorily determined in order that diffusion cell calibrations based on diffusion measurements need not be made.
3. The investigation of diffusion occurring in the two ternary systems, HT-H_2-CO_2 and HT-H_2-A and the binary system HT-H_2, for which no previous dense gas diffusion data had been taken.

Diffusion coefficients have been determined in this investigation at 35°C and 100°C for tritiated hydrogen, HT, diffusing through hydrogen and three mixtures each of H_2 and A and H_2 and CO_2 containing approximately 19, 62, and 93 percent hydrogen. Comparisons of the results have been made with the theory and results of other investigations where

similarities existed. The ensuing text is a presentation of applicable theory and the similar experimental investigations from the literature, the equipment and methods used in the present experimental work, and the results and comparisons related to the diffusion processes investigated.

II. SUMMARY OF WORK IN DIFFUSION

Gaseous diffusion is related to the state variables since diffusion occurs as a result of the same molecular movements which are responsible for the characteristic pressure effect of a confined specific quantity of gas at a given temperature. Diffusion, however, is also time dependent and it is normally defined as the net flow of a given component with respect to time which is caused by diffusion potential gradient, the diffusion occuring in the direction of reducing that gradient. This definition has been expanded to include self-diffusion in a single component system since it is convenient to think of selecting certain molecules of a system and considering their net migration into parts of the system where fewer selected molecules reside. This molecular selection in a one-component system can very nearly be carried out in the laboratory with use of radioactive isotopes, stereoisomers or ortho and para hydrogen. Theoretical and empirical attempts to predict diffusion are, then, necessarily associated with the state variables. The theory and experimental work reported in the literature having some direct bearing on this work will be presented in this section.

THEORY OF DIFFUSION

In the attempt to describe unknown phenomena, men search for relations between the unknown and familiar phenomena and make comparisons

between them. Scientists attempt to make quantitative comparisons by finding relations involving certain constants which are hopefully independent of one or more important variables affecting the phenomena. Diffusion is usually described quantitatively by Fick's Laws which relate the diffusion potential gradient to the rate of diffusion by means of a constant of proportionality, the diffusion coefficient, D. If the diffusion potential is taken to be concentration, Fick's first law of diffusion for steady state two component equal molar counter diffusion is:

$$J_1 = -D_{12} \nabla C_1 \qquad (1)$$

where J_i is the molar flux of component i, C_i is the concentration of component i, and D_{ij} is the diffusion coefficient of i in j. Actually, D_{ij} defined in this manner has been found to be dependent upon the concentration to some extent. According to the theoretical derivations of Enskog [13] and Chapman [8] this dependence could be a maximum of only thirteen percent in a binary system if the ratio of molecular masses of the diffusing components was infinite. This maximum dependence was derived by first letting the molar ratio of the two components approach zero and then infinity. Experimental determinations of this concentration dependence on the diffusion coefficient have been made on binary systems of the components involved in this investigation. Although the numerical results from the literature are presented later in this section,

a comparison of the latitude of the actual concentration dependence to the theory is warranted here. For the H_2 - D_2 system (having the same ratio of molecular masses as the HT - H_2 system) the maximum percent dependence was found to be three percent of the average. For H_2 - A the maximum dependence was seven percent; for H_2 - CO_2 it was nine percent. For diffusion determinations involving a sizable concentration difference this concentration dependence causes the resulting diffusion coefficients to be an integral average for the concentrations involved. For determinations involving only a trace amount of one of the components, the concentration dependence effect is negligible.

In a general two component system involving only diffusion for which diffusion flow is measured with respect to a stationary set of axes we must define the molar flux, N_i, of component i for which:

$$N_1 = J_1 + (N_1 + N_2)\, y_1 \qquad (2)$$

However when the molar average velocity past the stationary coordinates is zero, as with the use of negligible amount of a radioactive tracer, then $N_1 = -N_2$ and $N_1 = J_1$.

For one dimensional diffusion the change of concentration with respect to time of an element of volume of unit area cross section to flow and Δx thick is the difference between flux in and out divided by the thickness Δx, or:

$$\frac{\Delta C_1}{\Delta \theta} = \frac{(J_1)_x - (J_1)_{x+\Delta x}}{\Delta x} = \frac{D_{12}\left[\left(\frac{\partial C_1}{\partial x}\right)_{x+\Delta x} - \left(\frac{\partial C_1}{\partial x}\right)_x\right]}{\Delta x} \qquad (3)$$

As Δx, $\Delta \theta$, ΔC_1 approach zero:

$$\frac{\partial C_1}{\partial \theta} = D_{12} \frac{\partial^2 C_1}{\partial x^2} \qquad (4)$$

This relationship is frequently used as the basis of experimental determinations for the coefficient of diffusion and is often referred to as Fick's second law.

By the method of Enskog and Chapman, theoretical attempts to predict diffusion coefficients are based upon a choice of molecular model which in turn describes the manner by which molecules affect each other. The mathematical models which best predict these interactions are complicated in nature and become very difficult to manipulate except in the most ideal conditions. One such mathematical model with which a considerable amount of work has been done is the Lennard-Jones, or 6-12, potential model. A rather complete treatment of this model can be found in reference (17) and therefore only a cursory description will be included here. Attractive and repulsive potentials for this model are based on the distance between centers of the interacting molecules. The attractive forces are inversely proportional to the sixth power of the separation; the repulsive forces are inversely proportional to the twelfth power

of the separation. If two such molecules directly approach each other, they first experience an increasing attraction and then a more violent repulsion as they become very close together. In space, two molecules could approach in other than a direct collision path and experience only an attractive force. If one considers all random approaches and the resulting angles of deflection and energy transfers as predicted by the potential function, one can calculate a "collision integral", $\Omega^{(1,1)*}$, which is dependent upon temperature and species of molecules colliding. This collision integral can be used to predict the first approximation diffusion coefficient, D_{12}, of a binary mixture of dilute gases where only two body collisions are likely to occur by the expression:

$$[D_{12}]_1 = \frac{3}{16} \frac{\sqrt{2\pi RT\left(\frac{M_1 + M_2}{M_1 M_2}\right)}}{n\pi \sigma_{12}^2 \Omega^{(1,1)*}} \qquad (5)$$

In this relation, the collision integral $\Omega^{(1,1)*}$ is a function of the reduced temperature, (KT/ϵ_{12}), where ϵ_{12}/K is a measure of the attractive force between the two components and σ_{12} is the collision diameter for (1,2) collisions occurring. The collision integrals for a large range of reduced temperatures are presented in tabular form in reference [17]. There is no reason to suspect that Equation (5) represents the best molecular model for theoretical prediction of diffusion coefficients. However, these predictions are probably within the experimental accuracy of most experimental diffusion determinations at low pressures.

Further approximations to dilute gas diffusion coefficients are based on concentration dependence and rarely predict coefficients which differ from the first approximation by more than five percent. Different methods of computing second approximations have been suggested by Chapman and Cowling [8] and by Kihara [22]. Both are complicated functions involving the temperature and molecular weights of the components as well as the composition. Mason [26] has surveyed these two methods of making second approximation calculations and noted that they predict nearly identical results even though the Kihara method is reported to be considerably easier to use. These further approximations take the form of corrective factors to the first approximation.

$$[D_{12}]_2 = [D_{12}]_1 \cdot f_{(C)}^{(2)} \tag{6}$$

Based on the principles of Stefan-Maxwell, Wilke [47] derived an equation which relates the average diffusion coefficient of a given component through a multicomponent mixture to the binary diffusivities of the given component with each of the others.

$$\frac{1-y_1}{D_1} = \frac{y_2}{D_{12}} + \frac{y_3}{D_{13}} + \cdots\cdots \tag{7}$$

In this equation y_i represents the mole fraction of component i, and D_{ij} is the binary diffusion coefficient. This relation has been found to predict the data of Chou [9,10] with excellent accuracy.

For gaseous systems which are compressed to high densities, a given molecule can be influenced by attractive and repulsive forces of more than one other molecule at a time. The assumption of only two body collisions necessary in the development of Equation (5) is no longer valid. In addition, for very dense gases the actual volume occupied by molecules themselves becomes appreciable and the shielding of one molecule by another will cause a different number of collisions than would be predicted by the motion of point masses in space. Many attempts have been made to derive applicable relations to represent the actual molecular interactions which govern the rate of diffusion at high densities. Because of the extreme complexity of the physical situation and the inability to completely describe this situation in a simple manner by mathematical means, a successful rigorous formula has not been derived which utilizes the more realistic molecular force models.

The closest approach to a rigorous and applicable relation to predict diffusion coefficients in dense gases was formulated by Enskog [13] and presented in considerable detail by Chapman and Cowling [8]. This theory is based on the rigid sphere molecular model only, but allows for the appreciable diameter of a molecule in a dense gas with respect to its mean free path. Further compensation for the proximity of molecules has not been included. The results are again in the form of a corrective factor, Y, which is applied to the dilute gas prediction, D_o, at the

high density:

$$D = D_o/Y \tag{8}$$

The factor, Y, accounts for the difference in the probability of collision between low and high density gases. Enskog made the derivation for self-diffusion in a system of identical molecules and represented Y by the function:

$$Y = y/\ \frac{2}{3}\pi n\sigma^3 = y/\ \frac{b_o}{V} \tag{9}$$

Where:

$$y = \frac{PV}{RT} - 1 = \frac{2}{3}\pi n\sigma^3 + 0.6250\ (\frac{2}{3}\pi n\sigma^3)^2 + 0.2869\ (\frac{2}{3}\pi n\sigma^3)^3 + 0.115\ (\frac{2}{3}\pi n\sigma^3)^4 + \text{-----} \tag{10}$$

In Equations (9) and (10), σ is the diameter of the rigid spherical molecule, n is the molecular density at the system conditions, and b_o is the second virial coefficient for the rigid sphere equation of state. Thorne (42) has modified the theory for use with diffusion in a two component system:

$$Y_{12} = 1 + \frac{\pi}{12} n_1 \sigma_1^3\ (8 - \frac{3\sigma_1}{\sigma_{12}}) + \frac{\pi}{12} n_2 \sigma_2^3\ (8 - \frac{3\sigma_2}{\sigma_{12}}) + \text{----} \tag{11}$$

Further expansion of Equation (11) has not been accomplished even though the further terms would make important contributions to Y_{12} at rather low densities.

Realizing the inadequacy of the rigid spherical model to represent actual molecular interactions, Enskog suggested that a better value of y might be obtained from state data by substitution of the "thermal pressure", $T(\partial P/\partial T)_{\underline{V}}$, for pressure, P, in the first part of Equation (9). The "thermal pressure" is part of the following differential relation for pressure which is derivable from thermodynamic considerations.

EXTERNAL PRESSURE = THERMAL PRESSURE + INTERNAL PRESSURE

$$P = T\left(\frac{\partial P}{\partial T}\right)_{\underline{V}} + \left(\frac{\partial \underline{U}}{\partial \underline{V}}\right)_T \tag{12}$$

If the internal pressure $(\partial U/\partial \underline{V})_T$ can be assumed negligible, then:

$$y = \frac{\underline{V}}{RT}\left[T\left(\frac{\partial P}{\partial T}\right)_{\underline{V}}\right] - 1 \tag{13}$$

In order that D approach D_o at low density then according to Equation (9) the product, y $\underline{V}$, must approach the value of the solid sphere model second virial coefficient, b_o, at low density. In order for this to occur, then:

$$b_o = B(T) + \frac{T dB(T)}{dT} \tag{14}$$

B(T) is the second virial coefficient for a real gas model, the virial equation being:

$$\frac{P\underline{V}}{RT} = 1 + \frac{B(T)}{\underline{V}} + \ldots \tag{15}$$

In the virial equation further terms become negligible as the density approaches zero. According to this treatment, the dense gas correction factor is a measure of the inability of the first two terms of the virial equation to represent the actual P-V-T relationship.

Slattery [41] has presented an empirical correlation for prediction of diffusivities which is based on the Enskog theory. Since the Enskog development includes the other transport properties as well as diffusion, Slattery has prepared a corresponding states correlation for the prediction of diffusion coefficients by using only state relations and viscosity data. This correlation is in the form of a chart and relates the ratio of the diffusivity-pressure product at the desired conditions and the same product at its dilute gas value, $PD/(PD)_o$, to the reduced pressure, P_R, with the reduced temperature, T_R, as parameter. The resulting chart is very similar in appearance to the corresponding states compressibility factor, Z, chart, and not without reason since:

$$\frac{PD}{(PD)_o} = Z \frac{\rho D}{(\rho D)_o} \qquad (16)$$

As has been stated, it is felt that density is the state variable which is best suited for correlation of diffusion coefficients.

PRIOR EXPERIMENTAL DIFFUSION INVESTIGATIONS

Many investigators have determined diffusion coefficients for the molecules of one gas into one or more other gases. Work was first done with gases at nearly ideal gas conditions in reasonably uncomplicated equipment. The experiments were normally based on the two statements of Fick's laws, Equations (1) and (4), the former describing experimental systems in steady-state or quasi steady-state, the latter describing unsteady-state experiments the analysis of which may require complicated mathematics relating the boundary values necessitated by the experimental procedures chosen.

With an increase of interest concerning the interactions between like and unlike molecules, experimental investigations were carried out with near self-diffusion and diffusion at conditions where ideal gas conditions no longer exist. Because of the large number of diffusion investigations which have been made only the ones with some direct bearing on the present work will be included here.

Several types of equipment have evolved from the attempts to determine diffusion coefficients but only two have thus far been used in dense gas measurements. The quasi steady-state equipment of interest is described in detail in Section III of this dissertation since it is

the method used for experimental results presented here. The unsteady-state, or Loschmidt [25] type, equipment is usually made up of two similar cylindrical sections initially containing dissimilar gases at the same pressure which can be connected either by turning them into conjunction or by removing a partition between them. Normally the determinations are made by connecting the sections for a measured length of time, then disconnecting them and determining the mixed average concentrations of the samples remaining in each of the two sections. Since only initial and final integrated concentrations are determined, the mathematical analysis becomes a boundary value problem. Certain procedure variations have been utilized which change the type of boundary values encountered. See Jost [21] or Crank [11] for specific examples.

No low pressure diffusion data for the ternary systems of the present investigation, HT-H_2-CO_2 and HT-H_2-A, have been taken, although diffusion coefficients have been determined for the single component and binary systems of the components involved. Perhaps the best laboratory determination of self-diffusion coefficients involved the diffusion of para-hydrogen in normal hydrogen by Harteck and Schmidt [15]. Other approximations to determination of self-diffusion of hydrogen at low pressure involved the use of deuterium in the binary system D_2-H_2 in the works of Heath, Ibbs, and Wild [16], Waldmann [46], and Groth and Harteck [14]. Satisfactory agreement was found between the four

separate determinations after the D_2-H_2 results had been corrected for the molecular weight dependence predicted by Equation (5) where:

$$D_{12} \alpha \left[\frac{M_1 + M_2}{M_1 M_2}\right]^{1/2} \tag{17}$$

Thus, for converting isotopic diffusion to self-diffusion:

$$D_{11} = D_{12} \left[\frac{2M_2}{M_1 + M_2}\right]^{1/2} \tag{18}$$

For Equation (18), 1 denotes natural hydrogen and 2 denotes deuterium for this application. The deuterium investigations were made in unsteady-state modified Loschmidt-type equipment. The Waldmann experimental work was primarily designed for thermal diffusion determinations with the ordinary diffusion coefficient being derived as a secondary result.

Several studies of binary diffusion of hydrogen and argon at low pressure have been made. Groth and Harteck [14] also measured concentration effects on the diffusivities of binary mixtures. For several systems they reported an increase in the diffusion coefficient for increased mole fraction of the heavier component. Waldman [46] made thermal diffusion studies for mutual diffusion in the H_2-A system and reported ordinary diffusion coefficients for this system as well. Boardman and Wild [5] modified the Loschmidt type equipment and made atmospheric binary diffusion determinations for the H_2-A system and the H_2-CO_2 system. Several other investigators have studied diffusion

between hydrogen and carbon dioxide in the unsteady-state or Loschmidt-type cell. Boyd, Stein, Steingrimsson, and Rumpel [6] used interferometric methods of gas composition analysis within the cell in their determinations. Roth [39] and Lonius [24] also determined mutual diffusion coefficients of H_2-CO_2 at atmospheric conditions.

Schafer, Corte, and Moesta [40] used a quasi steady-state type cell in their determinations of the temperature and concentration effects on diffusivity in the H_2-CO_2 system at atmospheric pressure. Table I is a composite presentation of self diffusion and binary diffusion coefficients in systems of interest with respect to the present work. These results, when corrected to present experimental conditions, will be compared to extrapolated results from the data taken in conjunction with this dissertation.

TABLE I

DIFFUSION COEFFICIENTS AT ONE ATMOSPHERE

Investigators		Temperature °C	D, cm^2/sec
H_2 - Self Diffusion:			
Harteck and Schmidt	(15)	0	1.285 ± 0.0025
Heath (D_2-H_2)	(16)	15	1.24
Groth and Harteck	(14)		
99 percent D2(D2-H2)		0	1.135
99 percent H_2(D_2-H_2)		0	1.166
Waldmann (D_2-H_2)	(46)	20	1.21

TABLE I (cont.)

Investigators		Temperature °C	D, cm^2/sec
H_2-A Binary Diffusion:			
Boardman and Wild	(5)	20	0.77
Waldmann	(46)	20	0.77
Groth and Harteck	(14)		
99 percent H_2(H_2-A)		0	0.7418
99 percent A (H_2-A)		0	0.6905
99 percent D_2(D_2-A)		0	0.5345
99 percent A (D_2-A)		0	0.4999
H_2 - CO_2 Binary Diffusion:			
Boardman and Wild	(5)	20	0.639
Boyd	(6)	25	0.646
Schafer, Corte, Moesta	(40)		
100 percent CO_2(H_2-CO_2)		35	0.720
100 percent H_2 (H -CO_2)		35	0.656
Waldmann	(46)	20	0.60
Roth	(39)	0	0.544
Lonius	(24)	20	0.622
Chapman and Cowling	(8)	0	0.550

DENSE GAS EXPERIMENTAL WORK

High pressure gaseous diffusion measurements have been limited in number and scope. Most such determinations have been made using a radioactive tracer material as the measured diffusing component. All have been for the ultimate purpose of determining Fick diffusion coefficients, as defined by Equation (1), for the systems and conditions studied. The experimental procedures varied considerably and both unsteady-state and steady-state techniques are represented in published dense gas diffusion data determinations.

Several investigations involving carbon dioxide have been made because of the relative ease of the preparation of samples containing known amounts of carbon-14 dioxide. Timmerhaus and Drickamer [43,44] and Robb and Drickamer [38] have determined self-diffusion coefficients of carbon dioxide in a range of pressures from half an atmosphere to 1000 atmospheres. Although data from these investigations were considerably scattered, a definite trend of disagreement from the Enskog dense gas theory was noted at the higher densities. Enskog calculations for the comparison were made using collision diameters derived from the Lennard-Jones potential molecular model. The measurements were made with a series of packed columns; different size columns were used for different pressure ranges. Column calibrations were accomplished at low density by comparison of data with known diffusivities and then overlapping the ranges of succeedingly higher density columns. Radiation from continously increasing concentrations of carbon-14 dioxide at the low concentration end of the column was detected by means of a scintillation crystal and counter. Jefferies and Drickamer [19] used the same equipment for determinations of self-diffusion in methane to 300 atmospheres using tritiated methane as the traced diffusing component. Results agreed well with Enskog calculations to moderate densities. In a later work these authors [20] measured dense gas diffusion coefficients in the CO_2-CH_4 system with carbon-14 dioxide as the traced material in an attempt to

verify the agreement and disagreement with Enskog's theory for systems of self-diffusion in CH_4 and CO_2 respectively. To 225 atmospheres, a fifty-fifty molar percent mixture of these compounds was reported to agree with the dense gas theory. For a seventy-five molar percent CO_2 mixture, a definite deviation was noted at the higher densities.

O'Hern and Martin [30,31] also studied self-diffusion in CO_2 using a $C^{14}O_2$ diffusing component. Diffusion coefficients were determined within a temperature range of 0-100°C and within a pressure range from 2 to 205 atmospheres. The very consistant results of O'Hern, if plotted as the diffusivity-density product against the density, indicate a small initial increase in the product to intermediate densities but a general overall insensitivity of the product to density over the entire range of experimental pressures. These results are not in agreement with Enskog theory predictions based on the solid sphere molecular model which indicate a decreasing ρD-product for increasing density. The diffusion cell used was of the quasi steady-state type, the analysis of which was based upon Fick's first law of diffusion, Equation (1). Since a porous bronze plug was used as the diffusion path for the O'Hern investigation, a calibration of the cell was necessary in which high density diffusivity trends were extrapolated to low density where accurate absolute diffusion measurements have been made.

Chou and Martin [9,10] used the O'Hern diffusion equipment in studying diffusivities of $C^{14}O_2$ in four mixtures of CO_2 and H_2 and three mixtures of CO_2 and C_3H_8. Experimental work was carried out between 6 and 250 atmospheres at temperatures of 35°, 38.5° and 100° centigrade. The same insensitivity of the diffusion coefficient-density product as a function of density was noted for these two systems. The form of the Wilke equation, Equation (7), for predicting multicomponent diffusion coefficients from binary coefficients predicts the results within eight percent over the entire density range investigated. Chou found that D for the $C^{14}O_2$-CO_2-H_2 system varied approximately as the absolute temperature raised to the 1.27 power. This form of temperature dependence is based on some of the earlier forms of equations proposed for predicting diffusion coefficients which were in turn based on an ideal gas.

Becker, Vogell, and Zigan [1] studied nitrogen self-diffusion at 20°C between pressures of 20 and 90 atmospheres and found that the density-diffusivity product was independent of pressure in this range. Nitrogen-15 was used as the traced component in this system. A similar investigation by these authors for CO_2 using $C^{13}O_2$ indicated a thirty percent increase of the product between pressures of 15 and 52 atmospheres. The suggested explanation for this increase was that carbon dioxide molecules tended to coagulate at the higher densities.

Berry and Koeller [3] have measured rates of diffusion of binary systems of hydrogen-nitrogen and methane-ethane at 40°C, 60°C, and 77°C to 670 atmospheres and of binary systems of nitrogen-methane and nitrogen-ethane at 40°C to 170 atmospheres. They found that the calculated diffusion coefficients based on the Lennard-Jones model with Thorne's binary dense gas correction diverged below their experimental data for increasing densities. However, the experimental diffusivities also gradually diverge below dilute gas predictions. As would be expected the data was predicted with reasonable accuracy by the Slattery corresponding state correlation. The diffusion cell used for the Berry and Koeller investigation was a high pressure modification of the Loschmidt unsteady-state cell. It was similar to the cell used by Drickamer and coworkers excepting that it lacked the column packing which necessitated cell calibrations in the work of the latter. Another difference involved the determination of concentrations, which was accomplished at the end of a given run by mass spectrometry by Berry and Koeller. Temperature dependence was found to be exponential in form, similar to the dependence predicted by equations for liquid diffusion.

$$D_L = b_2 e^{-E/RT} \tag{19}$$

Timmerhaus and Drickamer [44] also found that their data was predicted by a temperature function of this form.

Mifflin and Bennett [29] have determined diffusion coefficients by the quasi steady-state method employed by O'Hern [30] and Chou [9]. Self-diffusion in Argon was studied using the radioisotope Argon-37 at 49.4°C in a pressure range between 68 and 291 atmospheres. Although the results were considerably scattered, agreement with the Enskog dense gas theory based on actual P-V-T relationships was reported. The data was said to tend below ideal gas predictions and above Enskog predictions based on the solid spherical molecular model.

III. DESCRIPTION OF EXPERIMENTAL APPARATUS

Much of the equipment used in this investigation was the same or similar to equipment used by O'Hern (30) and Chou (9) in experimental work for their doctoral dissertations at The University of Michigan. The major differences from their equipment were in the diffusion cell, itself, and in the sample preparation apparatus. In an attempt toward brevity, the chief purpose of this section will be to thoroughly describe the innovations produced in this work and to treat the equipment introduced by their works in brief descriptions concerned mainly with operating characteristics. It is felt that the sample preparation equipment can be best described in conjunction with the actual samples prepared. For this reason, description of that equipment is included in Appendix C together with the analyses of samples prepared. Therefore, equipment described in this section will be limited to apparatus utilized during an actual diffusion run.

THE DIFFUSION CELL

The diffusion cell used for the experimental work presented in this dissertation was similar to the one used by O'Hern and Chou in their experimental work. There were two chief differences which will be pointed out in the ensuing description of the cell. Figure 1 is a sectional drawing of the diffusion cell.

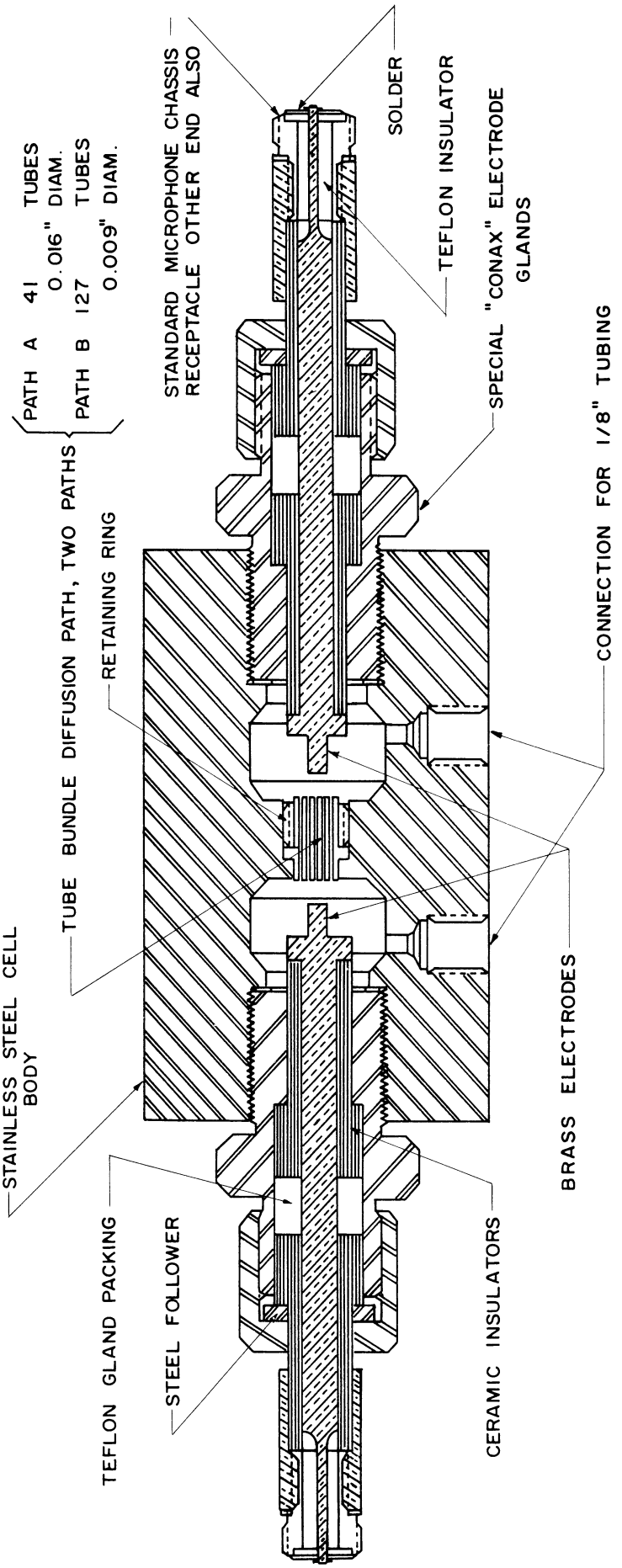

Figure 1. The Diffusion Cell.

The cell consisted of two chambers, one above the other, connected by a permeable diffusion path which was designed to curtail bulk flow between the chambers once an equilibrium pressure was reached after charging. In the diffusion measurements, gases introduced into these chambers ideally had exactly the same composition except for a trace of radioactive isotope which was introduced in greater concentration into the upper chamber. This radioactive isotope served as the traced diffusing component in the experiment. The concentration of the isotope in either chamber at any time was determined by an ionization chamber technique. The cell body was designed in such a manner that an electrode extended into each chamber which was entirely insulated from the body of the cell. A 200 volt direct current potential was maintained between the electrode in each chamber and the cell body. There was no appreciable potential difference between the two inserted electrodes although they were not connected electrically. Radiation from the radioactive material caused ionization of the gas within the chambers, and the ions were collected by the electrodes and walls.

The current resulting from such a collection can be measured and is related to the concentration of the radioactive material in the chamber. If the concentration of the radioactive material is low enough, this relation is a direct proportion. In order to simplify the analysis

of the results, ionization current calibrations of the cell were made to determine the concentration below which this direct proportion relationship was valid.

The results of these calibrations are located in Appendix D. For all experimental runs, concentrations of the tracer were small enough that direct proportionality held between the concentration of radioactive material and current measured. Continuous current measurements were made for each chamber of the cell, and the result was an accurate time-concentration relationship for the diffusing component. The desired diffusion coefficients were determined from these time-concentration relationships.

Because diffusion measurements were desired at pressures of greater than 5000 pounds per square inch, the cell and fittings were designed and pressure tested for greater than one and one-half times this pressure. The cell itself was constructed from a solid stainless steel block 2 1/4" x 2 1/4" x 3 3/4". The positive electrodes were introduced at opposite ends of the cell body in one inch threaded electrode plugs that screw into similarly threaded sockets in the cell body. Two one-eighth inch pressure tubing fitting threaded sockets were machined into one face of the cell body to provide an entrance for the gaseous systems into each of the two chambers. The chambers themselves were cylindrical

shaped, approximately one inch in diameter, and half an inch deep. A partially threaded receptacle was machined through the one-half inch of steel separating the chambers to accept a flanged permeable diffusion path.

This diffusion path, a major difference from previous equipment, was a bundle of fine stainless steel hypodermic needle tubes. Two such tube bundles were constructed, one from tubes having an inside diameter of approximately 0.009 inch, the second from tubes with approximately 0.017 inch inside diameter. The bundles were formed in such a manner that the interstices between individual tubes were completely filled. Bundle A, with 0.017 inch tubes, consisted of 47 tubes, of which six were accidentally sealed off during construction. It was constructed by inserting one-inch lengths of the tubing sealed at both ends into a one-half inch long flanged diffusion path shell, dipping the result into hydrochloric acid and then into molten solder which flowed into the interstices and was solidified. The sealed ends of the tubes were then cut off with a cutting wheel and the cut surfaces were ground flat with a fine grinding wheel. At this point it was found that many of the tubes were filled with burrs caused by the grinding or by the grinding material itself. All but six were successfully cleaned out by drilling. The final length of this bundle was 0.451 inch.

Diffusion path B, with 0.009 inch tubes, consisted of 136 tubes of which nine were sealed up during construction. The clogging of holes caused in the construction of bundle A indicated that another method of construction would be necessary for a bundle of tubes of smaller diameter. A two inch length of 0.006 inch wire was inserted into each of 136 one-inch lengths of 0.009 inch inside diameter hypodermic needle tubing. One end of each tube was sealed, sealing the wire in place. The tubes were then placed, one by one, into a one half inch long flanged diffusion path shell, which contained a solidifying epoxy resin mixture, in such a manner that the unsealed ends of tubes with wires protruding were not wetted by the liquid resin. After the resin solidified, the sealed ends of the tubes were cut off and ground to a flat surface with a surface grinding machine. The wires were then removed from the tubes and reinserted from the finished end. The remaining unfinished end was then ground to a flat surface and the wires were again removed leaving the tubes open. Particles of grinding material, grease, and dust were removed in an ultrasonic cleaning instrument bath which contained water and ordinary kitchen detergent. The ends of the holes were inspected and measured by a microscope before installation in the diffusion cell. The measurements of hole diameters and diffusion path length are recorded in Appendix F.

Figures 2 and 3 are photographs taken through a microscope of diffusion paths A and B. A closer visual examination of the tube bundle ends through a microscope reveals the openings to be clean and almost perfectly circular in shape. The measurements of these tube openings are listed in Appendix F. The average deviation of diameters measured from the average of all tubes measured was almost exactly one percent for diffusion path B.

The pressure limitation imposed by the electrode plug design was perhaps the most serious shortcoming of the diffusion cell used by O'Hern and Chou. The teflon insulation used in these plugs offered excellent resistivity characteristics, but lacked rigidity under the maximum pressures attained in these investigations, about 3750 pounds per square inch. In order to increase the pressure range available to this cell, a type of plug was developed which had both the necessary resistivity and strength to withstand high pressures.

Since the ionization currents to be measured were of the order of 10^{-11} to 10^{-12} amperes, it is clear that the electrode plug insulation resistivity must be of the order of 10^{17} ohms or higher if the background currents produced by the 200 volt potential across the electrode insulation are to be negligible. Since no commercially available electrodes could match this resistivity and yet withstand pressures of the

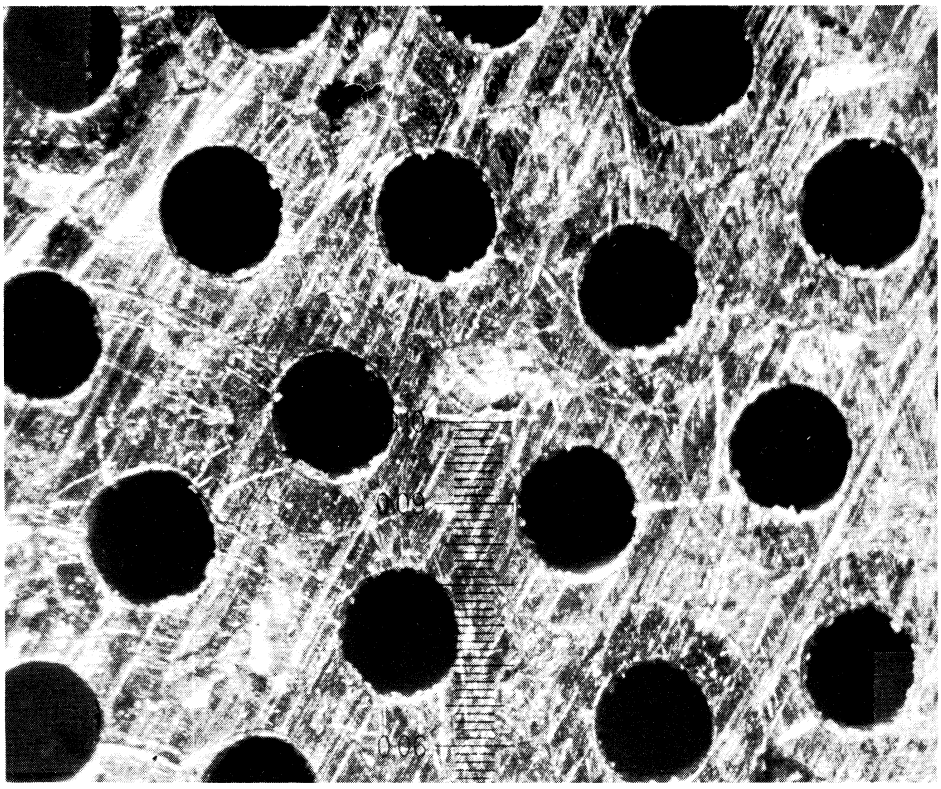

Figure 2. Microscopic Photograph of Diffusion Path A. Magnification 46X.

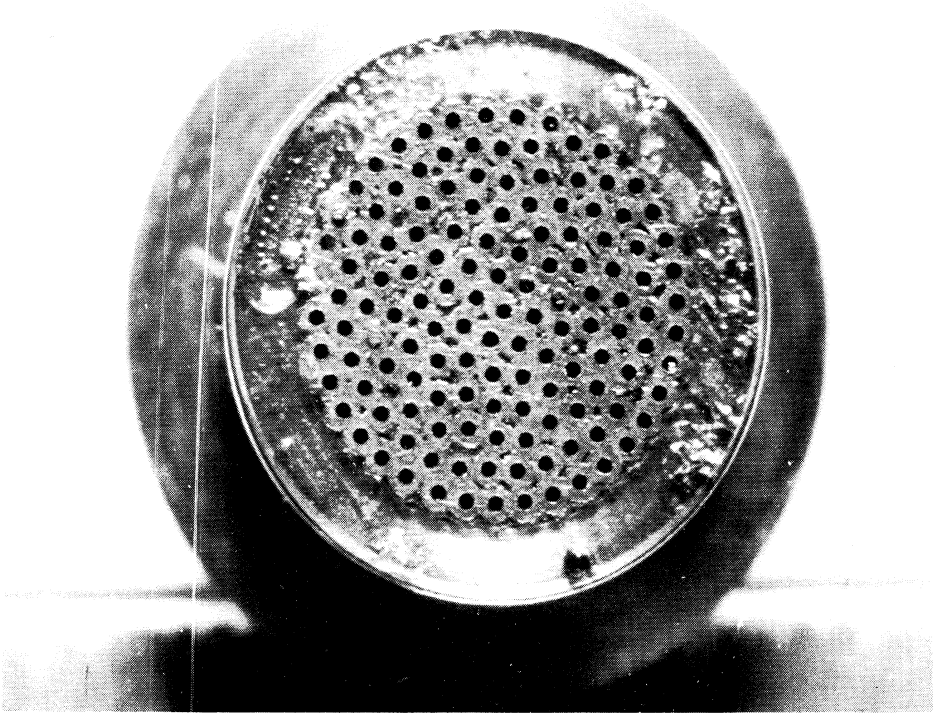

Figure 3. Microscopic Photograph of Diffusion Path B. Magnification 9X.

order of 9,000 pounds per square inch with a negligible leakage of hydrogen, the decision was made to attempt to convert an available high pressure electrode making it conform to the resistivity requirements. The attempt was successful. Two modified Conax electrode glands were purchased which would satisfy the pressure requirements. The ceramic insulators and specially designed electrodes were varnished with Dow-Corning NO. 994 silicone varnish and baked for 25 minutes at 275°C. Using a teflon packing, the carefully assembled plugs satisfied the resistivity requirements. Background currents were not entirely eliminated, however, and were corrected for in diffusion coefficient calculations. The background calibrations included in Appendix F show that this background was less than one percent of average measurements for 35°C runs. Background currents were somewhat higher for the 100°C runs.

THE CURRENT MEASURING CIRCUIT

The ionization currents caused by tritium disintegration and collected by maintaining a 200 volt potential between the electrodes and the cell body were measured by a sensitive current-detecting instrument, a Beckman Ultrohmeter. The instrument was actually used as a current amplifier in this investigation. The current from the cell, the order of magnitude of which being micro-micro amperes, was passed through a high internal resistance in the Ultrohmeter. The voltage across this

resistance was determined electronically and amplified for output to a continuous recorder. The input signal to the Ultrohmeter, being such a small current, was extremely sensitive to fluctuation. For this reason, careful pains were taken to shield the input cables and cable connections. In order that capacitance and resistance effects of shielding do not cause transient measuring difficulties, the Ultrohmeter electronically maintains the potential of the shield to within a few millivolts of the potential of the input lead without sacrificing shielding characteristics. Figure 4 is a schematic drawing of the circuitry employed in measuring ionization currents.

For equipment simplification, it was desired to alternately amplify the currents from the two cell chambers with the Ultrohmeter, and record both amplifications on the same recorder chart. This was accomplished by switching the input to the Ultrohmeter from one electrode to the other at convenient time intervals. Since some of the runs lasted approximately two days, this switching was done with a Flexopulse automatic time switch which allows variable equal measuring periods for the two channels of up to one hour. In order to maintain the two electrodes at the same potential and thereby eliminate a potential gradient through the diffusion path, a double-pole double-throw switching arrangement was employed which shorted one electrode to shield potential while the other electrode was connected to the Ultrohmeter input.

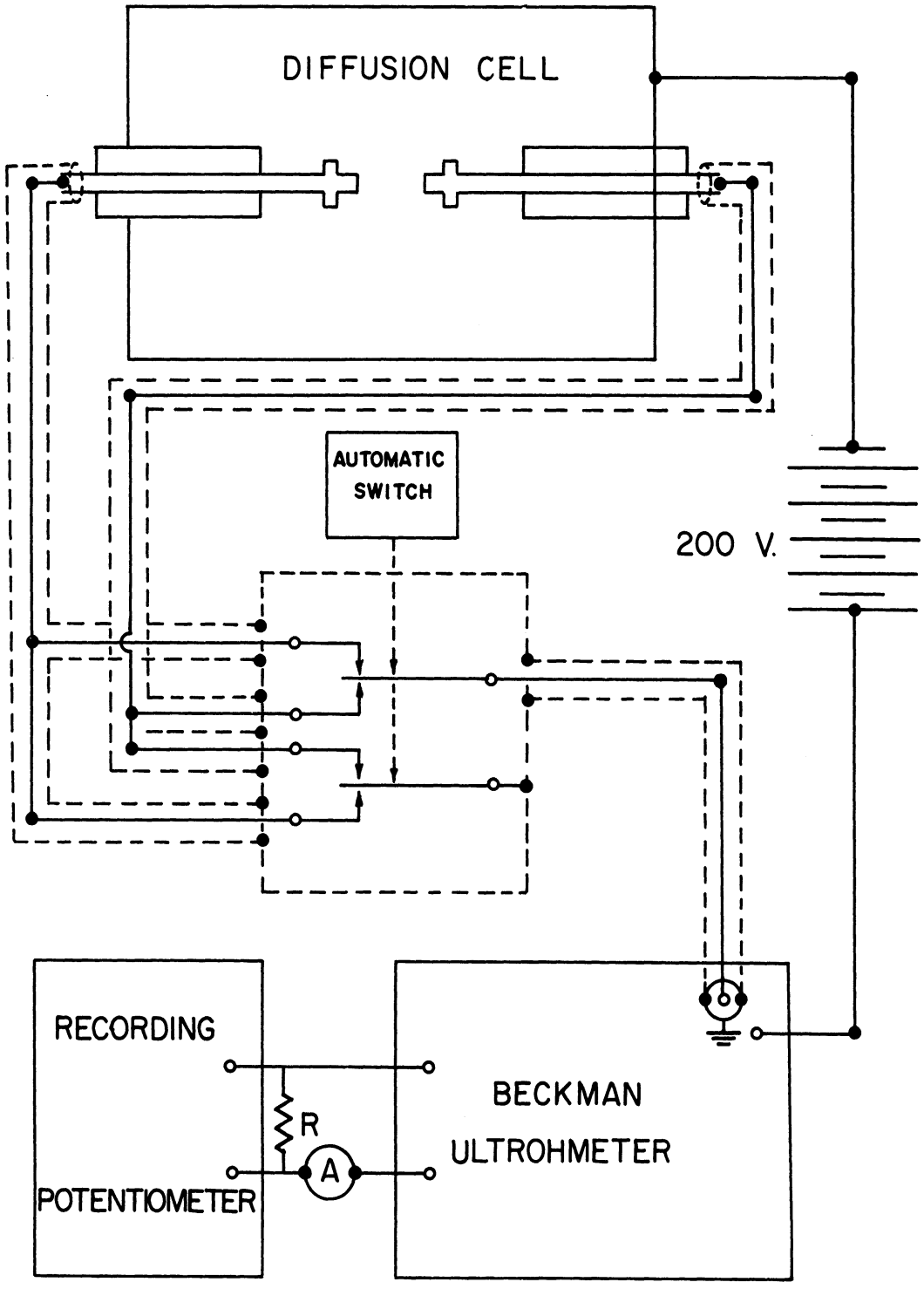

Figure 4. The Ionization Current Measuring Circuit.

Serious disturbances caused by the switching were effectively eliminated by carefully shielding and desiccating the switched circuit. Two single-pole double-throw microswitches were employed which were mechanically switched by eccentric cams driven by the timing mechanism of the Flexo-pulse timer.

The output signal from the Ultrohmeter is a current which is proportional to the input current. This output current is passed through a wire-wound resistor which is connected between the terminals of a Brown Recording Potentiometer. The resulting recorder chart trace is proportional to the ionization current produced in the diffusion cell chambers. An accurate 500 micro-ampere ammeter was used for balancing the Ultrohmeter output to zero for zero input.

Figure 5 is a typical recorder trace taken during diffusion run number 84B. Note the alternate periods of recording the currents from the two diffusion cell chambers. Segments of the broken curves have been connected by lines drawn with ships curves.

THE CELL CHARGING SYSTEM

The diffusion cell was charged through one-eighth inch steel high pressure tubing which was connected directly to the cell body into the two one-eighth inch fitting sockets. The tubing connected to the lower chamber was used chiefly for entrance of non-radioactive gas sample, the upper for entrance of radioactive gas sample. Each tube contained

FIGURE 5

RECORDER TRACE OF IONIZATION CURRENTS

RUN NUMBER 84B

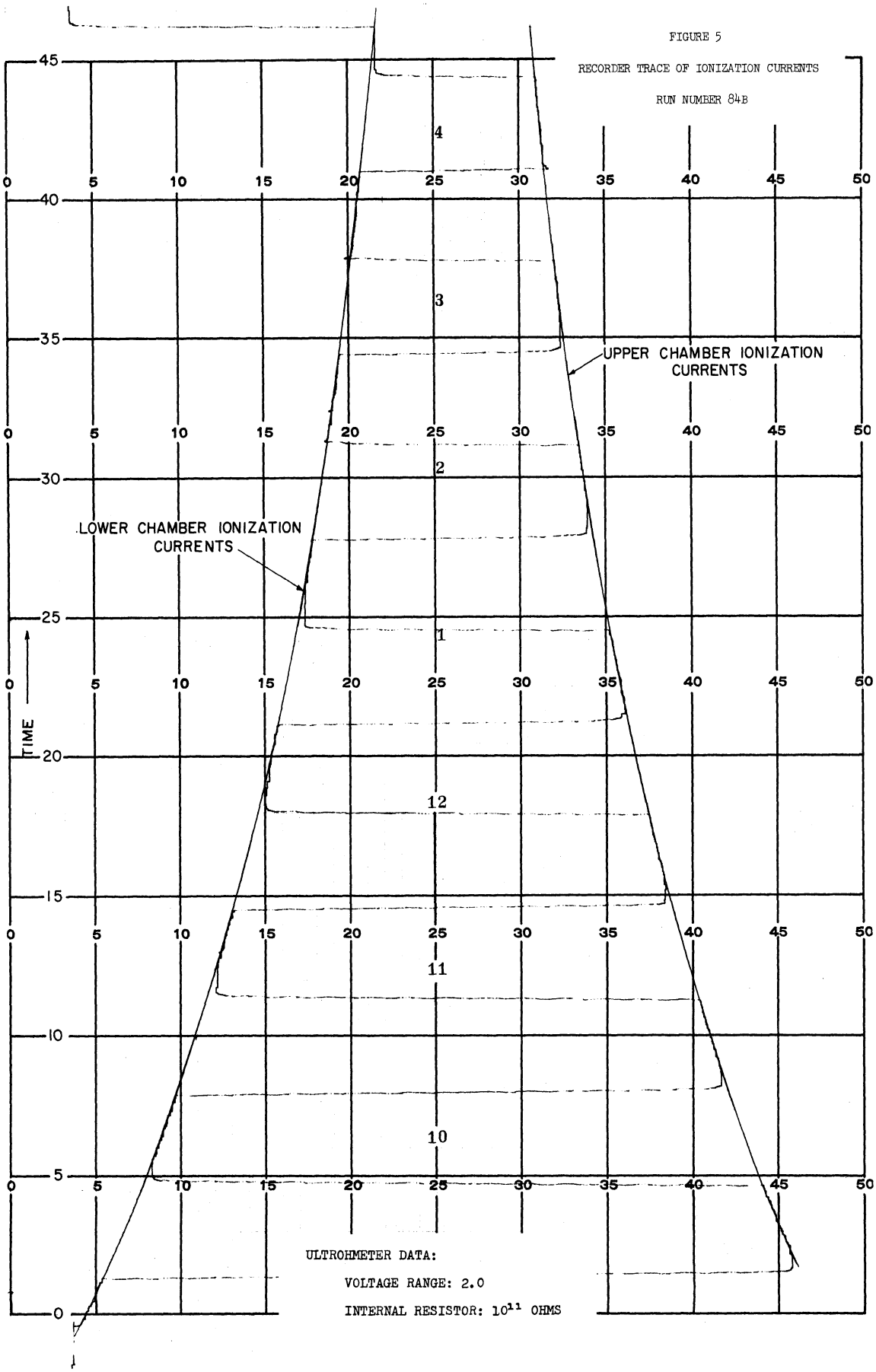

ULTROHMETER DATA:

VOLTAGE RANGE: 2.0

INTERNAL RESISTOR: 10^{11} OHMS

No. 14 copper wire to reduce diffusion into or out of the respective chamber through the tubing mouth. Diffusion run pressures were measured by one of two pressure gauges which were connected to the cell through the tubing to the lower chamber. These gauges had ranges of 0-1500 pounds per square inch for the lower pressure runs, and 0-10,000 pounds per square inch for the high pressure runs. The gauges were calibrated before and after the diffusion runs, the calibration data being presented in Appendix F.

The cell was pressurized to operating pressures by a manually operated hydraulic pressure generator which pumped oil over mercury in one leg of a U-shaped tube, thus compressing gas over mercury in the other leg. This pressurizing system is shown in Figure 6 together with the remainder of the equipment necessary for the cell charging. Non-radioactive gas from bottles (N) was allowed to expand into the pressurizing system through one side of a two-way valve after passing through silica gel for drying. The valve was closed and the manual generator was cranked until the ambient diffusion cell pressure was attained, the diffusion cell side of the two-way valve was opened, and cranking was resumed until either the desired pressure was attained or the crank came to its end. A thirty cubic-centimeter volume of gas could be elevated in pressure for each complete stroke of the generator, the mass quantity of gas per stroke being

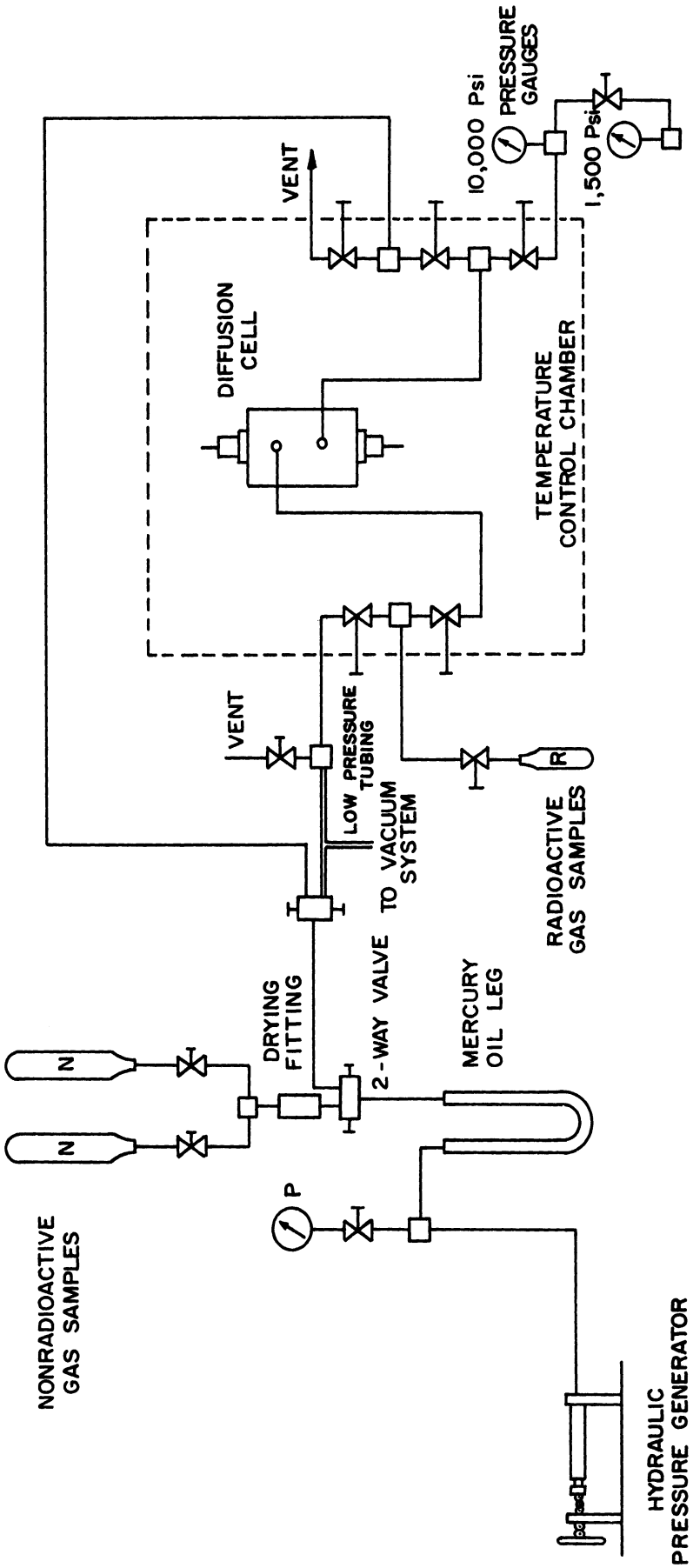

Figure 6. The Cell Charging System.

dependent upon the available gas pressure. For the highest pressure runs as many as ten complete strokes of the generator were necessary to bring the diffusion cell to run pressure. Radioactive gas was always added to the diffusion cell when the cell pressure was sufficiently less than the radioactive sample bottle pressure so that no additional pressurizing was necessary to transfer the desired amount of radioactive sample.

THE CONSTANT TEMPERATURE CHAMBER

This part of the O'Hern-Chou experimental equipment was used without modification except for insignificant repairs which were required because the chamber had set idle for several years. It is described more completely in references [9] and [30]. The chamber itself was an air bath constructed of insulating blocks which were cemented together with asbestos. The dimensions of its interior were 18" x 18" x 31". The chamber was heated by four electrical resistance heaters; one was utilized for rapid heating, two large variable output heaters were used for maintaining a constant heating effect during diffusion runs, and the fourth was used as a variable control heater which operated intermittantly during runs and was in turn controlled by a mercury expansion switch and temperature controller. Air was circulated within the chamber by a fan mounted at the rear of the chamber which drew air from the lower part of the chamber past the heaters and forced it out at the top.

Six copper-constantan thermocouples were placed inside the temperature chamber. Two were embedded in the diffusion cell itself, at opposite ends so that temperature inconsistencies could be detected. The calibrations of these thermocouples are recorded in Appendix F. The other four thermocouples were located at strategic points of the chamber. All six were connected through a six-position rotating switch to a common cold junction immersed in distilled ice water in a dewar flask and to a portable potentiometer which was used to determine the thermocouple potentials. The diffusion cell was clamped to a piece of transite insulating board at the center of the chamber and covered by a transite box which was lowered in place at the start of a diffusion run. Although the air temperature in the chamber itself varied as much as half of a degree centigrade during a control heater heating cycle at a chamber temperature of 100°C., the change of temperature of the cell, as indicated by the thermocouples embedded in the cell body, was entirely undetectable during a similar cycle. The diffusion cell temperature during an entire run was normally constant to within 0.2 of a degree centigrade.

Because the diffusion cell was positioned with one cell chamber above the other during diffusion measurements, it was important that the lower chamber should at no time contain gas of higher temperature than that in the upper chamber, since convection would most certainly occur through the tubes of the diffusion path. For this reason, the upper portion of the cell body was maintained at a slightly higher temperature than the lower portion, a temperature difference averaging

about 0.2 of a degree centigrade. This temperature difference was not difficult to maintain, in fact it would have been far more difficult to prevent, since the freshly heated air from the blower fan circulated from top to bottom in the portion of the constant temperature chamber containing the diffusion cell.

Figure 6 illustrating the charging system shows the extent of the equipment located within the constant temperature chamber. Valves on the charging lines to the cell body were mounted within the chamber to insure against tubing heat conductance effects being present in the cell. Although valve stems did necessarily stick through the temperature chamber walls, it was felt that heat conducted along these stems did not appreciably affect the cell. The equipment was designed in such a way that, barring difficulties, the constant temperature chamber could be sealed at the start of the first experimental diffusion run and not be opened until the last run had been completed. Actually, the chamber was opened on four occasions to repair leaks in the electrode plugs or the charging system.

IV. PROCEDURES USED IN THE DETERMINATION OF DIFFUSION COEFFICIENTS

The basic operation of the equipment used has been included along with the equipment descriptions covered in the previous section. This section will present the experimental work from the standpoint of actual steps followed, items of data recorded, and methods used in the analysis of the data in order that diffusion coefficients could be determined.

EXPERIMENTAL SYSTEMS

In the experimental work, diffusion was observed quantitatively in two ternary systems. In both systems tritiated hydrogen, HT, was the radioactive, traced diffusing component. The gaseous diffusion media were composed of, first, mixtures of hydrogen and carbon dioxide, and, second, mixtures of hydrogen and argon. An obvious degeneration of both ternary systems is the diffusion of HT in hydrogen, and this sub-system was also investigated. At first consideration, these systems seem to be two binary component systems with some of the molecules of one of the components tagged in such a manner that they can be detected in order to reveal the characteristics of the phenomenon of interest. Indeed, investigators have treated similar systems and phenomona in this manner. The physical dimensions and chemical properties of a HT molecule are very nearly identical with those of a H_2 molecule. Furthermore, an examination of gases used in the diffusion runs would not reveal the presence of a third component except due to radioactivity, since the actual

ratio of HT molecules to total molecules was approximately one to 2,000,000. However, due to the difference in masses between H_2 and HT, they cannot be treated as the same molecule in a diffusion analysis. Diffusion was investigated at two temperatures for each system, 35°C and 100°C.

EXPERIMENTAL PROCEDURE

The experimental work was divided into two basic parts, the preparation of equipment and samples to be utilized in the determination of diffusion coefficients, and the actual measurements pertaining to the phenomena which lead to the evaluation of the diffusion coefficients. The former part has already been covered in the equipment and sample preparation sections of the previous text and appendix. The function of this section will be to describe the latter procedures carried out with the previously prepared equipment and samples.

Since it was not necessary that the constant temperature chamber be opened except for repairs, a given temperature was maintained in the chamber during the entire series of runs with a given system at that temperature. Similarly, during runs with a given system composition, the cell did not require complete flushing between runs in order to insure the uncontaminated homogeneous distribution of the two major components. However, since the most general procedure is of interest, these items will be included in the description.

The experimental procedure for a data run started by first bringing the constant temperature chamber to the desired run temperature.

This was brought about by operating all four chamber heaters simultaneously until the chamber was at the approximate running temperature desired as measured by the four chamber thermocouples. The mercury expansion switch was adjusted to make and break contact at this temperature by either adding or removing mercury, a coarse adjustment, or by raising or lowering the contact wire, a fine adjustment. The chamber was then allowed to operate overnight in order that it and the diffusion cell come to equilibrium temperatures. The following day a check was made with the thermocouples embedded in the cell body to see if an equilibrium temperature had been reached. If no further temperature increase was noted in half an hour, the procedure was continued.

The valve to the mercury leg of the cell pressure gauges was closed, and the cell and pressurizing leads were evacuated to a pressure of 50 microns of mercury. System gas was expanded into the evacuated portion and then removed by re-evacuation. System gas was again expanded into the evacuated equipment, and the cell was pressurized to approximately 200 psig as indicated by the pressure gauge in the pressurizing equipment. The valve to the cell pressure gauges was then opened and these gauges were used in further cell charging operations. At this point, radioactive gas, from the sample bottle containing the same concentration of major components as the particular system gas, was introduced into the upper chamber of the diffusion cell. The cell was pressurized to a total pressure of about 400 psig with radioactive gas, this pressure being dependent upon the desired run operating pressure. It was found that the most stable and accurate measurements of

the ionization current could be made at the highest range of the Ultrohmeter for which the concentration of HT-ionization current relationship was a direct proportion. The desirability of this direct proportionality has been discussed thoroughly in Appendix D. The Ultrohmeter range satisfying this condition occurred using the 10^{11} ohm internal resistor and the 2.0 voltage range scale. For this range a full scale recorder trace deflection corresponds to an ionization current of approximately 2×10^{-11} amperes. All diffusion runs except for a few exploratory runs near the beginning of the experimental work were made using this instrument range. In order to do so, the amount of radioactive sample to be added for a given run had to be calculated so that the right amount of HT was present in the upper chamber at the desired run pressure to give a nearly full scale recorder trace deflection for that chamber. It was desired that the recorder trace for the upper chamber be nearly full scale on the recorder chart in order to take the fullest advantage of the sensitivity of the instruments. Similarly, it was desired that the recorder trace for the lower chamber be close to zero at the start of a run in order that the concentration difference at that time be a maximum. By the method of charging being described, an initial ratio of tritium in the upper chamber to tritium in the lower chamber of ten was usually attained. The radioactive sample was slightly more rich in hydrogen than the corresponding non-radioactive sample due to the method of preparation of the tritiated samples which is discussed in Appendix C. This helped to prevent bulk convection which might have been caused by a slightly higher concentration of hydrogen and therefore lower density gas in the lower chamber.

After the radioactive material had been added, the cell was pressurized with non-radioactive sample through the lower chamber to slightly greater than the desired run pressure. A small amount of gas was then released to flush the upper chamber charging tube of tritium-rich gas, thereby reducing the possibility of HT entering the upper chamber during the run by diffusion. This flush was also valuable if the amount of tritium charged was greater than necessary to cause full scale chart deflection using the optimum instrument range.

The concentration of tritium in the cell chambers began equalizing by diffusion as soon as bulk flow through the diffusion path due to the charging operation subsided. As quickly as possible the Ultrohmeter was balanced to zero for shorted input and a satisfactory chart speed and time switch period were chosen and set. The recording potentiometer was then adjusted for zero and standardized and the recorder trace of the alternate chamber concentrations was started. The cell temperature was then determined and recorded from the two thermocouples embedded in the cell body. The cell pressure was read and recorded from the 1500 psi pressure gauge if the pressure was below this value or from the 10,000 psi gauge if above. For runs with pressures above 1500 psi, the 1500 psi gauge was isolated from the system by a valve.

Table II lists in abbreviated form the data recorded for a given experimental run.

TABLE II

EXPERIMENTAL DATA RECORDED

Item	Remarks
Run number and date	
Sample percent hydrogen	Measured after each run for H_2-CO_2 runs.
Other component	Carbon dioxide or argon.
Voltage range and internal resistor	Ultrohmeter range, $\frac{V.R.}{R}$ is approximately current (amps) required for full scale deflection.
Chart speed	Variable from 1 to 6 inches per hour in one inch increments.
Charging information	Samples used and to what pressure they were charged.
Pressure Upper end thermocouple Lower end thermocouple	These three measurements were usually made at several recorded times during a run. Frequently for overnight runs, only starting and finishing conditions were recorded.
Chart traces of ionization currents and zero current traces	Figure 5
Date and time of completion of run	
Background (each channel)	Taken at regular intervals between experimental runs is less than 1 percent of average ionization currents at 35°C.

The end of an experimental run was entirely a matter of judgment or convenience. Upon observing Figure 5 it is seen that the separate chamber ionization current traces approach each other as the concentrations equalize due to diffusion. If both chambers responded identically to equal concentrations of tritium, these traces would come together only after an infinite time. However, since the accuracy and resolution of the equipment and analysis was better when a large ratio of chamber concentrations was present than when the concentration ratio was small, runs were normally stopped, if it was convenient, when the ratio of currents was about a third of the initial current ratio. On a few occasions, the runs were allowed to proceed to "infinite time", or until the ratio ceased to vary. In each case the ionization current calibrations in Appendix D were corroborated; the ratio of lower chamber current to upper chamber current at equalized concentration was always approximately 0.96. As is pointed out in the appendix, this is also the approximate ratio of the respective chamber volumes.

After the end of an experimental run, the cell was vented into an operating hood which expelled the slightly radioactive gases above roof level three stories up. If further runs were to be made using the same concentration of major components, the venting was completed at a cell pressure of approximately 200 psig and charging for the next run was done with this as the starting pressure. If another concentration or system was to be run next, the cell was completely vented and flushed with the new system gas as previously described.

METHOD OF DATA ANALYSIS

The type of diffusion cell used in this investigation was initially chosen because of its simplicity and the relative ease of analyzing the data. It was one of a class of cells termed as quasi steady-state diffusion cells. The mathematical analysis from which a diffusion coefficient is determined from the data is dependent upon two important assumptions. The first is a multi-part assumption which concerns the gradient causing diffusion. It is assumed that concentration is at least proportional to this gradient. This part of the assumption is probably very good for this investigation since the diffusing component, HT, is present in such low molecular fraction, approximately 1 to 2,000,000. The other parts of this assumption are that this concentration gradient is linear through the diffusion path, and that the reference plane which defines the diffusion process is stationary with respect to the equipment. Since the net molar flow through the diffusion path is negligible, this latter part is probably a good assumption.

The second assumption is that there is complete mixing in the two chambers of the cell, that the only resistance to transfer by diffusion occurs in the diffusion path. This assumption is also a good one since the cross-sectional area of the chambers is very large in comparison to the cross-sectional area of the diffusion path.

Using these assumptions we then can relate the rate of change of concentration in the two chambers to a coefficient of diffusion, D, by Fick's Law.

For Chamber 1:

$$\frac{V_1 dC_1}{d\theta} = -DA\frac{dC}{dx} = -DA\ \frac{C_1 - C_2}{L} \qquad (20)$$

For Chamber 2:

$$\frac{V_2\ dC_2}{d\theta} = +\ DA\ \frac{dC}{dx} = +DA\ \frac{C_1 - C_2}{L} \qquad (21)$$

Where:

θ = time.

V_1, V_2 = Volumes of Chambers 1 and 2.

C_1, C_2 = Instantaneous concentration in Chambers 1 and 2.

A = Open cross sectional area of diffusion path.

L = Length of diffusion path.

Subtracting (21) from (20) and rearranging:

$$\frac{d(C_1 - C_2)}{(C_1 - C_2)} = -\frac{DA}{L}\left(\frac{1}{V_1} + \frac{1}{V_2}\right)d\theta \qquad (22)$$

This can be integrated to result in:

$$\ln\ (C_1 - C_2) = -\frac{DA}{L}\left(\frac{1}{V_1} + \frac{1}{V_2}\right)\ \theta + \text{constant}_1 \qquad (23)$$

For the concentrations of tritium used, the ionization current, I_j, is proportional to the concentration, C_j, in a given chamber, j. If the chamber geometry is different for two ionization chambers, a constant of proportionality, f, is necessary in order that a comparison be made between the respective currents produced by a given concentration of

tritium in the two chambers. For the cell used in this investigation this constant was determined experimentally and is very nearly equal to the ratio of the free volumes of the chambers. This calibration is presented in Appendix D. Substituting the respective ionization currents into E-quation (23) the result is then:

$$\ln (fI_1 - I_2) = - \frac{DA}{L} \left(\frac{1}{V_1} + \frac{1}{V_2} \right) \theta + \text{constant}_2 \qquad (24)$$

If the natural logarithm of the quantity, $(fI_1 - I_2)$, is plotted versus the elapsed time for a series of values of the currents, I_1 and I_2, at different times, θ, as recorded on the recording potentiometer trace, the slope of the resulting straight line will be KD, the product of the cell constant, $K = \frac{A}{L} \left(\frac{1}{V_1} + \frac{1}{V_2} \right)$, and the coefficient of diffu-sion at the conditions of the experimental run. Figure 7 is this plot for run 84B. Perhaps a more objective way is to fit the same experimental data to the equation of a straight line by the method of least squares. The equation fitted was:

$$- \frac{\ln(fI_1 - I_2)}{\frac{A}{L} \left(\frac{1}{V_1} + \frac{1}{V_2} \right)} = D\theta + \text{constant}_3 \qquad (25)$$

The coefficient of time in this equation, D, is the desired diffusion coefficient. The latter procedure is easier if an automatic digital computer is available, and was the method used for this investigation. The computer programming techniques are covered in Appendix G.

In the calculations, two more corrections were made in de-termining the Fick diffusion coefficients. The first is the previously mentioned background current which was subtracted from the respective

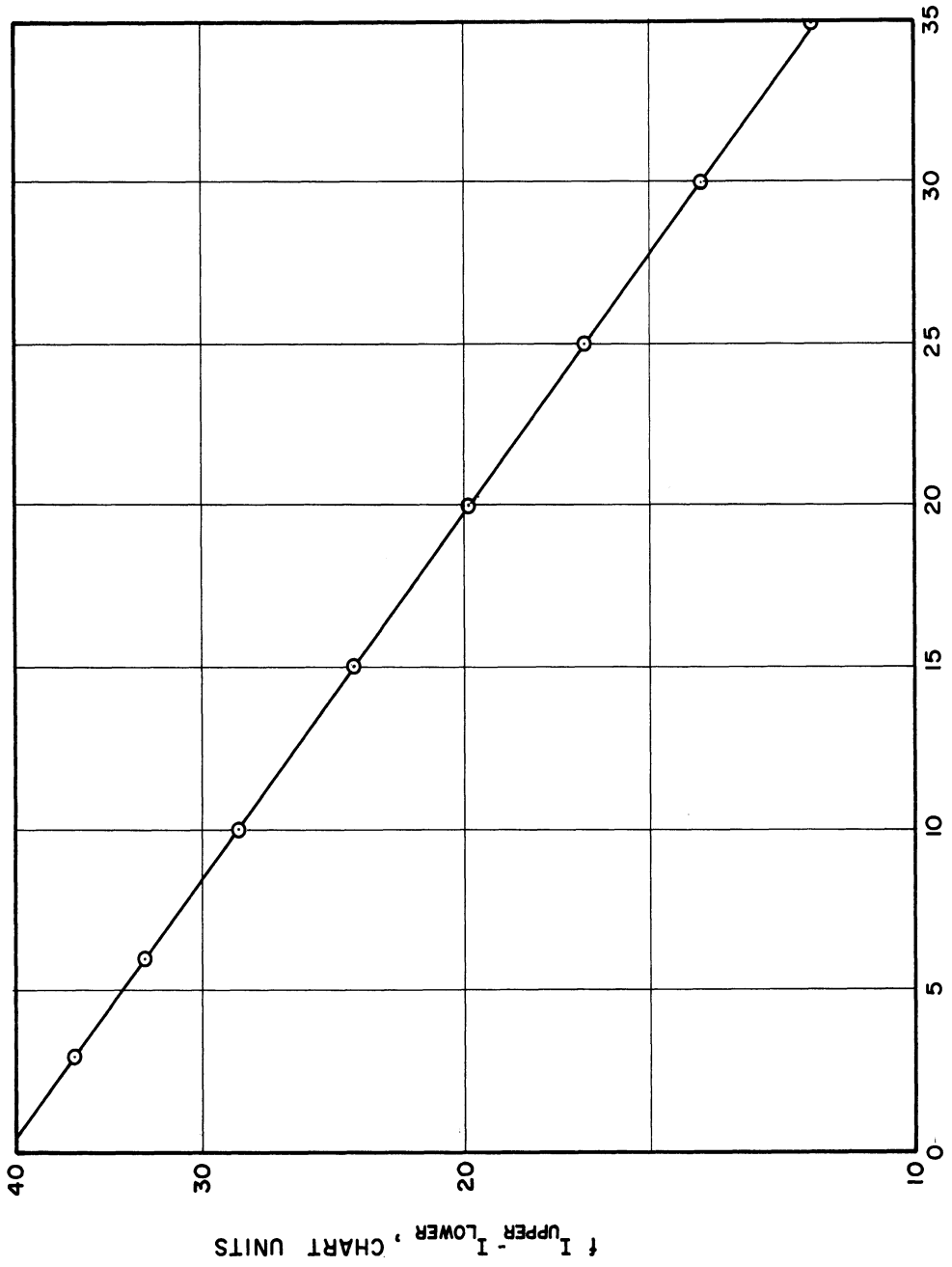

Figure 7. Semi-Log Plot of Ionization Current Difference Versus Elapsed Time for Diffusion Run 84B
HT-H_2-A at 35°C

ionization current from each cell chamber and which was probably caused by the very small conductivity of the electrode plugs. The second correction is made for the HT-H_2-CO_2 system only. Since the sample bottle storage temperature was below the critical temperature of one of the components, carbon dioxide, there was a possibility that two phases could exist in the storage cylinders. For this reason the vent gases after each run were analyzed in the Orsat-type analysis equipment. A small random variation in the hydrogen-carbon dioxide composition was noted between runs from the same storage bottle. The overall variance was at maximum about a percent and showed no definite trends as might be expected if two phases existed continually. Since the variation of composition was small, a correction was made in the calculations to base the runs on a single composition, the simple average. This correction was based on dilute gas diffusion theory, Equation (5), where:

$$D_{AB} \quad \alpha \sqrt{\frac{M_A + M_B}{M_A M_B}}, \quad D_{AC} \quad \alpha \quad \sqrt{\frac{M_A + M_C}{M_A M_C}} \qquad (17)$$

Letting A denote HT, B denote the pseudo property of the H_2-CO_2 mixture which occurred in the diffusion run, and C the pseudo property of the average composition of mixtures of runs made with the same sample bottle, then:

$$D_{AC} = D_{AB} \left[\frac{M_C (M_A + M_B)}{M_B (M_A + M_C)} \right]^{1/2} \qquad (26)$$

The corrections made by Equation (26) were never greater than half a percent of the resulting diffusion coefficient.

The Appendix A contains the following information recorded for each diffusion run made.

1. Run number.
2. Mole fraction hydrogen.
3. Chart speed.
4. Average absolute pressure.
5. Average readings of the two thermocouples embedded in the diffusion cell body.
6. Average cell temperature.
7. Compressibility factor of the diffusion mixture.
8. Ultrohmeter voltage range used for the diffusion run.
9. Values of time at which ionization currents were read from the recorder charts.
10. Ionization currents for each value of time.

    Upper chamber ionization current.

    Lower chamber ionization current.

    Zero current chart deflection.

V. EXPERIMENTAL DIFFUSION RESULTS

The diffusion coefficients calculated from the data taken as described in the previous section are presented in this section. The results are presented in three forms. The first is a complete tabulation, Tables III, IV, and V, of the diffusion coefficients determined for each run subdivided into sections of same composition and temperature. The second form of presentation is a series of four graphs, Figures 8, 9, 10 and 11, each plotting the relationship of the diffusion coefficient to the density for a system at a constant temperature. Curves have been drawn to associate the data results from each single concentration of sample. The third presentation of results is also a series of four graphs, Figures 12, 13, 14 and 15, each plotting the diffusion coefficient-density product versus the density. It can be seen from Equation (5) based on ideal gases that the diffusion coefficient is inversely proportional to the density at densities where the gas molecules behave ideally. The $D\rho$ versus ρ charts indicate at a glance the non-ideality of the particular system with respect to the density since Equation (5) would predict points along a line parallel with the abcissa.

The results from both diffusion path bundles are combined in all three presentations. This difference is indicated in each case. A minor portion of the total data was taken using the larger hole size path because it was felt that convection was more nearly eliminated by using the bundle of 0.009 inch tubes.

On each graph of $D\rho$ verses ρ at both temperatures appears a value for the diffusion of HT into hydrogen which represents the experimental atmospheric self-diffusion coefficient of hydrogen reported by Harteck and Schmidt [15]. The experimental value has been converted to the HT-H_2 system by the molecular weight correction, Equation (17), and to the experimental temperatures of the present investigation by the temperature dependence predicted in Equation (5) for dilute gases:

$$D \alpha \frac{T^{3/2}}{\Omega^{(1,1)*}} \tag{27}$$

Further comparisons of the present results to results from the literature will be made in a following section of this work.

TABLE III

DIFFUSION RESULTS, HT -H_2

Run No.	Pressure Psia	Density gm. moles/liter	Diffusivity, D $cm^2/sec \times 10^3$	$D\rho \times 10^3$
		HYDROGEN AT 35 °C		
40B	5394	11.83	4.49	53.16
32B	5244	11.57	4.48	51.83
37B	5231	11.53	4.55	52.47
38B	5174	11.43	4.70	53.73
72B	4388	9.97	5.37	53.55
36B	4076	9.38	5.59	52.46
34B	3699	8.63	5.98	51.61
31B	2866	6.90	7.71	53.19
35B	2652	6.43	8.20	52.73
29B	2469	6.04	8.58	51.82
33B	1994	4.96	10.65	52.83
87B	1671	4.20	12.56	52.80
39B	1474	3.75	14.57	54.56
30B	1057	2.732	20.14	55.01
88B	916	2.379	21.74	51.72
73B	819	2.135	24.93	53.22
		HYDROGEN AT 100 °C		
42B	5117	9.61	6.23	59.85
46B	4667	8.90	6.60	58.79
41B	3569	7.05	8.66	61.05
44B	2986	6.00	10.11	60.72
45B	2129	4.40	13.85	60.96
47B	2119	4.38	13.46	59.03
43B	1256	2.676	23.04	61.64

TABLE IV

DIFFUSION RESULTS, HT-H_2 -CO_2

Run No.	Pressure Psia	Density, ρ gm. moles/liter	Diffusivity, D $cm^2/sec \times 10^3$	$D\rho \times 10^3$
		$X_{H_2} = 0.628$ at 35°C		
14B	5074	12.84	1.966	25.24
16B	4021	10.60	2.507	26.57
4A	3543	9.46	3.11	29.40
10B	3091	8.34	3.43	28.62
11B	1912	5.24	5.56	29.11
3A	1361	3.73	7.46	27.80
12B	1124	3.07	9.54	29.32
15B	686	1.866	16.23	30.30
5A	623	1.692	17.71	29.95
		$X_{H_2} = 0.933$ at 35°C		
17B	5094	11.33	3.86	43.74
18B	4132	9.53	4.67	44.45
19B	3068	7.36	5.99	44.10
20B	1999	5.00	9.07	45.32
23B	1954	4.90	9.27	45.39
22B	884	2.305	20.01	46.11
		$X_{H_2} = 0.189$ at 35°C		
28B	4884	19.61	0.646	12.68
27B	3001	15.29	0.974	14.90
24B	2069	10.22	1.778	18.17
25B	1056	3.700	5.30	19.60
26B	513	1.544	13.36	20.63
		$X_{H_2} = 0.628$ at 100°C		
48B	4979	10.04	2.833	28.44
49B	4106	8.51	3.52	29.96
51B	2950	6.30	4.97	31.30
53B	2109	4.58	7.24	33.16
50B	1498	3.28	10.32	33.85
52B	756	1.670	20.73	34.61

TABLE IV (cont.)

Run No.	Pressure Psia	Density, ρ gm. moles/liter	Diffusivity, D $cm^2/sec \times 10^3$	$D\rho \times 10^3$
		X_{H_2} = 0.933 at 100°C		
54B	5114	9.61	5.17	49.70
59B	4122	7.99	6.51	52.00
56B	4109	7.97	6.12	48.80
55B	2554	5.22	10.15	52.92
57B	1508	3.19	16.38	52.25
60B	1024	2.200	24.11	53.06
58B	671	1.459	36.9	53.83
		X_{H_2} = 0.189 at 100°C		
61B	5063	14.06	1.246	17.52
62B	4353	12.51	1.460	18.27
63B	2834	8.15	2.637	21.48
64B	1489	3.84	5.92	22.73
65B	718	1.715	13.62	23.37

TABLE V

DIFFUSION RESULTS, HT-H_2- A

Run No.	Pressure Psia	Density, ρ gm. moles/liter	Diffusivity, D $cm^2/sec. \times 10^3$	$D\rho \times 10^3$
		X_{H_2} = 0.195 at 35°C		
74B	5051	12.51	1.682	21.04
75B	4272	10.93	1.952	21.33
78B	3300	8.71	2.440	21.25
77B	2401	6.51	3.65	23.76
79B	1472	4.01	6.07	24.33
76B	725	1.968	12.47	24.54
		X_{H_2} = 0.624 at 35°C		
81B	5204	11.92	2.695	32.12
85B	4398	10.36	3.09	31.99
1A	4074	9.72	3.45	33.50
80B	3544	8.62	3.83	32.98
86B	2775	6.93	4.85	33.55
82B	2099	5.35	6.47	34.61
83B	1253	3.27	9.99	32.74
2A	936	2.46	14.47	35.67
84B	769	2.033	17.53	35.62
		X_{H_2} = 0.926 at 35°C		
66B	5309	11.64	4.00	46.56
67B	4031	9.27	5.08	47.10
69B	3270	7.74	6.06	46.96
68B	2417	5.92	8.24	48.75
70B	1489	3.78	12.51	47.10
71B	816	2.127	22.53	47.27
		X_{H_2} = 0.195 at 100°C		
89B	5237	10.40	2.303	23.95
90B	4173	8.59	2.826	24.25
91B	3164	6.70	3.79	25.40
92B	1998	4.34	6.26	27.18
93B	1209	2.66	10.37	27.62
94B	633	1.402	20.11	28.19

TABLE V (cont.)

Run No.	Pressure Psia	Density, ρ gm. moles/liter	Diffusivity, D $cm^2/sec. \times 10^3$	$D\rho \times 10^3$
96B	5409	10.29	3.53	36.27
98B	4459	8.55	4.13	36.01
95B	3745	7.46	5.13	38.22
97B	2586	5.35	7.14	38.19
99B	1424	3.05	13.39	40.83
100B	724	1.577	25.29	39.88
		$X_{H_2} = 0.926$ at 100°C		
101B	5144	9.65	5.28	50.95
103B	4318	8.29	6.14	50.91
102B	3086	6.18	8.43	52.08
104B	2460	5.03	10.47	52.72
105B	1381	2.93	18.51	54.21
106B	815	1.762	30.4	53.63

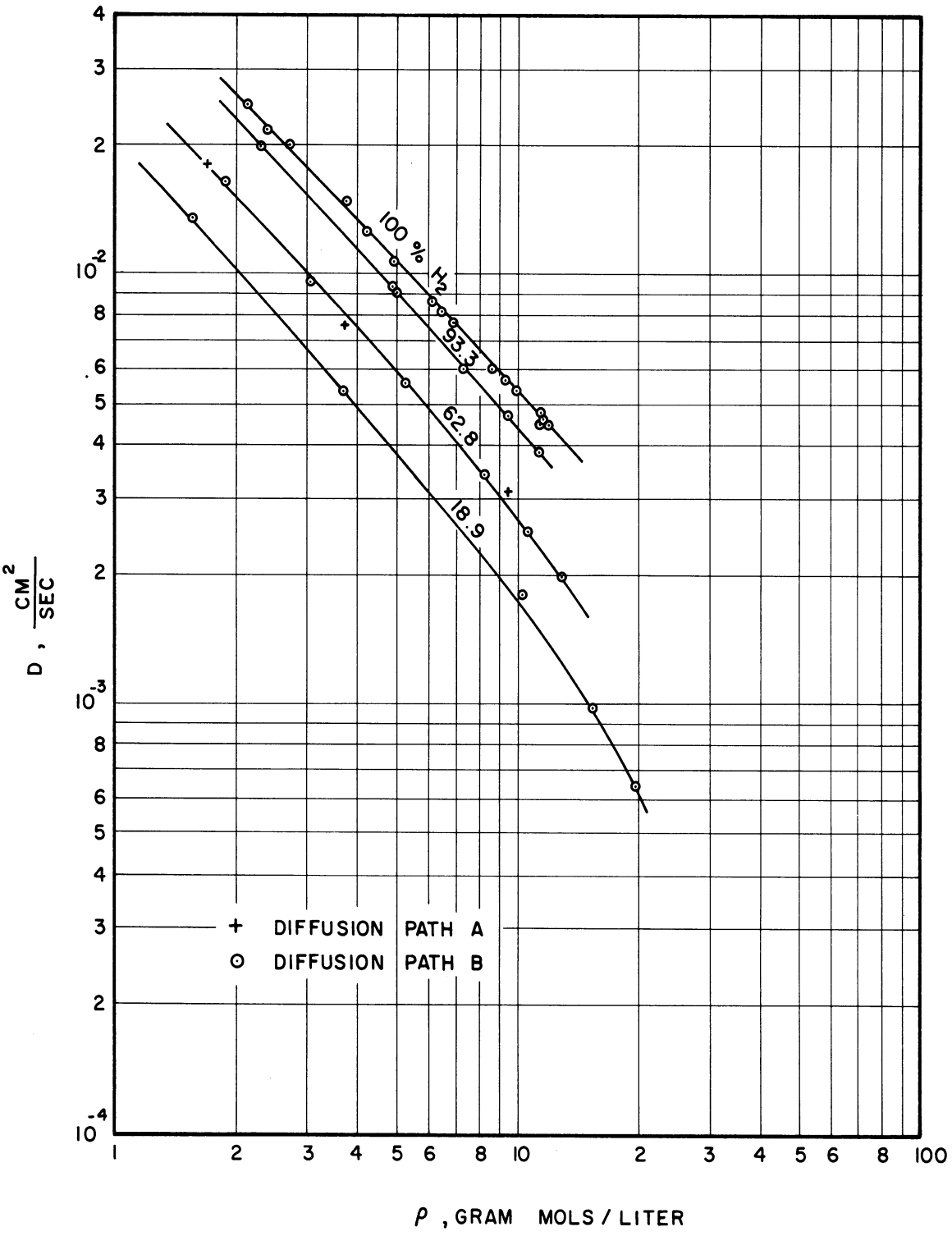

Figure 8. Diffusion Coefficient-Density Relationship for HT-H_2-CO_2 at 35°C.

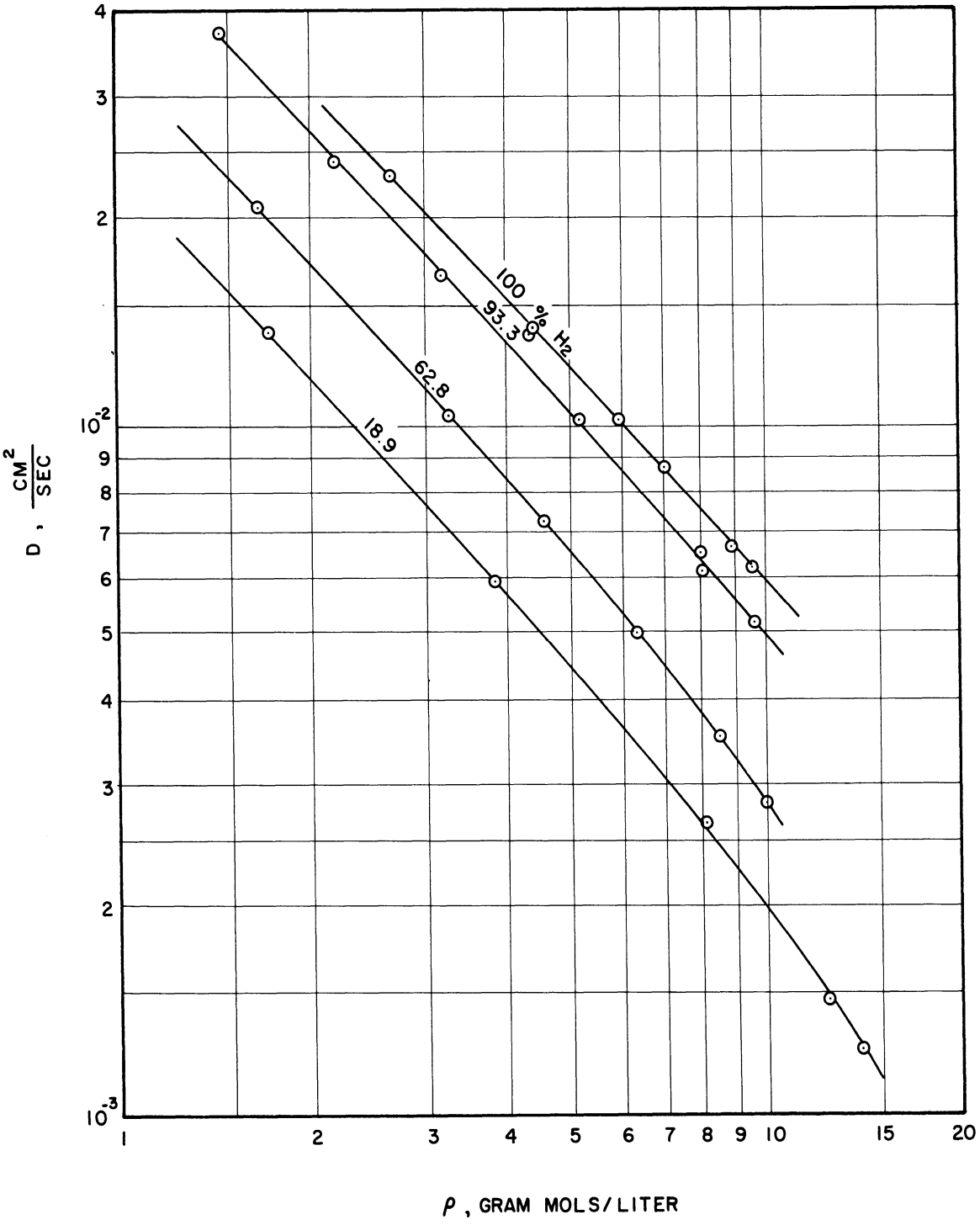

Figure 9. Diffusion Coefficient-Density Relationship for HT-H_2-CO_2 at 100°C.

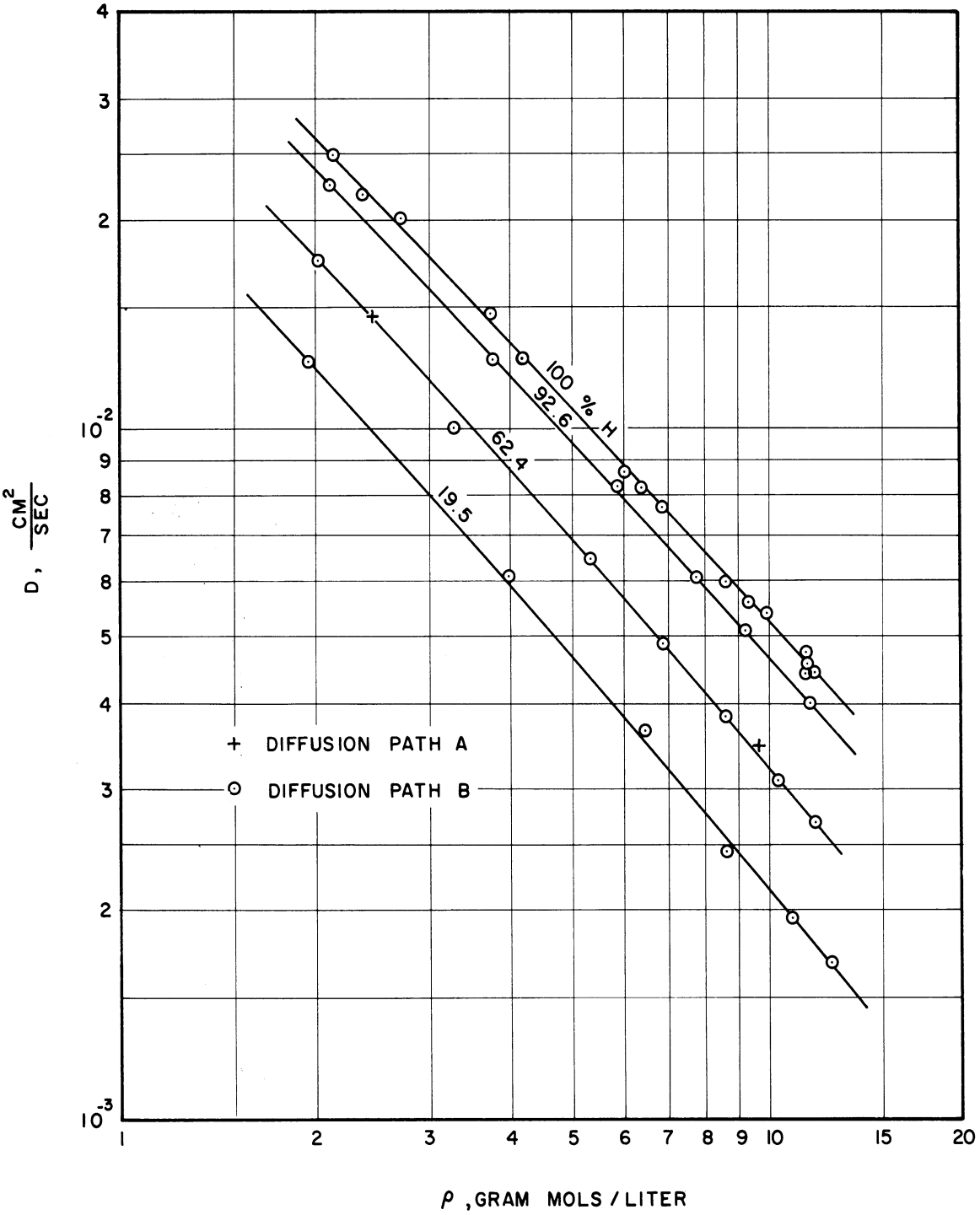

Figure 10. Diffusion Coefficient-Density Relationship for HT-H_2-A at 35°C.

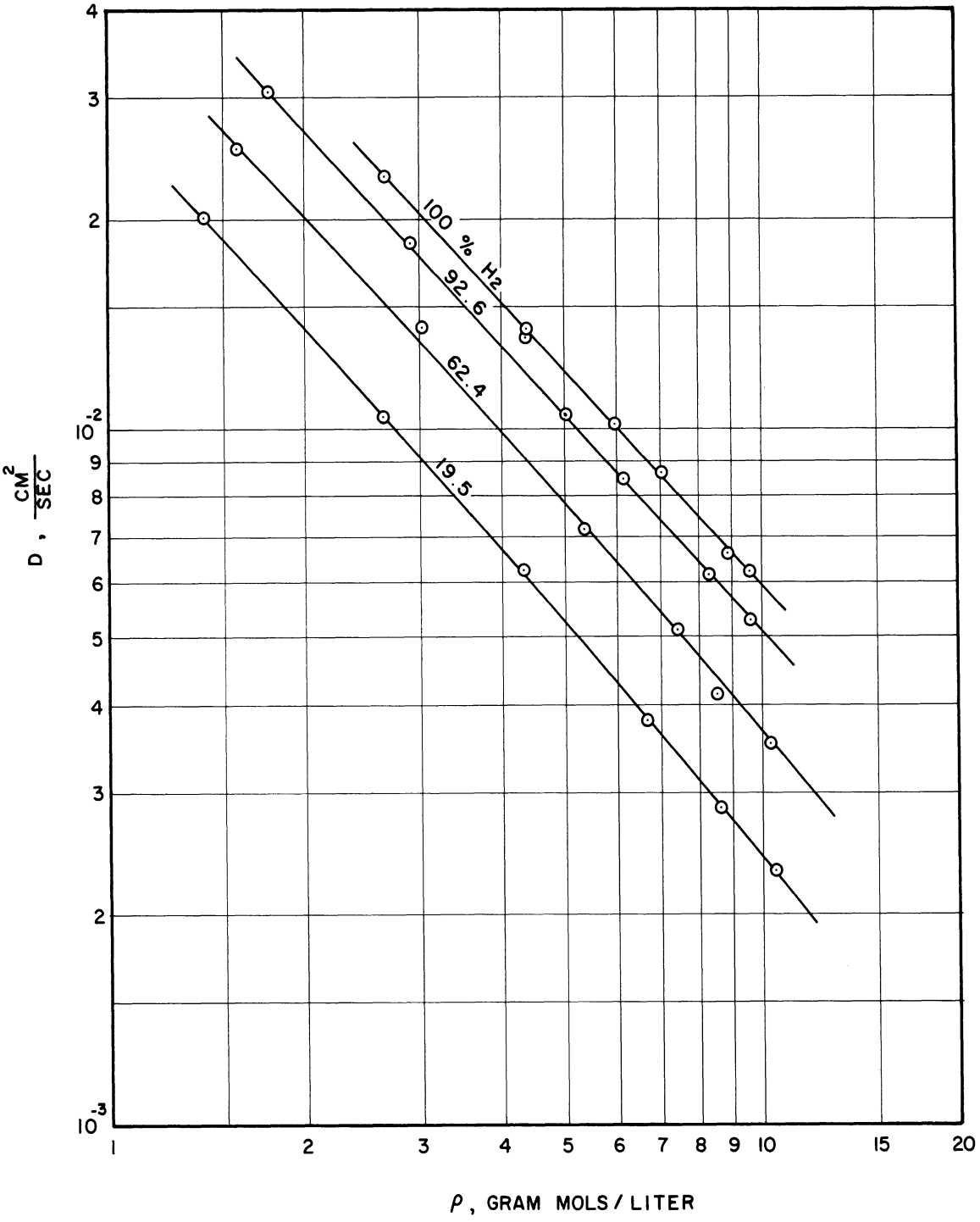

Figure 11. Diffusion Coefficient-Density Relationship for HT-H_2-A at 100°C.

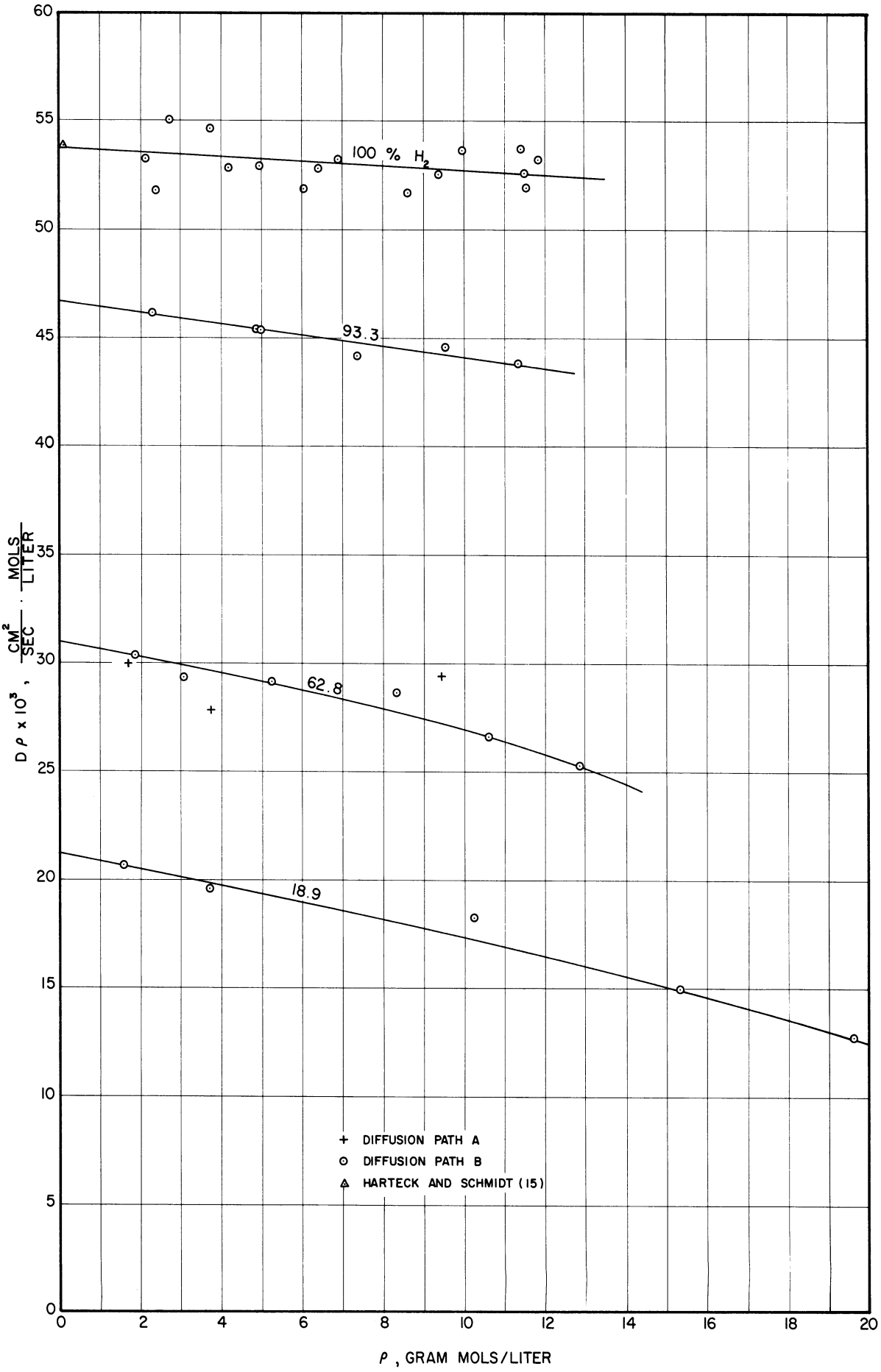

Figure 12. Diffusivity-Density Product as a Function of Density for HT-H_2-CO_2 at 35°C.

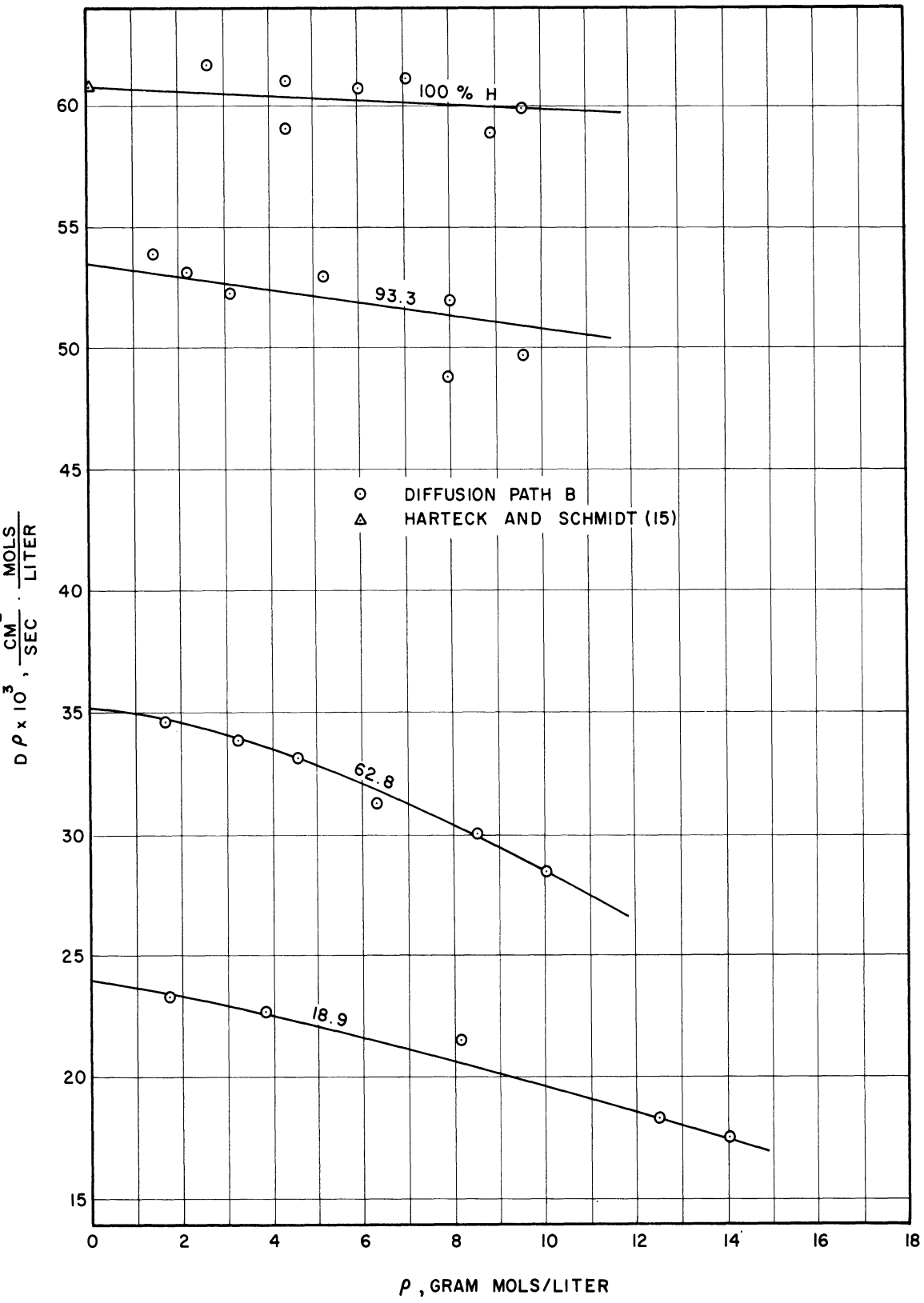

Figure 13. Diffusivity-Density Product as a Function of Density for HT-H_2-CO_2 at 100°C.

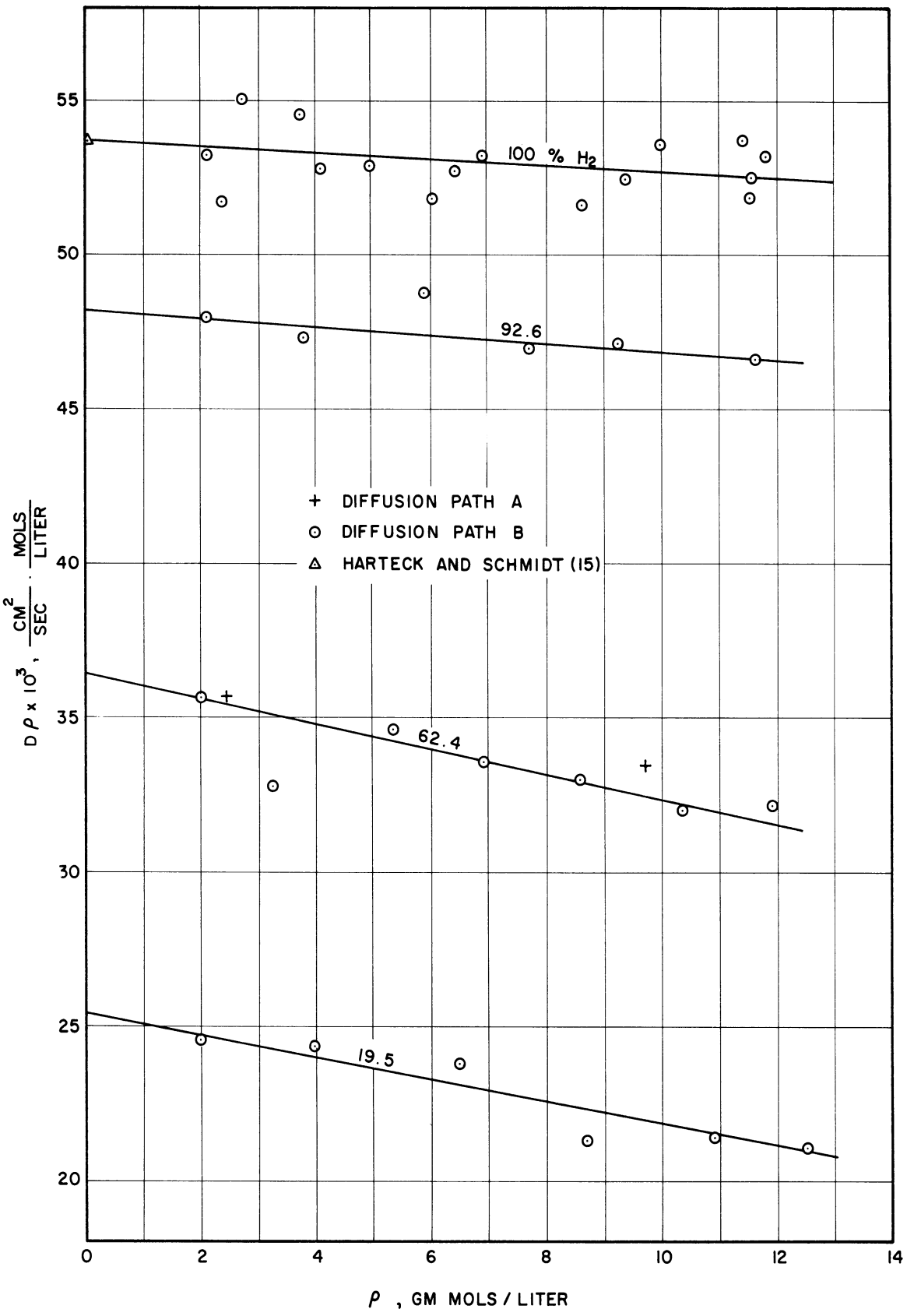

Figure 14. Diffusivity-Density Product as a Function of Density for HT-H_2-A at 35°C.

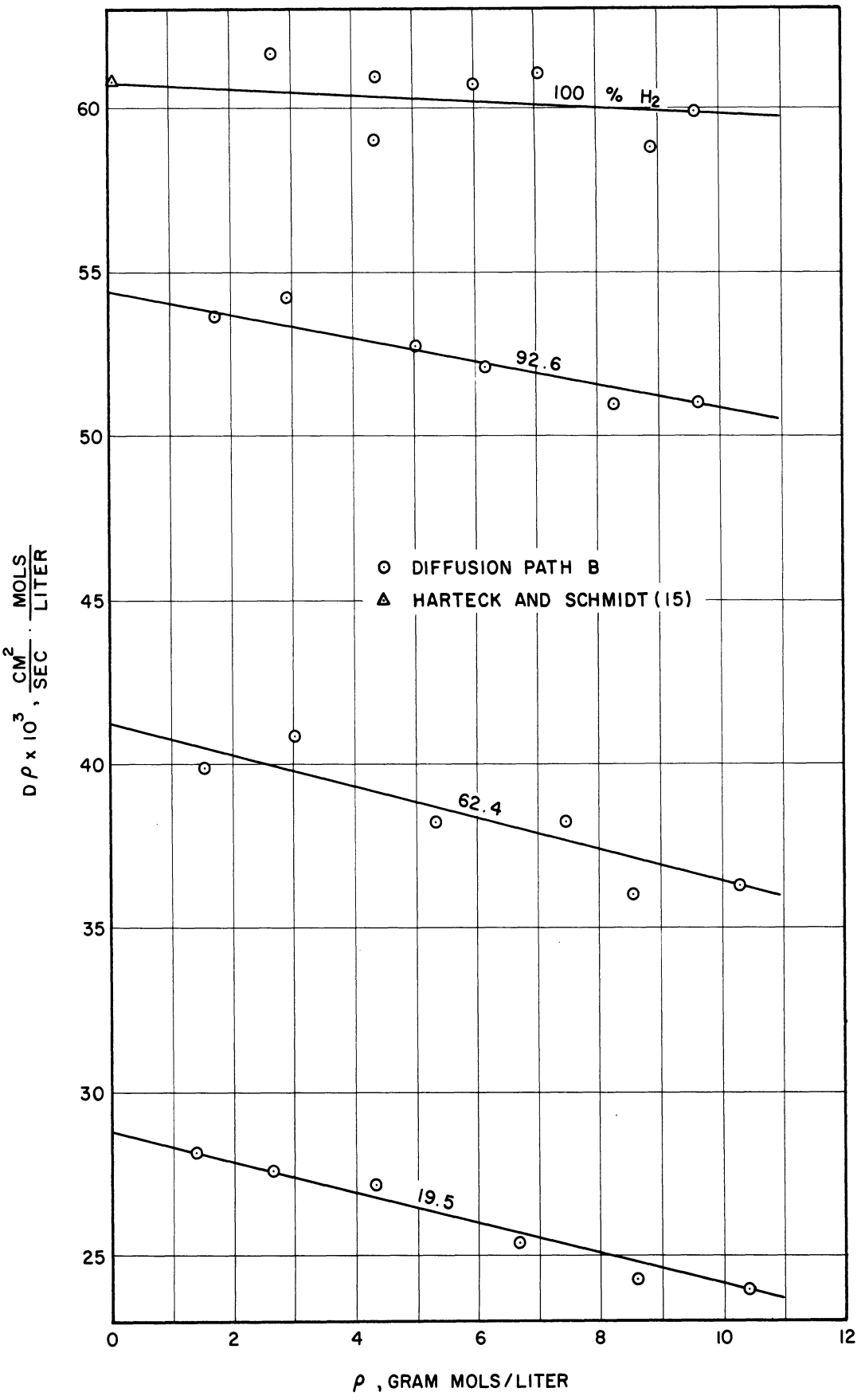

Figure 15. Diffusivity-Density Product as a Function of Density for HT-H_2-A at 100°C.

VI. COMPARISON OF RESULTS TO RELATED WORK

An attempt is made in this section of the dissertation to compare the experimental results presented in the previous section to experimental and theoretical works found in the literature which are related to the present work. Since little or no data is reported for the same systems as were studied here, extrapolations and conversions to similar reported systems were made using theoretical expressions which are available. In the first part, related low density binary and hydrogen self-diffusion coefficients were derived by extrapolation of the present data and compared to the reported atmospheric density coefficients for the same systems. The second part involves comparison of the present data with the accepted methods of predicting dense gas diffusion coefficients by theoretical or empirical means. Since the dense gas diffusion data of Chou [9,10] includes the system, $C^{14}O_2$-H_2-CO_2, which is very similar to the HT-H_2-CO_2 system reported here, special comparison is made between these results.

COMPARISON TO ATMOSPHERIC BINARY AND H_2 SELF-DIFFUSION COEFFICIENTS

In order to make a low density comparison of the present data with values from the literature, the trends of the dense gas diffusion results as plotted as the diffusivity-density product in Figures 12 through 15, were extrapolated back to zero density. By this means the low density product, $(D\,\rho)_o$, was evaluated for each system at each temperature for each composition of the major components. These extrapolated results are presented in the first part of Table VI.

TABLE VI

DIFFUSIVITY-DENSITY PRODUCT EXTRAPOLATED TO ZERO DENSITY WITH TEMPERATURE DEPENDENCE NOTED

Mole Fraction Hydrogen	$(D\rho)_o$ 35°C x 10^3	$(D\rho)_o$ 100°C x 10^3	Exponent of Absolute Temperature $D_{12} \alpha T^n$	Predicted Temperature Dependence of Equation (5)
HT-H_2			n	n
1.000	53.8	60.7	0.63	0.64
HT-H_2-A				
0.195	25.4	28.8	0.66	0.70
0.624	36.4	41.2	0.65	0.70
0.926	48.2	54.4	0.63	0.70
HT-H_2-CO_2				
0.189	21.2	24.0	0.64	0.72
0.628	31.0	35.2	0.66	0.72
0.933	46.7	53.4	0.70	0.72
$C^{14}O_2$-H_2-CO_2	(Chou data)		1.27	0.72

The remainder of Table VI indicates the temperature dependence of these extrapolated values and shows comparison between these values and the dependence predicted by the Lennard-Jones potential dilute gas theory, Equation (5). The classical form of temperature dependence is that the diffusion coefficient is proportional to the absolute temperature raised to a constant power, $D_{12} \alpha T^n$. Classical theory also predicts that the exponent, n, is 1 1/2. Since at constant low pressure the density is inversely proportional to temperature, this temperature exponent appears as 1/2 in expressions where the coefficient of diffusion is equated to a function involving temperature and density. Although the classical theory temperature dependence has been shown to not be valid over a wide temperature range, the form has been retained and experiments

reported in the International Critical Tables [18] indicate values between 0.5 and 1.00 for the constant exponent of temperature over moderate ranges of the temperature. Over the range of temperature covered in the present investigation, an exponent of 2/3 describes the temperature effect noted for the binary system, HT-H_2, and both ternary systems, HT-H_2-CO_2 and HT-H_2-A within seven tenths of a percent. The Lennard-Jones potential predicts an effective constant exponent of the absolute temperature of 0.64 for the HT-H_2 system, 0.72 for the HT-H_2-CO_2 system and 0.70 for the HT-H_2-A system. Chou [9] found that an exponent of 1.27 best described his data in the $C^{14}O_2$-H_2-CO_2 system. For the binary system of $C^{14}O_2$-CO_2 O'Hern's [30] experimental diffusion coefficients extrapolated to zero density by means of a diffusivity-density plot at 35°C and 100°C are proportional to the absolute temperature raised to the 0.95 power.

The low density product, $(D\ \rho)_o$, can be predicted accurately for any concentration of either experimental ternary system with respect to the major components, H_2-CO_2 or H_2-A, in the vicinity of the experimental temperatures, 35°C and 100°C, by Equation (28). This semi-emperical equation is based on the form of the Wilke equation, Equation (7), and relates $(D\ \rho)_o$ to the absolute temperature, T, and the mol fraction of hydrogen, y_{H_2}.

$$(D\ \rho)_o = \frac{a\ (T)^{2/3} * 10^{-3}}{1 - (1-0.853a)\ y_{H_2}} \qquad (28)$$

Where:

$(D\rho)_o$ is in $\frac{cm^2}{sec} \cdot \frac{gram\ mols}{liter}$

T is the absolute temperature in °K.

$a = 15.9/(\sigma_{12})^3$, σ_{12} is the Lennard-Jones "collision diameter" between the two major components, in Angstroms.

Values for the low density diffusivity-density product for HT-H_2 can be predicted as a trivial case of either ternary system. The fourteen values of $(D\rho)_o$ presented in Table VI for various experimental concentrations and temperatures of the investigated systems are predicted by Equation (28) with an average deviation of less than one percent.

Chou used a procedure for comparison of diffusion coefficients in a ternary mixture to binary and self-diffusion coefficients from the literature. Since such a comparison is desirable for the present work, a similar procedure will be used here. The systems of study, HT-H_2-CO_2 and HT-H_2-A, involve three binary mixtures of interest, HT-CO_2, HT-A, and HT-H_2. The diffusion coefficients of the last of these, HT-H_2, have been experimentally determined in this work. The Wilke [47] equation, Equation (7), is the basis of the extrapolation made to give values of the diffusivities for the remaining two binary systems of interest, HT-CO_2 and HT-A. As previously stated, this equation relates the diffusion coefficient of one component in a multicomponent mixture to the individual binary diffusion coefficients of the component with each of the remaining components separately. At constant density, ρ, for a

ternary mixture of components 1, 2, and 3 in which the mole fraction of component 1 is negligible, Equation (7) can be written:

$$\frac{1}{D_1 \rho} = y_2 \left(\frac{1}{D_{12} \rho} - \frac{1}{D_{13} \rho} \right) + \frac{1}{D_{13} \rho} \qquad (29)$$

This form of the equation indicates a linearity between the reciprocal diffusivity-density product of the trace component in a ternary mixture and the mole fraction of one of the other components. The values of this reciprocal at $y_2 = 0$ or $y_2 = 1$ are respectively the reciprocals of the products involving the two binary coefficients of diffusion.

Figures 16 and 17 are plots of the zero density reciprocal diffusivity-density products versus mole fraction of hydrogen for the two ternary systems studied. Although the four points for each isotherm do not fall exactly along a straight line, that form of representation is satisfactory within the experimental accuracy. Values for the diffusivity-density products of the related binary mixtures, HT-CO_2 and HT-A, were evaluated from these figures by extrapolation to the ordinate where the mole fraction of hydrogen is zero. This value of the product at $y_{H_2} = 0$ represents the diffusion coefficient at the particular temperature for dilute gas diffusion occuring as predicted by the dilute gas diffusion equation, Equation (5). Values for the coefficient of diffusion evaluated at one atmosphere from these extrapolated product values are presented in Table VII together with values obtained from the literature.

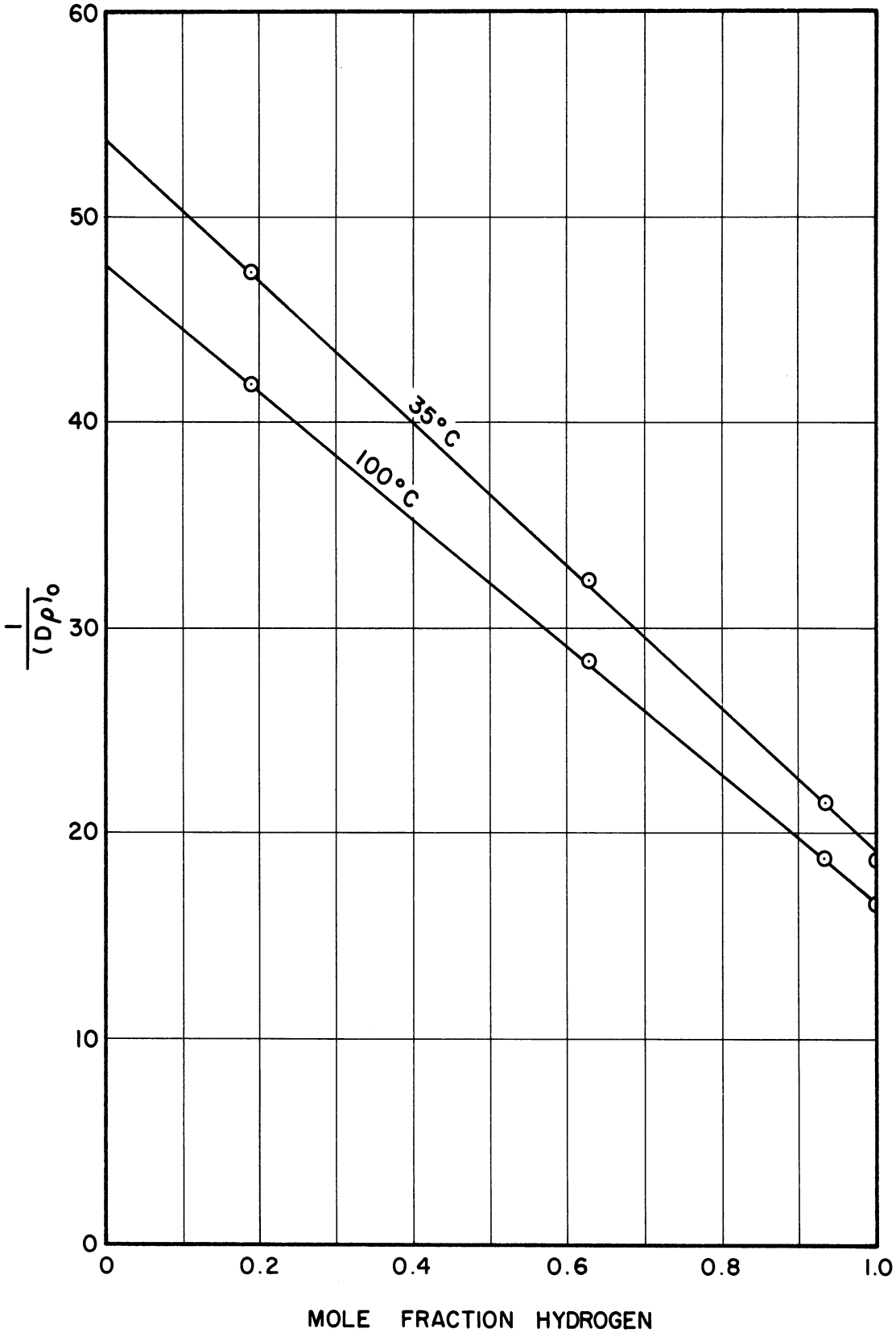

Figure 16. Reciprocal Diffusivity-Density Product for HT-H_2-CO_2 as a Function of Mol Fraction of Hydrogen.

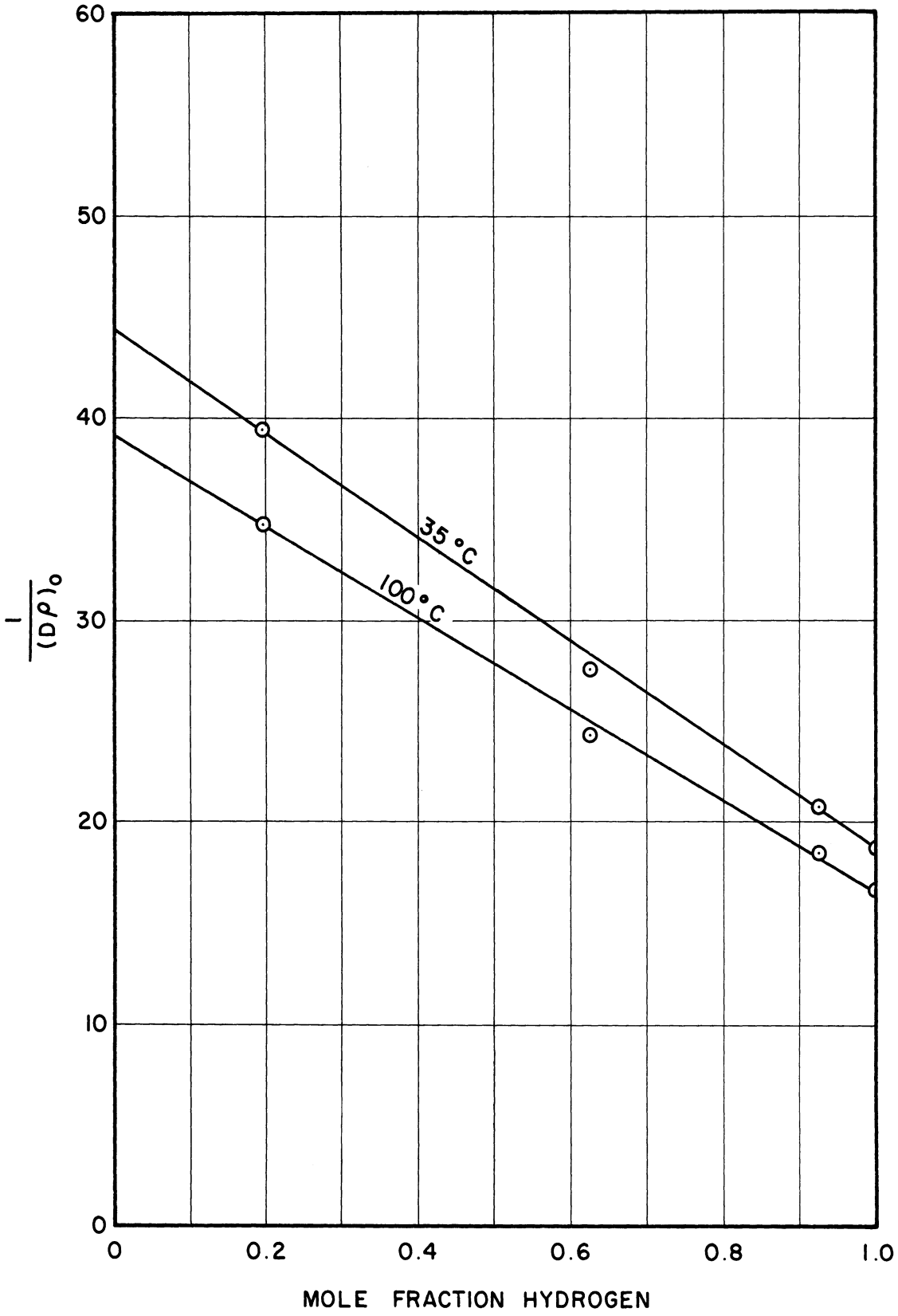

Figure 17. Reciprocal Diffusivity-Density Product for HT-H_2-A as a Function of Mol Fraction of Hydrogen.

TABLE VII

COMPARISON OF EXTRAPOLATED RESULTS TO DIFFUSION COEFFICIENTS, cm^2/sec FROM THE LITERATURE AT ONE ATMOSPHERE

	D_{HT-H_2}		D_{HT-CO_2}		D_{HT-A}	
	35°C	100°C	35°C	100°C	35°C	100°C
This Investigation	1.36	1.86	0.47	0.64	0.57	0.78
Harteck and Schmidt	1.362	1.862				
Heath, Ibbs, and Wild	1.39	1.90				
Waldmann	1.32	1.80	0.48	0.66	0.61	0.84
Groth and Harteck	1.389	1.899			0.615	0.852
Boardman and Wild			0.505	0.700	0.61	0.84
Boyd, Stein, Steingrimsson, Rumpel			0.495	0.688		
Schafer, Corte and Moesta			0.52	0.72		
Roth			0.485	0.675		
Lonius			0.492	0.682		
Chou			0.490	0.754		
Equation (5)	1.357		0.507		0.607	

The literature coefficients have been converted to the experimental temperatures by the dilute gas theoretical temperature dependence of Equation (5) which for constant pressure is:

$$D \alpha \frac{T^{3/2}}{\Omega^{(1,1)*}} \qquad (27)$$

Since some of the diffusivities reported in the literature regarded diffusion in mixtures containing ordinary hydrogen, a conversion was also necessary to account for the difference in molecular weight between tritiated hydrogen and ordinary diatomic hydrogen. This conversion was made according to the molecular weight dependence predicted

by dilute gas diffusion theory which is:

$$D_{12} \alpha \left[\frac{M_1 + M_2}{M_1 M_2}\right]^{1/2} \quad (17)$$

For the transposition of the coefficient of diffusion of a binary mixture to that of another binary mixture which differs from the first only in that one component of the second binary is another isotope of one of the original components, this expression can be expanded to:

$$D_{12} = D_{13} \left[\frac{M_2}{M_3} \cdot \frac{M_1 + M_3}{M_1 + M_2}\right]^{1/2} \quad (26)$$

Since the molecular weight difference between isotopes is normally small, inaccuracies which may be caused by this conversion are small.

The points attributed to Chou were transposed from values reported at 35°C and 100°C for the binary system of $C^{14}O_2$-H_2. These points were derived from the $C^{14}O_2$-H_2-CO_2 ternary system by the Wilke equation extrapolation used in the present work. The isotope conversion equation, Equation (18), was used to transpose the diffusivity for both members of the Chou binary system since the desired comparison was between data for the HT-CO_2 system. The Chou value of the diffusion coefficient at 35°C agrees well with the value derived in this investigation. However, at 100°C the values are considerably different. This fact was noted in the previous discussion concerning temperature dependence which indicates that the data from the present

investigation agree with the dilute gas theoretical predictions with respect to temperature effect better than do the data of Chou.

Comparison of the results, excepting those of Chou, shows the values of the diffusion coefficients derived from the present investigation for the binary systems, HT-H_2, HT-CO_2, and HT-A, to be respectively 0.4, 5.2, and 6.9 percent below the average of the converted values from the literature at 35°C. At 100°C the respective values are 0.3, 6.8, and 7.6 percent below the literature values. It must be pointed out that this extrapolation is at best an approximation and should only be regarded as a rough check of results.

DENSE GAS COMPARISONS.

The theoretical treatment of Enskog and Chapman which was outlined in the theoretical section of this dissertation is the only non-empirical reference of comparison of the dense gas diffusion data presented here. As was stated,this theory was developed for the solid spherical molecular model and allows for the size of individual molecules to be appreciable with respect to the distance between molecules. Calculations for the systems of this study have been made assuming the ternary systems to be binary systems composed of the two major components in each, H_2-CO_2 and H_2-A. This approximation is satisfactory since the theory is chiefly based on volumetric or state considerations and the ternary mixtures investigated here were binary mixtures from this viewpoint; the molecular fraction of HT in each case was negligible, about 5×10^{-7}. The results of this comparison are presented in Figures 18,

19, 20, and 21 for the HT-H_2-CO_2 and the HT-H_2-A systems at 35°C and 100°C respectively. At a given density, ρ, Equation (8) can be re-written as:

$$D\rho = \frac{(D\rho)_o}{Y} \tag{30}$$

where $(D\rho)_o$ is the dilute gas prediction at that density. This dilute gas product is constant with respect to density since according to dilute gas theory the diffusivity is inversely proportional to density. The theoretical curves on each graph for HT-H_2 are calculated using the extrapolation, $(D\rho)_o$, as the dilute gas prediction and calculating the correction factor, Y, by the Enskog relation, Equation (10), for a single component gas. The theoretical curves for mixtures of H_2-CO_2 and H_2-A were calculated by the Thorne relation, Equation (11), for binary gas mixtures using the $(D\rho)_o$'s extrapolated from the data.

It will be noted that the theoretical predictions based on the solid spherical model diverge below the experimental data in each case. It appears that the theoretical curves calculated by the Thorne expansion approach the data at the higher densities. This is due to the fact that unavailable further terms of the Thorne expansion are becoming important at the higher densities. The Enskog expansion for single component systems includes a sufficient number of terms so that further terms are neglibible within the experimental density range. It is clear that theoretical predictions based on the solid spherical molecular model are inadequate for the prediction of diffusion at high densities for the systems studied.

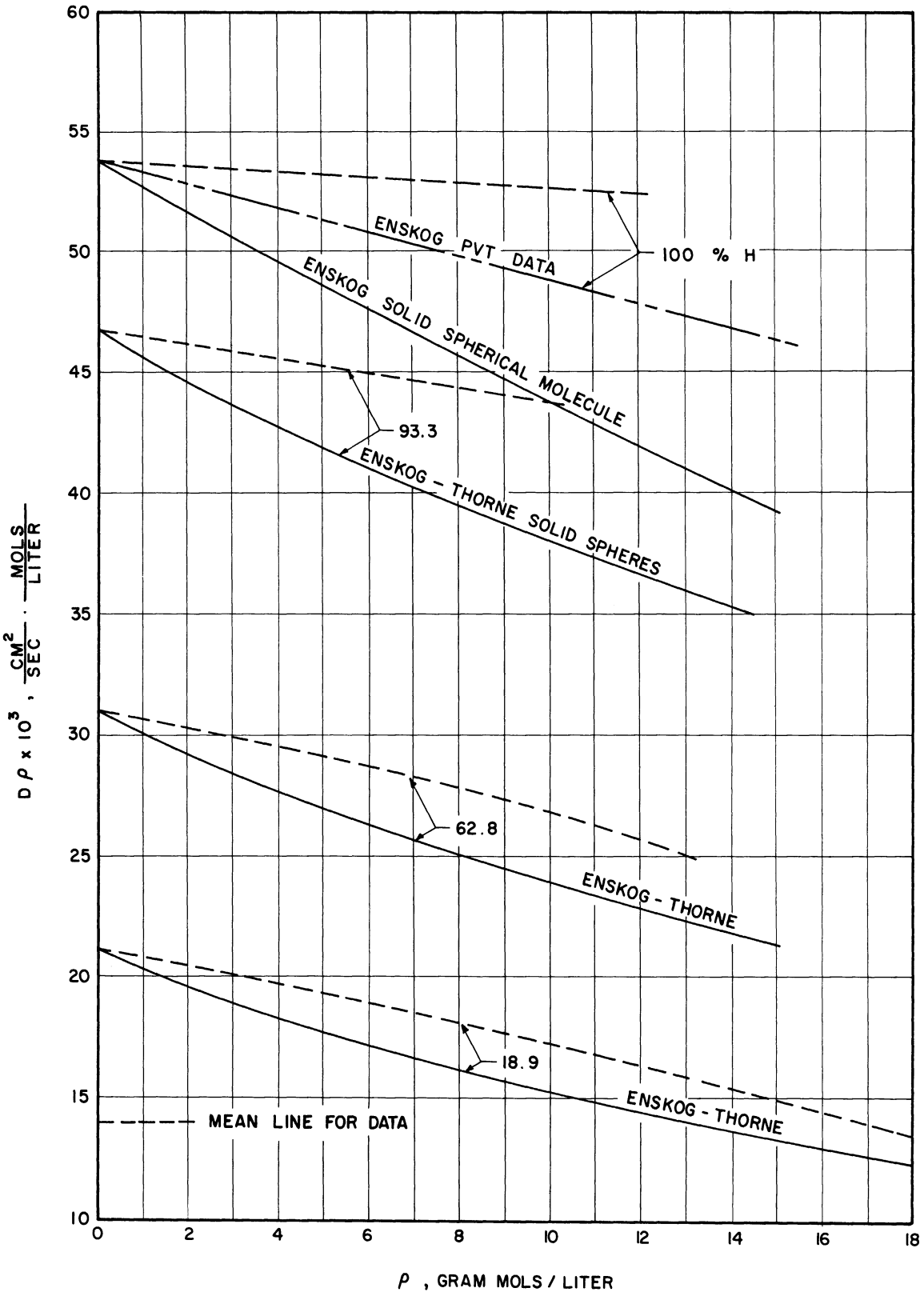

Figure 18. Enskog Theoretical Predictions Compared to Experimental Results for HT-H_2-CO_2 at 35°C.

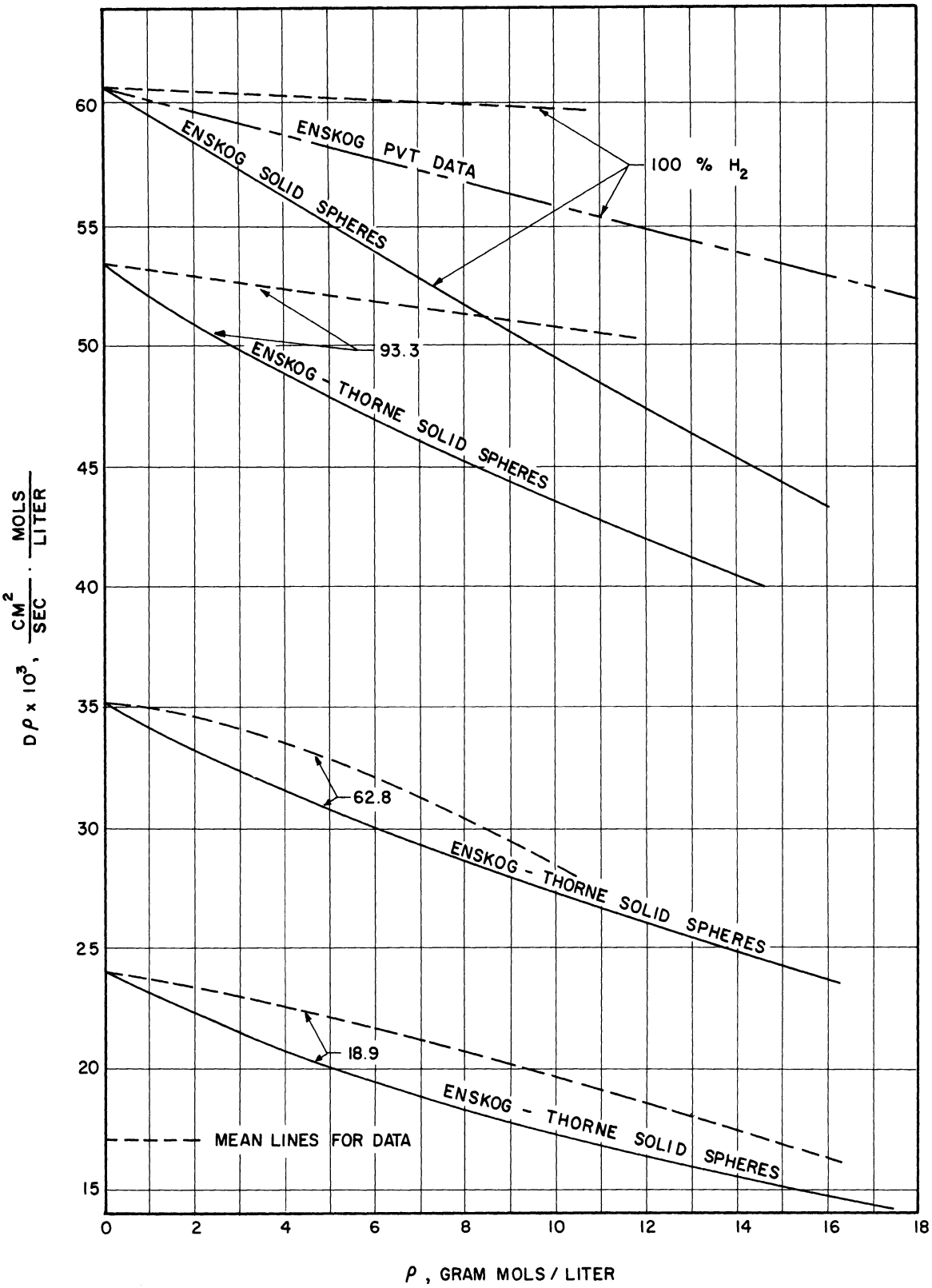

Figure 19. Enskog Theoretical Predictions Compared to Experimental Results for HT-H_2-CO_2 at 100°C.

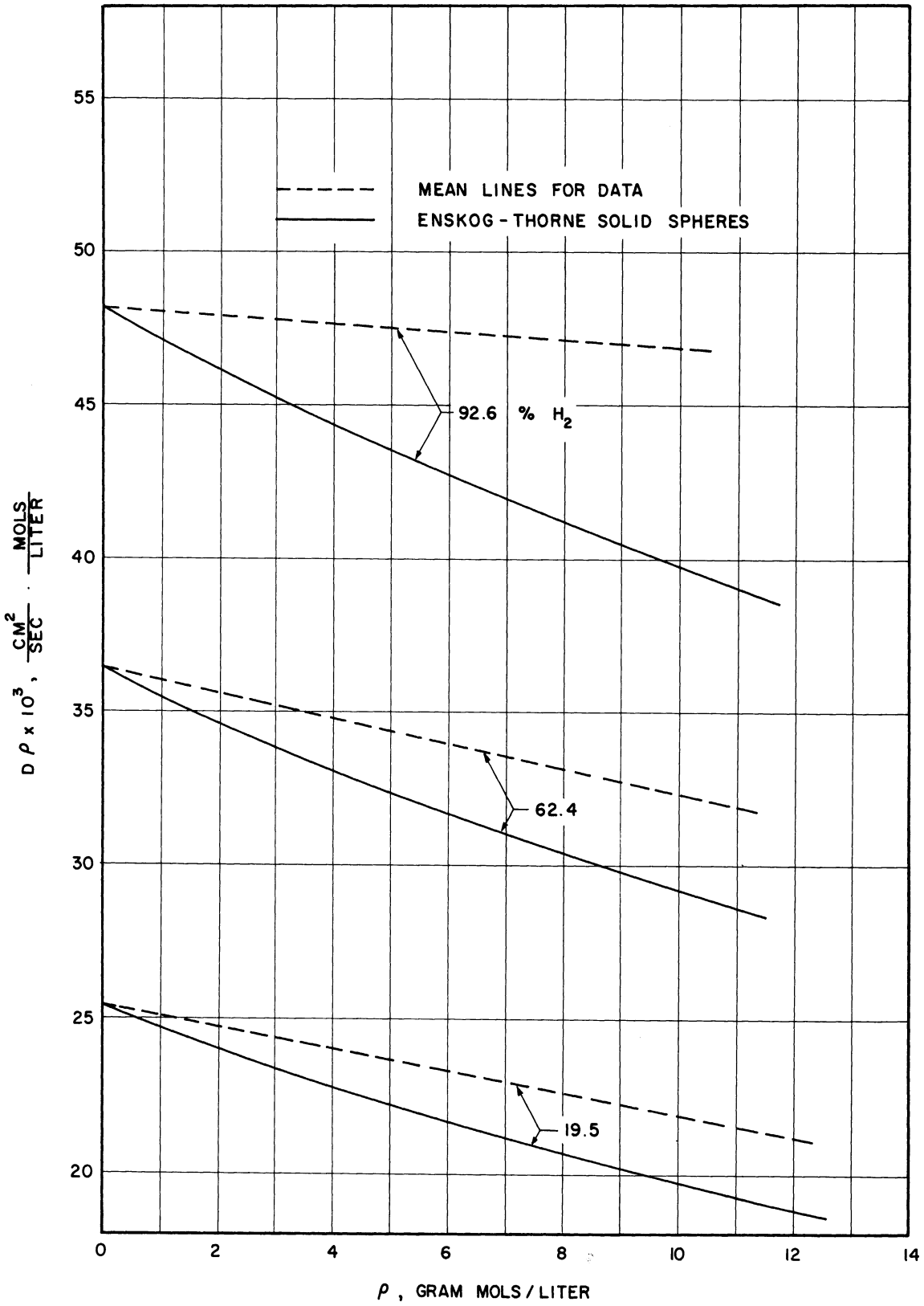

Figure 20. Enskog Theoretical Predictions Compared to Experimental Results for HT-H_2-A at 35°C

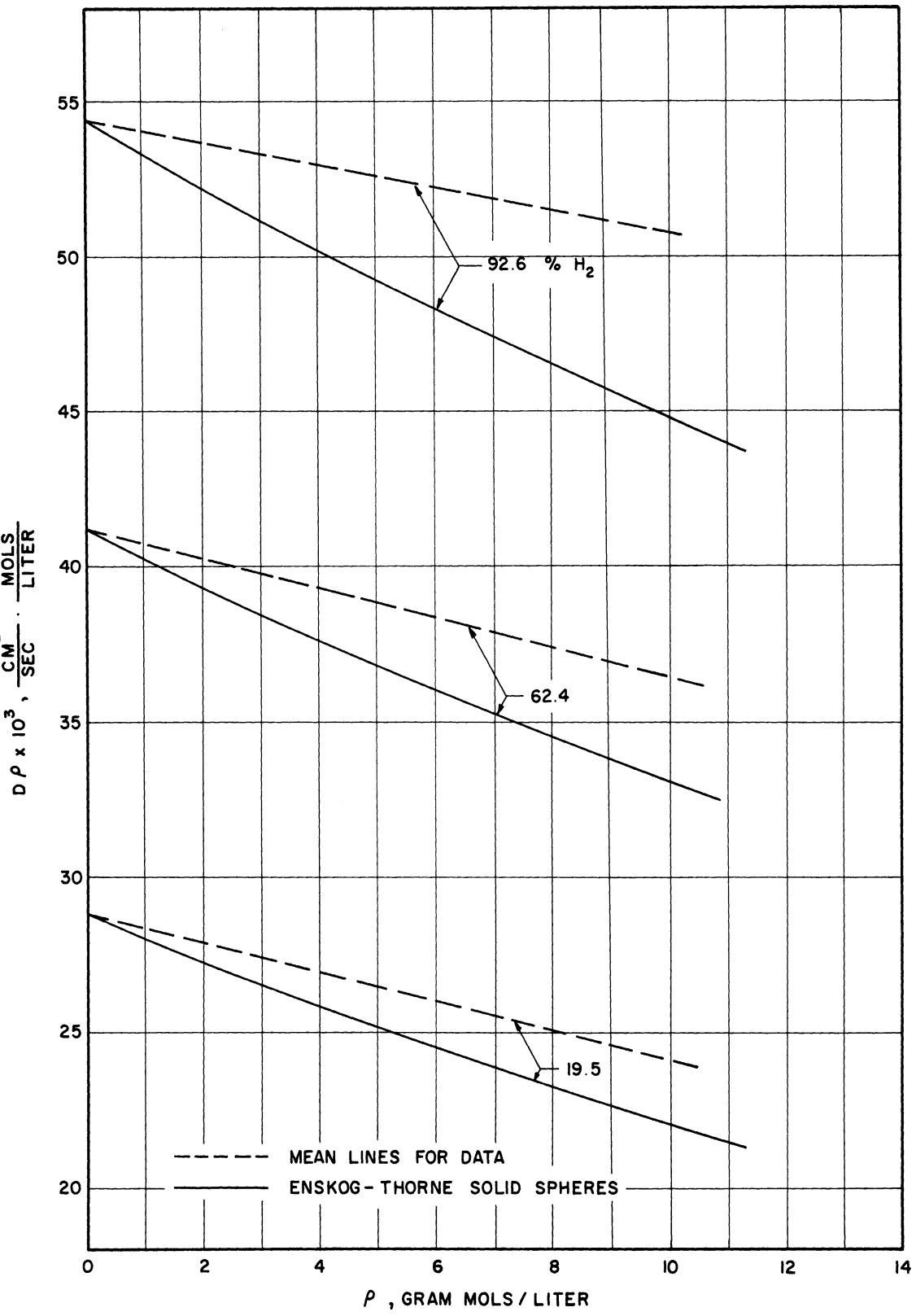

Figure 21. Enskog Theoretical Predictions Compared to Experimental Results for HT-H_2-A at 100°C.

Enskog realized that although the solid spherical model made the mathematical solution to dense gas transport property predictions possible, that that model would not be representative of real gas molecules. He suggested, then, that the "thermal pressure" of the gas species, determined from experimental data at the desired conditions, be substituted into the derived equations in place of the pressure evaluated according to the equation of state for solid spheres. This "thermal pressure" and its substitution into the Enskog theory has been treated in the theoretical portion of this paper.

Since experimental state data can be represented by a compressibility factor, $Z(T,\underline{V})$, in the equation of state:

$$P\underline{V} = Z_{(T,\underline{V})}\, RT \tag{31}$$

Then the partial derivative of pressure, P, with respect to temperature, T, at constant specific volume, $\underline{V}$, can be evaluated:

$$\left(\frac{\partial P}{\partial T}\right)_{\underline{V}} = \frac{R}{\underline{V}}\left[Z_{(T,\underline{V})} + T\left(\frac{\partial Z_{(T,\underline{V})}}{\partial T}\right)_{\underline{V}}\right] \tag{32}$$

Substituting this expression into Equations (13) and (9) and making cancellations where possible, the resulting expression for the Enskog density correction factor, Y, to the diffusion coefficient is:

$$Y = \frac{\underline{V}}{b_o}\left[Z_{(T,\underline{V})} + T\left(\frac{\partial Z_{(T,\underline{V})}}{\partial T}\right)_{\underline{V}} - 1\right] \tag{33}$$

where:

$$b_o = B(T) + \frac{T dB(T)}{dT} \qquad (14)$$

If accurate data for the second virial coefficient, B(T), and the compressibility, Z, are known, a more realistic prediction for the diffusion coefficient can be made.

Using the excellent synopsis of data for hydrogen prepared by the National Bureau of Standards [48], this method of computation of the dense gas diffusion coefficient was carried out for hydrogen for the experimental range investigated. The results of this calculation are presented in Figures 18 and 19 together with the predictions based on the solid spherical molecular model. It is to be noted that this method better predicts the data of this investigation than does the method based on the rigid sphere model.

The theory of corresponding states has been used by Slattery[41] to prepare charts for predicting dense gas coefficients of diffusion. Figure 22 is a reproduction of the corresponding states chart with the results of this investigation for the HT-H_2-CO_2 system superimposed upon it. A similar chart can be found in reference [37] upon which the bulk of dense gas diffusion data is superimposed. The apparent agreement noted at higher densities is to a large part due to the fact that the chart as presented differs from a compressibility factor chart only by the factor of $D/(D)_o$ which is never very far from unity within the range of the chart.

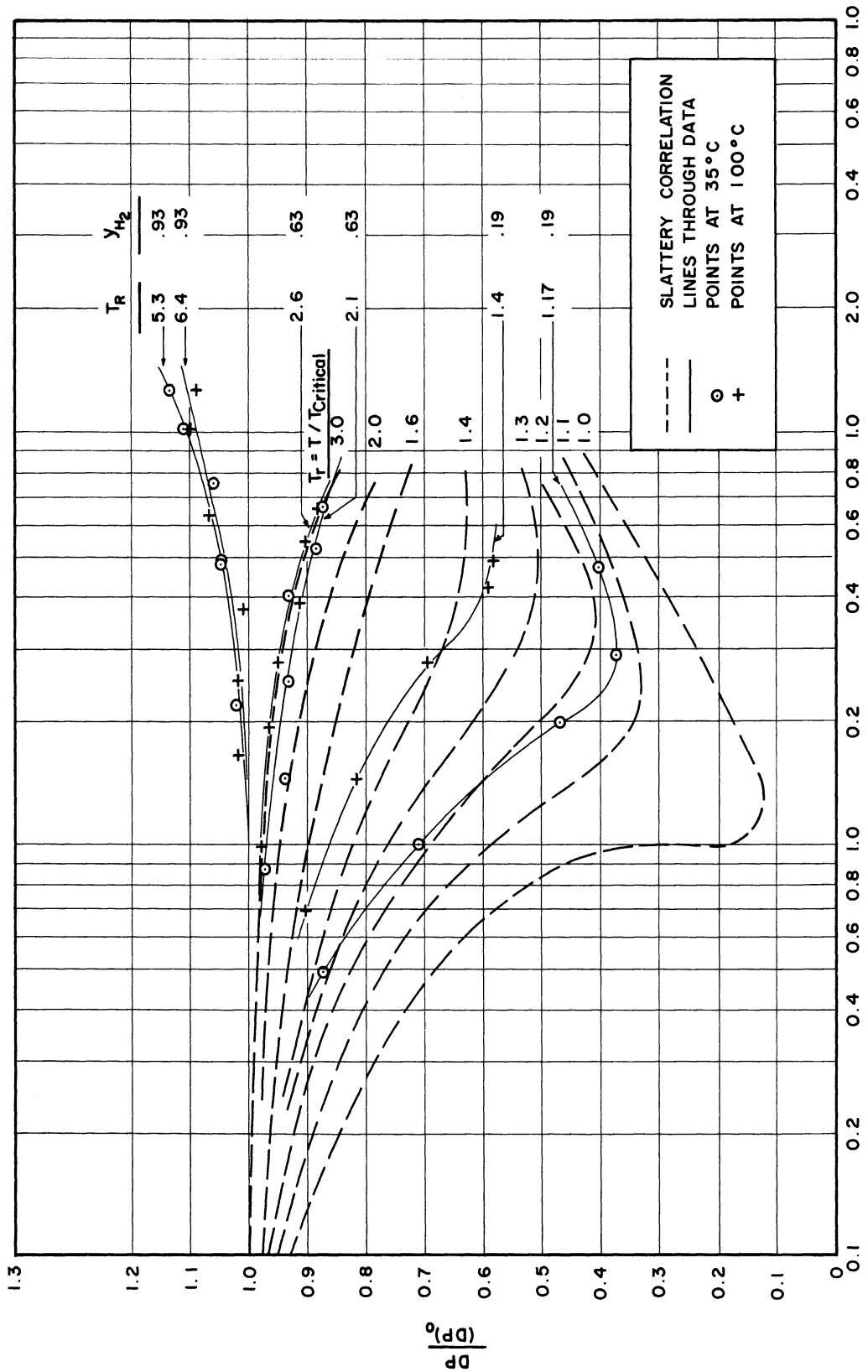

Figure 22. Experimental Results for HT-H_2-CO_2 Superimposed Upon the Slattery[41] Corresponding States Correlation.

The only quantitative comparison with dense gas diffusion data which will be made here involves a ternary system which very closely resembles the HT-H_2-CO_2 system of this investigation, the diffusion data reported by Chou [10] with the $C^{14}O_2$-H_2-CO_2 system. Chou fitted his data empirically to an equation the form of which was based on the Wilke equation for predicting multicomponent diffusion coefficients. Since the Chou data diffusion coefficient-density product did not vary appreciably with density, the empirical equation contains the inverse proportionality of diffusivity to density predicted by dilute gas theory.

$$D_{C^{14}O_2} = \frac{3.2 \times 10^{-6} T^{1.27}}{\rho\,(1-0.82\, y'_H)} \qquad (34)$$

where $y'_H = y_{H_2}/(1-y_{C^{14}O_2})$. Since $y_{C^{14}O_2}$ was negligible for each diffusion run, $y'_H = y_{H_2}$. In order to convert the diffusion coefficient of $C^{14}O_2$ through mixtures of H_2 and CO_2 predicted by this equation to the coefficient of HT through mixtures of H_2 and CO_2, dilute gas theory relationships were used. This is justified since Equation (34) is basically the form of dilute gas theory with respect to the important variables of temperature, density and composition. The conversion used corrects for the molecular weight, M, the effective collision diameter, σ, and the collision integral, $\Omega^{(1,1)*}$, of the diffusing component with respect to the major components, hydrogen and carbon dioxide.

(35)

$$D_{HT} = D_{C^{14}O_2}\left[\frac{M_{C^{14}O_2}}{M_{HT}} \cdot \frac{M_{HT} + M_{avg}}{M_{C^{14}O_2} + M_{avg}}\right]^{1/2}\left[\frac{(\sigma^2\Omega^{(1,1)*})_{C^{14}O_2}}{(\sigma^2\Omega^{(1,1)*})_{HT}}\right]$$

In this relation M_{avg} represents the average molecular weight of the mixture in which diffusion is occurring. The resulting comparison between converted values from the Chou empirical equation and the data points from this investigation taken for the HT-H_2-CO_2 system at 35°C is presented in Figure 23. The converted equation values for the diffusivity-density product agree well with the extrapolated low density products, $(D\rho)_o$ of the data from this investigation. Table VIII presents this comparison numerically. However, except for the high hydrogen content mixtures, where the transposition made is likely to be less accurate, the HT-H_2-CO_2 results diverge below the converted Chou predictions with increasing density.

TABLE VIII

LOW DENSITY COMPARISON BETWEEN DIFFUSIVITY-DENSITY PRODUCT OF CONVERTED VALUES FROM EQUATION (34) AND EXTRAPOLATED DATA FOR HT-H_2- CO_2 AT 35°C

Mole Fraction H_2	$(D\rho)_{EQN.\ (34)}$ x 10^3	$(D\rho)_o$ x 10^3	Percent Difference*
0.189	20.9	21.2	1.4
0.628	30.4	31.0	2.0
0.933	44.9	46.7	4.0
1.000	51.9	53.8	4.0

* Percent Difference $= 100 \cdot \dfrac{(D\rho)_o - (D\rho)_{EQN.\ (34)}}{(D\rho)_{EQN\ (34)}}$

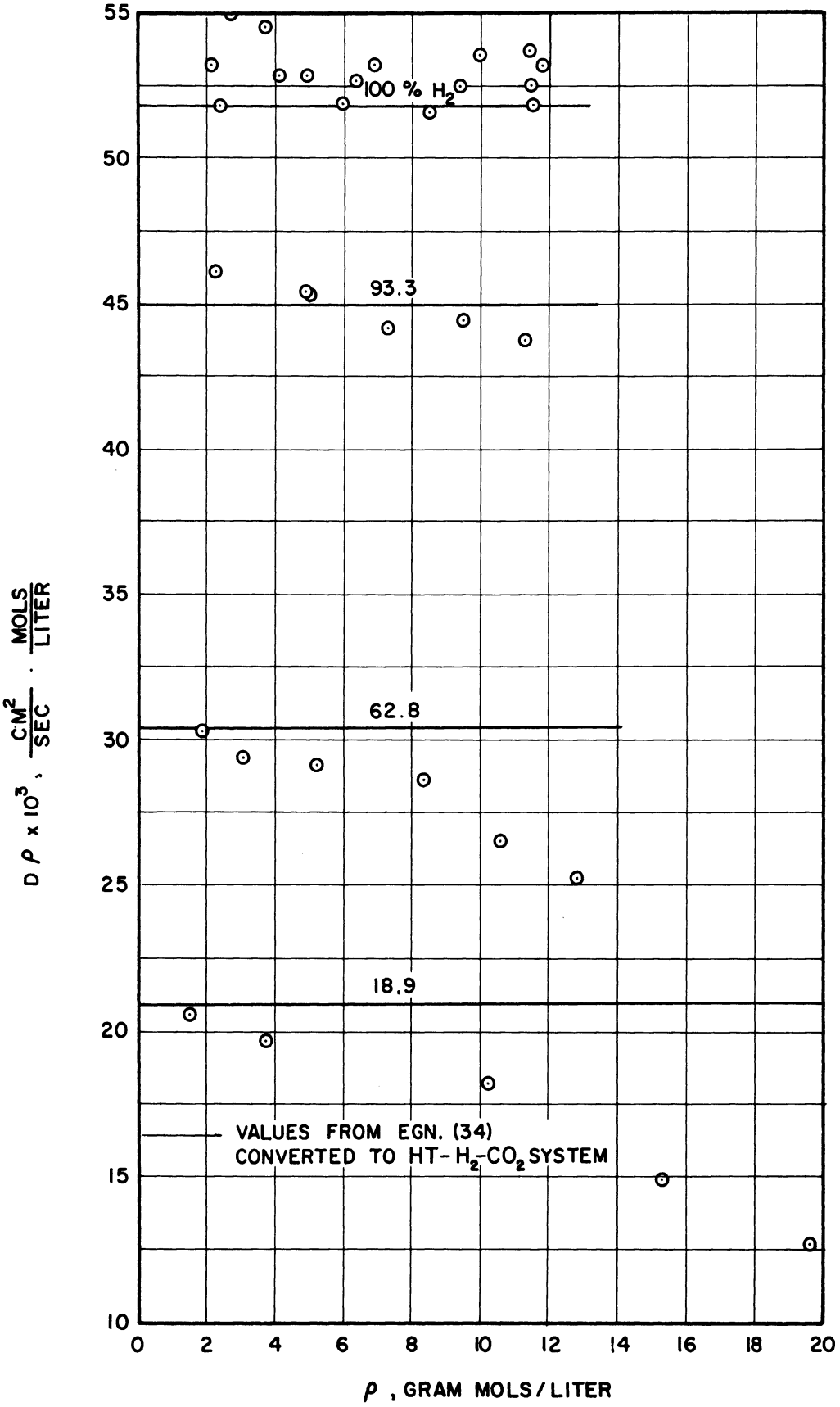

Figure 23. Comparison of Data to Chou Equation Converted to HT-H_2-CO_2 System by Dilute Gas Diffusion Theory.

VII. DISCUSSION OF ERRORS AND DIFFICULTIES

Since the experimental works of O'Hern and Chou were carried out with much of the same equipment used in this investigation, many of the sources of errors and difficulties were the same as those described in their dissertations. However, the introduction of new equipment, materials, and techniques into the present work has created a few new ideas to be discussed with the old ones in this section.

ACCURACY OF RESULTS

The comparison of the results of this investigation to the theoretical and experimental results of other works has been presented in the previous section. This comparison reflects the general accuracy of the results presented here. In order to show the consistency of the results of this investigation, smooth arbitrary lines have been drawn on the respective graphs of results which appear to best fit the data at each single temperature and composition of gas. Since the graphs of the diffusion coefficient-density product, Figures 12, 13, 14, and 15, most clearly indicate the deviations from these smoothed result lines, they have been chosen for use as the basis of the discussion concerning consistency.

With the exception of the two runs, runs 13B and 21B, for which no diffusivity could be evaluated, the average percent deviation from the smoothed results is about one percent. Only two, runs 24B and 83B, of the ninety-five successful diffusion data runs with the smaller hole diffusion path, path B, show greater than five percent

deviation from the lines drawn. A total of eight runs have greater than a three percent deviation. The five experimental runs made with the larger hole diffusion path, path A, in place have a considerably larger average deviation percent from the smoothed results, slightly less than four percent. A greater deviation might be expected for runs with this path since bulk convection is more likely to occur through the larger holes. However, no trend of deviation between the runs with different diffusion paths was noted.

Sixteen diffusion runs were made with the HT-H_2 system at 35°C. The average deviation of these runs is less than one and one-half percent. Because of the large number of points taken for this single temperature and composition, perhaps this is the best estimate of the overall consistency of results. However, although the data seem to be inclusively consistant, several systematic sources of error to be considered here might well cause the absolute error of the results to be different from the error indicated by the percent deviation from the arbitrarily drawn smooth lines.

Most of the possible causes of error to be considered here would cause deviations which would show up in the mathematical analysis of the results. According to the analysis of the diffusion cell, the Fick coefficient of diffusion is determined from the slope of the linear relationship between the logarithm of the concentration difference between chambers of the cell and the elapsed time of the diffusion run. Sizeable error caused by a phenomenon which is not proportional to the

concentration difference would result in curvature of this supposed linear relationship. Only the analyses of the two unsuccessful runs, runs 13B and 21B showed evidence of curvature of this relationship over the entire duration of the run. Some other runs showed curvature during the first ten percent of the run which could be attributed to the period when the system was coming to quasi steady-state or during the last part of the run when the chamber concentration differences were too close to equilibrium to give accurate results.

MASS TRANSFER AT THE SURFACE

Use of a diffusion path which restricts transfer by bulk convective processes may introduce transfer by a mechanism which is related to the amount of surface area per unit length parallel to diffusional transfer. Unless the driving force associated with the surface transfer is the same as that causing diffusion, an appreciable surface transfer would cause curvature in the semi-log straight line relationship just discussed. The two diffusion paths with different sized hole were used in order to detect surface transfer which might be proportional to the diffusion gradient. Diffusion path A, constructed of tubes with an average inside diameter of 0.0428 centimeter has a ratio of cross sectional open area to parallel surface area which is 1.9 times as great as the same ratio for path B with tubes having an average inside diameter of 0.0228 centimeter. Although the proof of the absence of surface transfer is not irrefutable because of the scatter of the data,

the virtual agreement between results using the two diffusion paths indicates that surface transfer is not a substantial part of the mass transfer occurring between chambers of the cell.

More conclusive proof could have been gained if an even greater variance of the open area to surface area had been attained. However, construction of a bundle of smaller tubes than those used in path B would have been a nearly impossible task. Threat of convective transfer would have seriously curtailed the use of a bundle having much larger diameter holes than those in path A.

END EFFECT OR CONCENTRATION GRADIENT IN THE CHAMBERS

The mathematical analysis of experimental work was partially based on the assumption of complete mixing in the two cell chambers. This assumption disregards the presence of end effects at the openings of the tubes of the diffusion path. The close agreement of the results with low density values from the literature is an indirect indication of the lack of important end effects since the cell constant was entirely determined from cell geometry. The ratio of diffusion path to chamber cross sectional areas was almost exactly one percent. The resistance to diffusional transfer of the diffusion path was therefore nearly completely controlling, and very little of the total concentration gradient could have been maintained in the chambers. It is felt that no appreciable error was caused by end effects.

CAPILLARY EFFECT

In order that the results be representative coefficients of diffusion for the gaseous mixtures studied in the investigation, the number of collisions of gaseous molecules with molecules in the walls of the diffusion path must be negligible in comparison with inter-gaseous molecular collisions. A comparison involving the path minimum tube diameter to the maximum mean free path of molecules at diffusion run conditions indicates compliance to this condition. The mean free path of a hydrogen molecule at the minimum experimental density of 1.402 gram moles per liter is 3.1×10^{-7} cm. Pollard and Present [34] have derived an expression which predicts the diffusion coefficient, D, of rigid spherical molecules in a capillary from the diffusion coefficient in free space, D_{FS}.

$$D = D_{FS} \left(1 - \frac{3}{4} \frac{\lambda}{d}\right) \qquad (36)$$

where λ is the mean free path and d is the diameter of the capillary tube. The term $3/4\ \lambda/d$ is, then, the fractional correction which must be made for diffusion occurring in a capillary. The maximum value of this term for the experimental conditions is 0.000010. Although the expression is valid only for rigid spherical molecules it serves as a satisfactory indication of order of magnitude of the capillary effect. The error introduced by using the bundles of tubes as diffusion paths is probably negligible.

MEASUREMENT OF CELL GEOMETRY

There is a possibility of error resulting in incorrect values for the cell constants of the two cell configurations. Perhaps the largest uncertainty could be attributed to the measurement of tube diameters. Although considerable care was taken to remove burrs covering portions of the ends of tubes which might have been caused during the construction of the tube bundles, the measurement of the ends of the individual tubes may have caused the introduction of error. The incomplete sample of tubes actually measured may have introduced error, although the averaged results for the two entirely independent sets of measurements for tube bundle B produced the same average tube diameter well within one tenth of a percent. The measurements on path B, themselves, had an average deviation from the average of approximately one percent. Additional error could have been introduced by determinations of the volumes of the cell chambers and diffusion path length. Average deviations from the averages of these measurements were considerably less than one tenth of a percent, however. It is estimated that the maximum possible error in determination of the respective cell constants is two percent.

DENSITY DETERMINATION

The results of this investigation as presented as functions of the density of the diffusing gases are relatively sensitive to errors made in determining the densities. Since excellent data concerning the state behavior of hydrogen at the experimental conditions are available,

little error was introduced here. However, PVT data for mixtures of carbon dioxide and hydrogen and argon and hydrogen are not available for the greater part of the experimental conditions. For the lower fraction hydrogen runs generalized compressibility correlations were used to predict the experimental densities from the experimental temperatures and pressures. Pseudo-critical properties were calculated by the methods of Prausnitz [35,36] for use in conjunction with the Pitzer [32,33] compressibility tables. State conditions for mixtures of carbon dioxide and hydrogen were predicted with a maximum deviation of 2.2 percent and an average deviation of 1.3 percent in the temperature range between 273°K and 473°K and in the pressure range between 3000 and 7500 pounds per square inch absolute by these correlations. Further discussion concerning the state relations is presented in Appendix E. It is felt that the compressibilities of mixtures of hydrogen and argon are predicted by the Pitzer-Prausnitz relations with at least as good an accuracy as the less ideal mixtures of hydrogen and carbon dioxide.

CONVECTIVE TRANSFER

The temperature of the cell body was maintained at a non-fluctuating temperature by surrounding it with insulating material within the constant temperature chamber to eliminate "thermal pumping" which might occur between the cell chambers. The diffusion path was constructed of small diameter tubing in order to reduce the possibility of convective currents causing transfer of material between the chambers.

With the diffusion cell resting with one chamber above the other, two further measures were undertaken to reduce tendencies toward convection in the cell. The upper chamber was maintained at approximately one tenth of a degree centigrade higher temperature than the lower chamber during 35°C runs and three tenths of a degree centigrade higher temperature during the 100°C runs. The radioactive gas mixture introduced into the upper chamber contained approximately one percent more hydrogen than the mixture in the lower chamber. This radioactive mixture, on the average about one tenth of the total amount of gas in the upper chamber, caused a result of about a tenth of a percent higher hydrogen content in the upper chamber. Both of these measures made the gas in the upper chamber slightly less dense than that in the lower chamber, thus reducing the possibility of interchamber convection. Although convective transfer could probably not be totally eliminated, it is believed that convection between chambers was reduced to a negligible amount except for runs 13B and 21B which indicate a definite non-linear relationship between the log of the concentration difference and time.

IONIZATION CURRENT MEASUREMENT

The chief difficulties encountered encountered during the investigation involved the reduction of errors and inconsistencies introduced by measurement of the ionization currents. The small order of magnitude of the currents measured was responsible for these difficulties. A considerable length of time was required for the preparation of a measuring circuit for which the background and leakage currents

were small with respect to the desired ionization currents. Detailed descriptions of the circuit components are located in Section III of this dissertation. The background currents were never entirely eliminated. For runs at 35°C the background current for each channel was less than one percent of average current measurements. For runs at 100°C the background currents varied, although they remained reasonably constant for a given series of runs at that temperature. After each of the two occasions of electrode plug insulation repair the values for the background current of both channels differed from those from before the repair. The first repair was necessitated after soap solution had been placed on the electrodes to locate a gas leak which had been detected at the start of a series of runs at 100°C. The soap solution destroyed the coating of silicone varnish which had been used to increase the resistivity of the electrode plug ceramic insulators. The second repair was necessitated after mercury from the compression leg had entered the diffusion cell and similarly destroyed the varnish coating. On both occasions operations were shut down for about a week while satisfactory varnish coatings were replaced. Backgrounds for both channels varied from two to about five percent of average current readings for runs at 100°C.

The error introduced by background currents at 35°C is probably not appreciable. The variation from constancy of the backgrounds at 100°C could conceivably have introduced an error of as much as three percent into the results. This error is probably smaller, however, since the difference between backgrounds of the two channels of current

measurement is the important quantity. The close agreement between the temperature dependency of the experimental results and the values predicted by dilute gas theory and from data in the literature indirectly indicates that the error caused by uncertainty in the measurements of the background currents at 100°C is small. The background measurements are covered in greater detail in Appendix F.

The absolute accuracy of the Beckman Ultrohmeter is stated to be between three and five percent for the range of measurements of this investigation. However since only relative accuracy is required for the measurements resulting in diffusion coefficients, the error introduced by this instrument is believed to be considerably less than one percent. The recorder speeds of from one to six inches per hour were all checked and found to be accurate to within one-tenth of a percent.

MATERIAL LEAKAGE

Although various amounts of gas leakage were detected during the investigation after a change in operating temperature and once due to valve wear, there was no occasion of serious leakage during a diffusion run. The maximum percent leakage per unit time occurred during run 102B at a pressure of 3086 pounds per square inch and a temperature of 100°C during which a 0.8 percent drop in pressure occurred in the 4 1/2 hour duration of the run. For most runs no appreciable drop in pressure was noted. The maximum fractional error introduced by a material leak would be equal to the fractional drop in pressure divided by the total fractional change in concentration in a unit of time. This

maximum possible error amounts to 1.0 percent for the run having the greatest percent leakage.

CHEMICAL REACTION

It is conceivable that components of the diffusion mixtures could react together and thereby cause erroneous results. Hydrogen and argon do not react together. The possible reaction between hydrogen and carbon dioxide,

$$H_2 + CO_2 = H_2O + CO \qquad (37)$$

has been discussed by Chou in connection with his diffusion work. He found that the maximum equilibrium concentrations of CO and H_2O would be 0.68 percent and 0.22 percent at 100°C and 35°C. There is considerable question as to whether equilibrium would be reached in a reasonable length of time. The effect of even the equilibrium concentrations of these materials would be considerably less than the sum of the percentages of CO and H_2O since the diffusion coefficient is not sensitive to the presence of small amounts of impurities.

The diffusion coefficient could be affected by the radiation and surface catalyzed reaction,

$$2HT = H_2 + T_2 \qquad (38)$$

since HT is the traced diffusing component. Since the concentration of H_2 is extremely large with respect to the other members of the reaction and since T_2 is a comparatively unstable molecule at room

temperature, one of tritium's chief desirable characteristics is its affinity for replacing hydrogen in organic compounds and thereby "tagging" molecules, there is little chance of an appreciable amount of T_2 being present in the diffusion mixture with respect to the amount of HT present. The calculated equilibrium ratio of T_2 to HT is 0.000055 at 28°C for the most concentrated radioactive sample handled in the investigation after the initial tritium dilution. The values of the equilibrium constants used for the calculation were reported by Mattraw, Pachuchi, and Dorfman [27].

ADDITIONAL SOURCES OF ERROR

Some other possible sources of error which have been thoroughly discussed by Chou and O'Hern will be mentioned only briefly here because it is thought unlikely that an appreciable error could result from them.

Diffusion through the tubing connections to the cell body could conceivably cause small amounts of tritium to enter or leave the cell chambers and thereby introduce error into the results. The open cross sectional areas have been reduced to a minimum by insertion of 14 gauge copper wire into the tube openings. High concentration HT gas was flushed from the tubing to the upper chamber before the start of a run to reduce the driving force causing diffusion through this tubing entrance.

The presence of radioactivity in the diffusion cell might possibly cause reduction or enhancement of the diffusion occurring. O'Hern made three diffusion runs at approximately the same density with

widely different concentrations of $C^{14}O_2$, the radioactive component. He reported that radioactivity had no apparent effect upon the diffusion coefficients determined by the type of cell used in the present investigation.

The pressure and temperature expansion difficulties associated with the cell used by O'Hern and Chou which changed the chamber volumes and were caused by the flexability of the teflon insulators was no problem in the cell used in this investigation, since only rigid materials were exposed to the conditions in the chambers.

Although the total absolute error introduced by these possible sources could conceivably exceed five percent, it is felt that the actual error is less than two percent.

DIFFICULTY IN DIFFUSION PATH CONSTRUCTION

The most time consuming task connected with this investigation involved the construction of the diffusion paths used. The detailed methods of construction of each are described in Section III of the dissertation. Each path was the result of many unsuccessful attempts over a period of months. These pains were taken because it is felt that the resulting tube bundles were the heart of the investigation.

CONCLUSION AND SUMMARY

The primary purpose of the work covered in this dissertation was to investigate diffusion in the dense gas phase for systems for which there has been no such data available. Accordingly, Fick diffusion coefficients have been determined and are reported here for two ternary systems, HT-H_2-CO_2 and HT-H_2-A, and one binary system, HT-H_2, at temperatures of 35°C and 100°C and to pressures of 370 atmospheres. Three mixtures each of the two ternary systems were investigated; the mixtures contained approximately 19, 62, and 93 percent of hydrogen and negligible traces of HT, the remainder in each case being respectively carbon dioxide or argon. Except for the larger molecular weight of tritiated hydrogen, diffusion in the HT-H_2 system could be thought of as self-diffusion since the physical sizes of the two species of hydrogen molecule are nearly identical.

The diffusion coefficient-density product for each constant composition of the systems studied decreased with respect to increasing density at both experimental temperatures. This decrease with increasing density was less pronounced for the high hydrogen content mixtures than for the high carbon dioxide or argon content mixtures. The maximum percentage decrease noted within the range of densities investigated occurred for the 19 percent hydrogen, 81 percent carbon dioxide sample at 35°C which had a 40 percent drop of the product below the value of the diffusivity-density product extrapolated back to zero density. The results presented for the systems are consistant with

respect to themselves, the maximum and average percent deviation of the individual data points from arbitrary smooth lines drawn through the points at each given concentration and temperature being six and one percent respectively.

The diffusion cell used for the investigation is of the quasi steady-state type. It is felt that this cell is superior to others used in similar investigations in some respects. One advantage stems from the automatic continuous monitoring of concentration in both chambers throughout the entire diffusion run. This type of concentration determination quickly indicates irregularities which may occur and makes possible the utilization of the data from only the best part of the diffusion run. Methods involving only initial and final composition measurements produce results which must include transients which occur at the start of a run. The mathematical simulation of a diffusion determination for the cell of this investigation is also far less complicated than of those which require the solution of boundary value equations based on Fick's second law.

The cell used in the present work required no calibration based upon diffusion results. The construction of tube bundles from fine stainless steel hypodermic needle tubing allowed the determination of the cell constant to be made entirely from measurements of the cell geometry. Electrode modifications made in this investigation extended the density range of the O'Hern cell substantially, and did away with chamber volume expansion due to internal pressure since only rigid materials of the electrodes were in contact with the internal conditions.

The results of the investigation were found to compare reasonably well with results from the literature. The results, extrapolated to low density showed good agreement with the Wilke [47] equation for prediction of multicomponent diffusion coefficients from binary coefficients of the components.

$$\frac{1-y_1}{D_1} = \frac{y_2}{D_{12}} + \frac{y_3}{D_{13}} + \text{----} \qquad (7)$$

The binary coefficients of diffusion for HT-CO_2 and HT-A evaluated by the extrapolation of the Wilke equation to zero mole fraction of hydrogen show fair agreement with values of the binary coefficients from the literature which have been converted to allow for the difference in molecular weight between H_2 and HT. The experimentally determined values for the diffusivity of HT in hydrogen extrapolated to one atmosphere agree to within 0.4 percent of the average of converted values from the literature.

The temperature dependence of the extrapolated low pressure values of the diffusivity agrees well with dilute gas theory predictions based on the realistic Lennard-Jones potential. Values of the diffusivity-density product extrapolated to low density are proportional to the absolute temperature raised to the 2/3 power to within 0.7 percent for all compositions of the three systems studied. The Lennard-Jones potential theory predicts an effective constant exponent of 0.64 for HT-H_2, 0.70 for HT-H_2-CO_2 and 0.72 for HT-H_2-A for the temperatures investigated.

The predictions of the Enskog [13] dense gas theory based on the solid spherical molecular model diverge below the experimental results for the diffusion coefficients for increasing density. The apparent fair agreement between the experimental results and the Thorne [42] expansion for the dense gas correction to dilute gas theory occurs because important further terms of the Thorne expansion have not been derived theoretically nor evaluated. The Enskog theory based on evaluation of the "thermal pressure", $T\left(\frac{\partial P}{\partial T}\right)_{\underline{V}}$, from actual state data of the diffusion mixture shows closer agreement to the results for HT-H_2 than do the Enskog calculations based on the solid spherical molecule. It is believed that similar calculations based on actual $\underline{PVT}$ data of the respective H_2-CO_2 and H_2-A systems would predict the experimental diffusion coefficients at the investigated densities with reasonable accuracy. However, the lack of such state data makes this prediction impossible.

The results of this investigation have fair agreement with the Slattery corresponding states correlation, but the ultimate value of this chart is questioned since the major contribution of the deviation from the low density values, to which the correlation compares high density values, is due to the compressibility of the gases of the diffusion mixture rather than to the diffusion coefficient.

Since part of the dense gas diffusivity experimental data reported by Chou [10] involved a system, $C^{14}O_2$-H_2-CO_2, which was very similar to the system, HT-H_2-CO_2, of this investigation, a special comparison between these results was made. The respective values agree to

within four percent at low densities but the values from the present work are increasingly lower than the Chou values at higher densities. The values attributed to Chou which were converted to the HT-H_2-CO_2 system by dilute gas theory relationships for this comparison were evaluated from his empirical equation which predicts inverse proportionality between the diffusion coefficient and the density at all densities investigated. The larger than theoretically predicted temperature dependence noted by Chou for the $C^{14}O_2$-H_2-CO_2 system was not observed for the similar HT-H_2-CO_2 system of this investigation.

Recent data reported by Berry and Koeller [3] and Mifflin and Bennett [29] indicate the systematic decrease of the diffusivity-density product with increasing density which was noted for the results of this investigation.

The author would like to recommend further attempts to relate the dense gas diffusion data with either theoretical or empirical state investigations. Since diffusion in a binary mixture is chiefly a function of (1,2) collisions, or interactions between the two different species of the mixture rather than between members of the same species, perhaps an investigation involving the non-idealities of mixing of gases would clarify the dense gas diffusion picture to some extent.

APPENDIX A

TABULATION OF DIFFUSION RUN DATA

1. Table IX, Run Data Excepting Ionization Current Data.

2. Table X, Ionization Current Data.

The uncorrected ionization currents listed in this appendix are in chart units since the analysis of the slopes in order to determine diffusion coefficients did not require further conversion to current units in amperes nor to concentration in mass units per unit volume. However, the necessary equations to make these conversions will be presented here in case such a conversion is desired. It will be remembered that the absolute accuracy of the Ultrohmeter is stated to be from three to five percent for the ranges utilized in this investigation. Although this accuracy probably did not enter appreciably into the diffusion results of this work, it must be taken into account for any conversion from chart units to absolute current units. The relation for conversion from chart units on a 20 space full scale chart is:

$$I, \text{ amps} = \frac{(I, \text{chart units})(\text{Voltage Range})}{(\text{Internal Resistor})(17.36)} \qquad (39)$$

The voltage range refers to the Ultrohmeter range and is listed for each run in Table IX. The internal resistance for every run of the investigation was 10^{11} ohms. For runs taken using a 50 space full scale chart, the factor, 17.36, must be replaced by a factor which is 5/2 times larger, 43.40. The currents converted by this formula must first be corrected for the chart deflection for zero current and the background currents listed in Appendix F.

The respective concentrations may be determined from the thus determined currents by determining the concentration-current ratio for the particular run pressure from Figure 26 of Appendix D.

TABLE IX

TABULATED DATA, EXCEPTING
IONIZATION CURRENTS

Run Number	H_2 Mole Fraction	Chart Speed	Pressure Psia	Average Millivolts Thermocouple		Avg. Temp. °C	Compressibility Factor	Voltage Range
				Upper	Lower			
1A	0.624	1	4074	1.407	1.403	35.0	1.128	2.0
2A	0.624	6	936	1.408	1.403	35.0	1.022	2.0
3A	0.628	6	1361	1.418	1.414	35.2	0.910	2.0
4A	0.628	2	3543	1.417	1.414	35.2	0.910	0.5
5A	0.628	6	623	1.402	1.398	34.9	0.960	1.0
10B	0.628	3	3091	1.405	1.401	34.9	0.997	5.0
11B	0.628	3	1912	1.401	1.399	34.9	0.982	5.0
12B	0.628	3	1124	1.406	1.403	35.0	0.984	2.0
13B	0.628	1	4176	1.408	1.404	35.0	1.039	0.5
14B	0.628	1	5074	1.407	1.404	35.0	1.063	2.0
15B	0.628	6	686	1.401	1.398	34.8	0.989	2.0
16B	0.628	2	4021	1.402	1.399	34.9	1.021	2.0
17B	0.9396	1	5094	1.406	1.404	35.0	1.210	5.0
18B	0.9334	2	4132	1.409	1.406	35.0	1.167	2.0
19B	0.9316	2	3068	1.407	1.405	35.0	1.121	1.0
20B	0.9335	4	1999	1.409	1.407	35.0	1.076	1.0
21B	0.9390	6	909	1.404	1.402	34.9	1.037	5.0
22B	0.9330	6	884	1.403	1.401	34.9	1.032	2.0
23B	0.9264	4	1954	1.403	1.400	34.9	1.074	2.0
24B	0.1889	1	2069	1.403	1.401	34.9	0.545	1.0
25B	0.1820	2	1056	1.403	1.401	34.9	0.768	1.0
26B	0.1921	4	513	1.403	1.401	34.9	0.894	2.0
27B	0.1839	1	3001	1.405	1.403	34.9	0.528	1.0
28B	0.1924	1	4884	1.406	1.404	35.0	0.670	2.0
29B	1.000	4	2469	1.407	1.403	35.0	1.101	2.0
30B	1.000	6	1057	1.404	1.402	34.9	1.041	5.0
31B	1.000	4	2866	1.407	1.404	35.0	1.118	2.0
32B	1.000	2	5244	1.406	1.404	35.0	1.220	2.0
33B	1.000	4	1944	1.401	1.399	34.9	1.082	2.0
34B	1.000	3	3699	1.404	1.402	34.9	1.153	2.0
35B	1.000	3	2652	1.408	1.406	35.0	1.109	2.0
36B	1.000	2	4076	1.406	1.404	35.0	1.169	2.0
37B	1.000	2	5231	1.404	1.402	34.9	1.221	5.0
38B	1.000	2	5174	1.409	1.407	35.0	1.218	2.0
39B	1.000	6	1474	1.402	1.399	34.9	1.059	2.0
40B	1.000	2	5394	1.406	1.403	35.0	1.227	2.0

TABLE IX (cont.)

Run Number	H_2 Mole Fraction	Chart Speed	Pressure Psia	Average Millivolts Thermocouple Upper	Lower	Avg. Temp. °C	Compressibility Factor	Voltage Range
41B	1.000	3	3569	4.291	4.271	100.4	1.126	2.0
42B	1.000	2	5117	4.271	4.252	100.1	1.183	2.0
43B	1.000	6	1256	4.277	4.262	100.1	1.043	2.0
44B	1.000	4	2986	4.277	4.262	100.1	1.105	1.0
45B	1.000	5	2129	4.282	4.268	100.2	1.075	5.0
46B	1.000	3	4667	4.259	4.245	99.8	1.165	2.0
47B	1.000	6	2119	4.258	4.247	99.8	1.075	2.0
48B	0.6342	1	4979	4.268	4.247	99.9	1.102	2.0
49B	0.6277	1	4106	4.267	4.248	99.9	1.072	2.0
50B	0.6380	3	1498	4.267	4.247	99.9	1.015	2.0
51B	0.6264	2	2950	4.261	4.246	99.8	1.040	2.0
52B	0.6272	6	756	4.262	4.243	99.7	1.006	2.0
53B	0.6264	3	2109	4.268	4.248	99.9	1.024	2.0
54B	0.9329	2	5114	4.268	4.251	99.9	1.183	2.0
55B	0.9268	4	2554	4.267	4.251	99.9	1.088	2.0
56B	0.9279	3	4109	4.268	4.250	99.9	1.145	2.0
57B	0.9352	6	1508	4.262	4.245	99.7	1.050	2.0
58B	0.9323	6	671	4.261	4.246	99.7	1.022	2.0
59B	0.9287	3	4122	4.265	4.253	99.9	1.146	2.0
60B	0.9257	6	1024	4.262	4.246	99.8	1.034	2.0
61B	0.1924	1	5063	4.269	4.255	99.9	0.800	2.0
62B	0.1925	1	4353	4.272	4.262	100.0	0.773	2.0
63B	0.1975	1	2834	4.268	4.257	100.0	0.773	2.0
64B	0.1894	2	1489	4.266	4.253	99.9	0.862	2.0
65B	0.1905	4	718	4.266	4.253	99.8	0.930	2.0
66B	0.926	2	5309	1.409	1.405	35.0	1.227	2.0
67B	0.926	2	4031	1.410	1.407	35.1	1.170	2.0
68B	0.926	4	2417	1.408	1.405	35.0	1.099	2.0
69B	0.926	3	3270	1.409	1.406	35.0	1.136	2.0
70B	0.926	5	1489	1.409	1.406	35.0	1.060	2.0
71B	0.926	6	816	1.409	1.407	35.0	1.032	2.0
72B	1.000	2	4388	1.410	1.407	35.1	1.184	2.0
73B	1.000	6	819	1.409	1.405	35.0	1.032	2.0
74B	0.195	1	5015	1.408	1.405	35.0	1.086	2.0
75B	0.195	1	4272	1.410	1.408	35.1	1.052	2.0
76B	0.195	4	725	1.409	1.407	35.0	0.991	2.0
77B	0.195	2	2401	1.409	1.405	35.0	0.993	2.0
78B	0.195	1	3300	1.410	1.406	35.1	1.019	2.0
79B	0.195	3	1472	1.410	1.407	35.1	0.989	2.0
80B	0.624	3	3544	1.409	1.406	35.0	1.106	2.0

TABLE IX (cont.)

Run Number	H_2 Mole Fraction	Chart Speed	Pressure Psia	Average Millivolts Thermocouple Upper	Lower	Avg. Temp. °C	Compressibility Factor	Voltage Range
81B	0.624	1	5204	1.409	1.406	35.0	1.175	2.0
82B	0.624	3	2099	1.409	1.407	35.0	1.055	2.0
83B	0.624	5	1253	1.408	1.405	35.0	1.030	2.0
84B	0.624	6	769	1.410	1.408	35.1	1.018	2.0
85B	0.624	2	4398	1.411	1.408	35.1	1.142	2.0
86B	0.624	3	2775	1.409	1.406	35.0	1.078	2.0
87B	1.000	6	1671	1.404	1.402	34.9	1.068	2.0
88B	1.000	6	916	1.407	1.405	35.0	1.035	2.0
89B	0.195	1	5237	4.267	4.246	99.8	1.119	2.0
90B	0.195	1	4173	4.273	4.253	100.0	1.080	2.0
91B	0.195	1	3164	4.276	4.255	100.0	1.049	2.0
92B	0.195	2	1998	4.280	4.256	100.1	1.022	2.0
93B	0.195	4	1209	4.281	4.262	100.2	1.009	2.0
94B	0.195	6	633	4.270	4.253	100.0	1.003	2.0
95B	0.624	2	3745	4.285	4.265	100.2	1.116	2.0
96B	0.624	1	5409	4.287	4.266	100.3	1.168	2.0
97B	0.624	3	2586	4.286	4.264	100.2	1.074	2.0
98B	0.624	1	4459	4.285	4.263	100.2	1.137	2.0
99B	0.624	5	1424	4.284	4.260	100.2	1.038	2.0
100B	0.624	6	724	4.284	4.264	100.2	1.020	2.0
101B	0.926	1	5144	4.283	4.260	100.2	1.185	2.0
102B	0.926	3	3086	4.281	4.258	100.1	1.110	2.0
103B	0.926	2	4318	4.282	4.260	100.2	1.158	2.0
104B	0.926	4	2460	4.257	4.247	99.9	1.086	2.0
105B	0.926	6	1381	4.274	4.254	100.0	1.048	2.0
106B	0.926	6	815	4.274	4.254	100.0	1.028	2.0

TABLE X

IONIZATION CURRENT DATA

Run No.	Time (Chart Spaces)	Ionization Currents (Chart Units)		
		Lower	Upper	Zero
1A	2	7.43	47.84	3.65
	4	9.94	46.15	3.65
	6	12.15	44.55	3.65
	8	14.13	43.05	3.65
	10	15.82	41.64	3.65
	12	17.25	40.39	3.65
	14	18.55	39.27	3.65
2A	3	7.87	49.01	3.65
	6	10.53	47.23	3.65
	9	12.85	45.50	3.65
	12	14.94	43.91	3.65
	15	16.73	42.50	3.65
	20	19.23	40.51	3.65
	25	21.23	38.84	3.65
	30	22.84	37.40	3.65
3A	3	3.66	13.92	1.54
	12	4.55	13.07	1.53
	21	5.30	12.38	1.53
	30	5.88	11.81	1.53
	39	6.36	11.33	1.52
	48	6.77	10.95	1.52
	57	7.13	10.65	1.52
	66	7.39	10.39	1.53
	75	7.61	10.18	1.53
	84	7.80	10.01	1.52
	93	7.96	9.85	1.52
	102	8.09	9.74	1.51
4A	2	4.58	17.89	1.52
	10	5.44	17.22	1.52
	20	6.34	16.43	1.51
	30	7.06	15.76	1.51
	45	7.93	14.93	1.50
	60	8.60	14.30	1.54
	75	9.04	13.74	1.55
	90	9.46	13.34	1.53
	105	9.74	13.00	1.52
	120	10.11	12.87	1.53
	135	10.36	12.69	1.53
	150	10.50	12.53	1.51

TABLE X (cont.)

Run No.	Time (Chart Spaces)	Ionization Currents (Chart Units)		
		Lower	Upper	Zero
5A	2	4.43	17.48	1.59
	5	5.39	16.68	1.60
	10	6.67	15.53	1.61
	15	7.60	14.61	1.62
	20	8.36	13.88	1.61
	25	8.92	13.32	1.60
	30	9.33	12.88	1.60
	35	9.69	12.54	1.59
	40	9.95	12.28	1.59
	45	10.14	12.07	1.58
	50	10.29	11.92	1.58
	55	10.40	11.80	1.57
	60	10.52	11.71	1.56
10B	5	3.82	14.80	1.61
	15	4.59	14.31	1.62
	25	5.27	13.75	1.63
	35	5.84	13.28	1.63
	45	6.34	12.88	1.63
	55	6.77	12.48	1.63
	65	7.15	12.14	1.63
	75	7.47	11.87	1.63
	85	7.74	11.63	1.63
	95	7.98	11.40	1.63
11B	2	3.26	13.22	1.59
	5	4.11	12.90	1.58
	10	4.58	12.45	1.58
	20	5.36	11.68	1.57
	30	5.97	11.07	1.57
	40	6.44	10.57	1.57
	50	6.82	10.18	1.58
	60	7.13	9.91	1.59
	70	7.40	9.68	1.60
12B	2	5.23	17.46	1.58
	5	5.93	16.88	1.58
	10	6.88	16.04	1.58
	15	7.67	15.29	1.58
	20	8.32	14.67	1.57
	25	8.87	14.16	1.57
	30	9.28	13.72	1.56

TABLE X (cont.)

Run No.	Time (Chart Spaces)	Ionization Currents (Chart Units) Lower	Upper	Zero
	35	9.63	13.38	1.56
	40	9.94	13.08	1.60
13B	2	7.27	13.83	1.61
	5	8.08	13.20	1.60
	10	8.74	12.62	1.59
	15	9.11	12.29	1.58
	20	9.32	12.07	1.56
	25	9.48	11.92	1.54
14B	5	4.93	16.26	1.54
	10	5.80	15.87	1.54
	15	6.45	15.51	1.55
	20	7.02	15.13	1.55
	30	7.92	14.40	1.55
	35	8.29	14.06	1.55
	45	8.88	13.50	1.56
	55	9.38	13.08	1.56
	65	9.70	12.76	1.55
15B	2	5.52	18.90	1.58
	5	6.17	18.35	1.58
	10	7.11	17.52	1.58
	15	7.89	16.77	1.58
	25	9.11	15.63	1.58
	35	9.98	14.79	1.58
	45	10.58	14.20	1.58
	55	11.03	13.79	1.58
16B	5	4.91	17.91	1.59
	10	5.89	17.21	1.62
	15	6.82	16.52	1.63
	20	7.63	16.02	1.68
	25	8.26	15.49	1.68
	30	8.73	15.03	1.68
	35	9.17	14.63	1.68
	40	9.55	14.29	1.68
	45	9.88	14.02	1.68
	50	10.14	13.78	1.68
	55	10.35	13.57	1.68

TABLE X (cont.)

Run No.	Time (Chart Spaces)	Ionization Currents (Chart Units)		
		Lower	Upper	Zero
17B	5	3.73	13.68	1.60
	10	4.84	12.82	1.61
	15	5.70	12.06	1.62
	20	6.35	11.37	1.62
	25	6.86	10.92	1.61
	30	7.26	10.53	1.60
	35	7.57	10.22	1.59
	40	7.80	9.98	1.58
18B	5	5.76	17.63	1.62
	10	6.57	16.91	1.61
	15	7.28	16.30	1.60
	20	7.87	15.72	1.59
	25	8.38	15.23	1.58
	30	8.81	14.79	1.57
	35	9.17	14.43	1.56
	40	9.47	14.12	1.55
	45	9.72	13.83	1.54
	50	9.93	13.57	1.53
	55	10.14	13.36	1.52
19B	2	7.02	19.32	1.56
	5	7.68	18.72	1.55
	10	8.61	17.89	1.53
	15	9.37	17.18	1.51
	20	9.96	16.55	1.50
	25	10.48	16.04	1.49
	30	10.90	15.62	1.48
	35	11.23	15.27	1.46
	40	11.52	14.98	1.45
	45	11.74	14.77	1.44
	50	11.90	14.57	1.42
20B	2	5.63	13.88	1.61
	5	5.98	13.56	1.60
	10	6.48	13.11	1.60
	20	7.27	12.37	1.59

TABLE X (cont.)

Run No.	Time (Chart Spaces)	Ionization Currents (Chart Units)		
		Lower	Upper	Zero
	30	7.83	11.80	1.58
	40	8.26	11.39	1.58
	50	8.59	11.05	1.57
21B	10	5.24	14.59	1.56
	15	6.14	13.86	1.57
	20	6.90	13.19	1.58
	25	7.48	12.63	1.59
22B	10	4.31	13.47	1.58
	15	5.14	12.73	1.57
	20	5.83	12.10	1.57
	25	6.41	11.56	1.56
	30	6.86	11.14	1.56
	35	7.21	10.78	1.55
23B	10	4.47	16.92	1.52
	15	5.27	16.17	1.51
	20	6.00	15.50	1.49
	25	6.59	14.92	1.47
	30	7.13	14.39	1.45
	40	7.94	13.56	1.43
	50	8.55	12.92	1.43
	60	9.02	12.43	1.43
24B	5	4.63	17.16	1.40
	10	5.22	16.54	1.30
	15	5.77	15.97	1.20
	20	6.22	15.42	1.05
	25	6.61	14.90	.90
	30	6.95	14.43	.75
	35	7.27	14.00	.60
	40	7.50	13.60	.43
	45	7.68	13.23	.21
	50	9.23	14.27	1.54

TABLE X (cont.)

Run No.	Time (Chart Spaces)	Ionization Currents (Chart Units)		
		Lower	Upper	Zero
25B	5	5.98	18.42	1.58
	10	6.83	17.48	1.52
	20	8.09	15.92	1.37
	25	9.01	15.71	1.62
	30	9.42	15.21	1.61
	35	9.79	14.78	1.59
	40	10.08	14.43	1.57
	45	10.35	14.12	1.55
26B	6	4.07	16.71	1.57
	10	5.02	15.87	1.56
	15	6.00	14.92	1.55
	20	6.77	14.12	1.53
	25	7.45	13.47	1.51
	30	7.94	12.97	1.50
	35	8.32	12.54	1.49
	40	8.65	12.17	1.48
27B	30	7.63	16.47	1.60
	40	8.13	16.03	1.61
	50	8.57	15.65	1.63
	60	8.97	15.29	1.63
	70	9.29	14.97	1.61
28B	40	5.36	17.30	1.48
	50	5.84	16.93	1.46
	60	6.20	16.48	1.42
	70	6.78	16.33	1.60
	80	7.17	16.00	1.59
	90	7.49	15.69	1.58
	100	7.81	15.43	1.57
	110	8.11	15.17	1.56
	120	8.37	14.94	1.55
	130	8.57	14.69	1.53
	140	8.76	14.44	1.50

TABLE X (cont.)

Run No.	Time (Chart Spaces)	Ionization Currents (Chart Units) Lower	Upper	Zero
29B	3	2.82	18.16	1.56
	6	3.47	17.63	1.56
	10	4.25	17.00	1.56
	15	5.11	16.33	1.56
	20	5.84	15.75	1.56
	25	6.48	15.23	1.56
	30	7.03	14.78	1.56
	35	7.54	14.38	1.56
	40	7.97	14.03	1.56
	45	8.32	13.73	1.56
30B	10	7.16	18.17	1.57
	15	8.16	17.29	1.57
	20	9.01	16.52	1.57
	25	9.67	15.91	1.57
	30	10.21	15.38	1.57
	35	10.63	14.95	1.57
	40	11.00	14.60	1.57
	45	11.29	14.33	1.57
31B	5	5.10	15.49	1.56
	10	5.69	14.96	1.56
	15	6.21	14.50	1.56
	25	7.05	13.72	1.56
	35	7.74	13.05	1.56
	45	8.28	12.59	1.55
32B	10	5.66	18.28	1.54
	15	6.51	17.61	1.54
	20	7.22	16.97	1.55
	25	7.83	16.38	1.55
	30	8.35	15.88	1.55
	35	8.82	15.44	1.54
	40	9.22	15.03	1.54
	45	9.57	14.72	1.53
	50	9.89	14.45	1.53

TABLE X (cont.)

Run No.	Time (Chart Spaces)	Ionization Currents (Chart Units)		
		Lower	Upper	Zero
33B	5	6.85	16.73	1.53
	10	7.58	16.03	1.53
	15	8.20	15.47	1.53
	20	8.73	14.96	1.53
	25	9.17	14.53	1.53
	30	9.54	14.19	1.53
	35	9.87	13.89	1.53
34B	10	4.62	16.33	1.51
	15	5.37	15.83	1.52
	20	6.01	15.23	1.52
	25	6.56	14.86	1.51
	30	7.03	14.42	1.51
	40	7.81	13.70	1.51
	50	8.44	13.13	1.51
	60	8.90	12.69	1.51
35B	10	5.18	14.23	1.53
	15	5.91	13.63	1.53
	20	6.51	13.12	1.53
	25	7.01	12.68	1.53
	30	7.46	12.29	1.53
	35	7.82	11.97	1.53
	40	8.12	11.70	1.53
	45	8.37	11.47	1.53
36B	10	5.49	15.82	1.56
	15	6.31	15.17	1.56
	20	6.99	14.56	1.56
	25	7.60	14.03	1.56
	30	8.11	13.58	1.55
	35	8.52	13.21	1.55
	40	8.84	12.89	1.55
37B	10	5.80	14.10	1.53
	15	6.33	13.64	1.53
	20	6.81	13.21	1.54

TABLE X (cont.)

Run No.	Time (Chart Spaces)	Ionization Currents (Chart Units)		
		Lower	Upper	Zero
	25	7.21	12.83	1.54
	30	7.55	12.50	1.54
	35	7.86	12.21	1.55
	40	8.13	11.97	1.55
38B	5	3.27	18.92	1.54
	10	4.33	18.04	1.54
	15	5.27	17.17	1.54
	20	6.10	16.43	1.54
	25	6.76	15.79	1.54
	30	7.35	15.25	1.54
	35	7.86	14.77	1.54
	40	8.30	14.34	1.54
	45	8.71	13.97	1.54
39B	15	8.16	17.05	1.54
	20	8.76	16.52	1.56
	25	9.28	16.04	1.56
	30	9.73	15.64	1.57
	40	10.45	14.97	1.58
40B	5	3.73	19.90	1.57
	10	4.77	18.94	1.57
	15	5.71	18.10	1.57
	20	6.50	17.36	1.57
	25	7.21	16.72	1.57
	30	7.80	16.14	1.57
	35	8.30	15.66	1.57
	40	8.77	15.23	1.57
	45	9.13	14.85	1.57
41B	10	6.82	17.58	1.56
	15	7.67	16.79	1.55
	20	8.38	16.11	1.55
	25	8.98	15.55	1.54
	30	9.49	15.07	1.53
	35	9.89	14.66	1.52
	40	10.24	14.33	1.51
	45	10.53	14.05	1.50

TABLE X (cont.)

Run No.	Time (Chart Spaces)	Ionization Currents (Chart Units)		
		Lower	Upper	Zero
42B	10	6.76	18.78	1.57
	15	7.78	17.88	1.55
	20	8.61	17.01	1.53
	25	9.27	16.30	1.50
	30	9.83	15.70	1.48
	35	10.25	15.25	1.46
	40	10.63	14.86	1.43
	45	10.93	14.53	1.42
	50	11.19	14.27	1.41
43B	10	6.87	17.37	1.59
	15	7.90	16.39	1.56
	20	8.73	15.54	1.54
	25	9.35	14.86	1.53
44B	2	8.29	17.15	1.59
	5	8.61	16.72	1.58
	10	9.11	16.16	1.57
	15	9.53	15.66	1.56
	20	9.92	15.23	1.55
	25	10.24	14.87	1.54
45B	10	5.40	15.87	1.62
	15	6.25	15.18	1.61
	20	6.94	14.54	1.61
	25	7.50	13.99	1.60
	30	7.98	13.53	1.60
	35	8.36	13.13	1.59
46B	10	5.83	18.54	1.58
	15	6.70	17.92	1.58
	20	7.50	17.34	1.58
	25	8.14	16.80	1.58
	30	8.67	16.34	1.58
47B	5	4.42	18.78	1.57
	10	5.40	17.95	1.57
	15	6.28	17.28	1.57
	20	7.02	16.71	1.57

TABLE X (cont.)

Run No.	Time (Chart Spaces)	Ionization Currents (Chart Units) Lower	Upper	Zero
48B	5	5.76	19.67	1.57
	10	7.10	18.89	1.57
	15	8.12	18.16	1.57
	20	8.97	17.44	1.57
	25	9.64	16.87	1.57
	30	10.22	16.40	1.57
	35	10.68	15.98	1.56
	40	11.06	15.62	1.56
49B	5	4.83	18.67	1.60
	10	6.36	17.54	1.60
	15	7.53	16.72	1.60
50B	5	4.75	17.77	1.62
	10	6.04	16.60	1.62
	15	7.07	15.71	1.62
	20	7.88	14.97	1.62
	25	8.52	14.37	1.62
51B	5	4.25	19.17	1.60
	10	5.52	18.32	1.60
	15	6.56	17.58	1.60
	20	7.37	16.97	1.60
	25	8.08	16.46	1.60
52B	2	3.63	13.92	1.64
	5	4.24	13.31	1.64
	10	5.06	12.47	1.64
	15	5.76	11.84	1.64
53B	2	3.23	19.60	1.59
	5	3.97	18.95	1.59
	10	5.04	18.02	1.59
	15	5.94	17.21	1.59
	20	6.72	16.52	1.59
	25	7.40	15.95	1.59

TABLE X (cont.)

Run No.	Time (Chart Spaces)	Ionization Currents (Chart Units) Lower	Upper	Zero
54B	2	6.00	19.67	1.58
	5	6.72	19.22	1.58
	10	7.70	18.48	1.58
	15	8.53	17.78	1.58
	20	9.22	17.20	1.58
	25	9.82	16.68	1.58
	30	10.28	16.24	1.58
	35	10.68	15.87	1.58
	40	11.03	15.54	1.58
	45	11.35	15.27	1.58
55B	5	4.09	18.84	1.63
	10	5.31	17.89	1.63
	15	6.27	17.15	1.63
	20	7.09	16.47	1.62
56B	3	3.30	19.43	1.65
	6	3.97	18.95	1.65
	10	4.80	18.40	1.65
	15	5.67	17.76	1.65
	20	6.42	17.18	1.66
	25	7.11	16.65	1.66
57B	10	5.83	18.31	1.67
	15	6.85	17.41	1.67
	20	7.69	16.67	1.67
	25	8.37	16.04	1.68
	30	8.97	15.55	1.68
58B	4	6.57	17.88	1.65
	6	7.36	17.18	1.65
	8	8.03	16.57	1.65
	10	8.63	16.03	1.65
59B	2	2.87	18.13	1.58
	5	3.52	17.68	1.58
	10	4.53	16.97	1.58
	15	5.36	16.33	1.57

TABLE X (cont.)

Run No.	Time (Chart Spaces)	Ionization Currents (Chart Units)		
		Lower	Upper	Zero
60B	2	4.32	19.00	1.58
	5	5.36	18.03	1.58
	10	6.74	16.81	1.59
	15	7.85	15.83	1.59
61B	5	4.64	19.94	1.56
	10	5.33	19.50	1.55
	15	5.92	19.10	1.54
	20	6.43	18.71	1.53
	25	6.91	18.32	1.53
	30	7.33	17.94	1.52
	40	8.05	17.24	1.51
	50	8.69	16.63	1.50
	60	9.23	16.13	1.48
	70	9.67	15.73	1.45
62B	5	3.73	19.09	1.55
	10	4.52	18.54	1.55
	15	5.21	18.05	1.55
	20	5.78	17.61	1.54
	25	6.33	17.19	1.54
	30	6.82	16.83	1.53
63B	2	3.81	17.08	1.58
	5	4.55	16.63	1.57
	10	5.59	15.93	1.56
	15	6.44	15.34	1.55
64B	2	3.17	19.19	1.54
	5	4.07	18.44	1.54
	10	5.33	17.40	1.55
	15	6.36	16.55	1.55
65B	2	3.82	19.20	1.52
	5	4.82	18.38	1.52
	10	6.17	17.27	1.52
	15	7.26	16.38	1.53

TABLE X (cont.)

Run No.	Time (Chart Spaces)	Ionization Currents (Chart Units) Lower	Upper	Zero
66B	5	3.12	19.38	1.53
	10	4.12	18.64	1.53
	15	4.94	17.92	1.52
	20	5.68	17.23	1.52
	25	6.36	16.62	1.51
	30	6.93	16.04	1.51
	35	7.43	15.54	1.50
	40	7.87	15.10	1.50
	45	8.27	14.67	1.49
67B	3	5.88	41.59	3.70
	6	7.53	40.27	3.70
	10	9.45	38.58	3.69
	15	11.53	36.62	3.69
	20	13.29	34.93	3.68
	25	14.83	33.36	3.68
	30	16.05	32.14	3.67
	40	18.23	30.20	3.65
68B	3	3.50	16.83	1.53
	6	3.98	16.38	1.53
	10	4.59	15.84	1.53
	15	5.28	15.23	1.53
	20	5.87	14.70	1.53
	25	6.38	14.24	1.53
	30	6.87	13.84	1.53
	35	7.31	13.48	1.53
	40	7.62	13.19	1.53
69B	3	2.60	18.32	1.54
	6	3.20	17.83	1.54
	10	3.91	17.23	1.54
	15	4.71	16.52	1.54
	20	5.40	15.90	1.54
	25	6.02	15.37	1.54
	30	6.55	14.87	1.54
	35	7.04	14.43	1.54
	40	7.50	14.02	1.54

TABLE X (cont.)

Run No.	Time (Chart Spaces)	Ionization Currents (Chart Units)		
		Lower	Upper	Zero
70B	3	6.20	43.69	3.65
	6	7.90	42.43	3.65
	10	9.99	40.81	3.65
	15	12.23	38.87	3.65
	20	14.09	37.15	3.65
	25	15.66	35.60	3.65
	30	17.07	34.28	3.65
	35	18.26	33.18	3.65
	40	19.27	32.21	3.65
71B	2	6.77	46.83	3.69
	4	8.56	45.33	3.69
	6	10.25	43.87	3.69
	8	11.77	42.46	3.69
	10	13.14	41.24	3.69
	12	14.38	40.13	3.69
	14	15.52	39.12	3.69
	16	16.55	38.14	3.69
	18	17.47	37.27	3.69
	20	18.31	36.48	3.69
72B	5	3.23	18.64	1.53
	10	4.37	17.60	1.50
	15	5.30	16.62	1.48
	20	6.07	15.73	1.45
	25	6.78	15.03	1.40
	30	7.33	14.40	1.35
	35	7.83	13.90	1.30
	40	8.25	13.47	1.25
	45	8.62	13.10	1.20
73B	2	6.78	17.67	1.53
	4	7.38	17.17	1.53
	6	7.87	16.75	1.53
	8	8.30	16.37	1.53
	10	8.66	16.00	1.53
	12	9.00	15.69	1.53
	14	9.32	15.42	1.53
	16	9.60	15.15	1.53
	18	9.86	14.93	1.53

TABLE X (cont.)

Run No.	Time (Chart Spaces)	Ionization Currents (Chart Units)		
		Lower	Upper	Zero
74B	10	5.81	19.17	1.60
	15	6.50	18.65	1.60
	20	7.17	18.17	1.59
	25	7.79	17.77	1.58
	30	8.33	17.42	1.58
	35	8.80	17.04	1.57
	40	9.18	16.68	1.57
	45	9.52	16.32	1.56
	50	9.80	15.95	1.55
75B	10	6.29	19.06	1.56
	15	7.06	18.56	1.56
	20	7.75	18.07	1.56
	25	8.35	17.58	1.56
	30	8.88	17.12	1.56
	35	9.35	16.68	1.56
	40	9.74	16.34	1.56
	45	10.13	16.00	1.56
	50	10.45	15.72	1.56
76B	3	13.18	49.28	3.67
	6	15.23	47.64	3.67
	10	17.63	45.75	3.67
	15	20.10	43.63	3.67
	20	22.12	41.82	3.67
	25	23.77	40.24	3.67
	30	25.17	38.95	3.67
	35	26.26	37.92	3.67
	40	27.23	37.03	3.67
77B	3	5.42	18.85	1.57
	6	5.89	18.46	1.57
	10	6.50	17.99	1.57
	15	7.15	17.48	1.57
	20	7.69	16.98	1.57
	25	8.18	16.56	1.57
	30	8.63	16.18	1.57
	35	9.02	15.86	1.57
	40	9.42	15.56	1.57

TABLE X (cont.)

Run No.	Time (Chart Spaces)	Ionization Currents(Chart Units) Lower	Upper	Zero
78B	3	5.26	19.26	1.58
	6	5.94	18.90	1.58
	10	6.75	18.40	1.58
	15	7.66	17.79	1.58
	20	8.42	17.23	1.58
	25	9.02	16.68	1.58
	30	9.57	16.22	1.58
79B	3	5.27	19.49	1.56
	6	5.80	19.04	1.56
	10	6.47	18.49	1.56
	15	7.18	17.87	1.56
	20	7.83	17.31	1.56
	25	8.39	16.81	1.56
	30	8.87	16.38	1.56
	35	9.29	16.02	1.56
	40	9.68	15.68	1.56
80B	3	2.08	19.23	1.55
	6	2.50	18.90	1.55
	10	3.03	18.50	1.55
	15	3.67	17.99	1.55
	20	4.23	17.52	1.55
	25	4.74	17.06	1.55
	30	5.18	16.64	1.55
	35	5.63	16.25	1.55
	40	6.03	15.87	1.55
	45	6.42	15.55	1.55
	50	6.75	15.23	1.55
	55	7.07	14.93	1.55
81B	3	2.76	19.80	1.57
	6	3.63	19.18	1.57
	10	4.63	18.38	1.57
	15	5.72	17.43	1.57
	20	6.62	16.57	1.57
	25	7.37	15.90	1.57
	30	7.99	15.28	1.57

TABLE X (cont.)

Run No.	Time (Chart Spaces)	Ionization Currents (Chart Units)		
		Lower	Upper	Zero
82B	3	2.37	15.87	1.56
	6	2.91	15.37	1.56
	10	3.55	14.77	1.56
	15	4.25	14.12	1.56
	20	4.85	13.54	1.56
	25	5.39	13.04	1.56
	30	5.84	12.63	1.56
	35	6.24	12.25	1.56
	40	6.63	11.93	1.56
83B	3	2.53	18.68	1.55
	6	3.19	18.18	1.55
	10	3.94	17.61	1.55
	15	4.81	16.93	1.55
	20	5.56	16.34	1.55
	25	6.23	15.83	1.55
	30	6.84	15.37	1.55
	35	7.35	14.98	1.55
	40	7.77	14.63	1.55
84B	3	6.65	45.15	3.71
	6	8.60	43.24	3.71
	10	10.86	41.05	3.71
	15	13.29	38.67	3.71
	20	15.35	36.73	3.71
	25	17.03	35.11	3.70
	30	18.43	33.74	3.70
	35	19.54	32.58	3.70
	40	20.53	31.65	3.70
85B	5	2.73	18.99	1.56
	10	3.52	18.46	1.56
	15	4.27	17.93	1.56
	20	4.92	17.42	1.56
	25	5.48	16.92	1.56
	30	6.01	16.43	1.56
	35	6.50	16.00	1.56
	40	6.93	15.62	1.56
	45	7.33	15.25	1.56
	50	7.68	14.91	1.56

TABLE X (cont.)

Run No.	Time (Chart Spaces)	Ionization Currents (Chart Units)		
		Lower	Upper	Zero
86B	3	2.21	18.87	1.55
	6	2.71	18.44	1.55
	10	3.33	17.91	1.55
	15	4.06	17.29	1.55
	20	4.70	16.73	1.55
	25	5.29	16.23	1.56
	30	5.83	15.77	1.56
	35	6.31	15.37	1.56
	40	6.72	14.97	1.56
	45	7.12	14.63	1.56
87B	5	11.00	46.50	3.75
	10	13.48	45.26	3.75
	15	15.65	43.92	3.75
	20	17.57	42.59	3.75
	25	19.20	41.37	3.75
	30	20.65	40.33	3.75
	35	21.93	39.37	3.75
	40	23.03	38.47	3.75
	45	24.04	37.71	3.75
88B	3	7.93	47.26	3.78
	6	10.67	45.48	3.78
	10	13.74	43.19	3.78
	15	16.83	40.56	3.78
	20	19.22	38.47	3.78
	25	21.17	36.82	3.78
	30	22.73	35.47	3.78
	35	23.89	34.36	3.78
89B	10	17.36	49.90	3.67
	15	19.65	48.19	3.66
	20	21.58	46.82	3.65
	25	23.27	45.56	3.64
	30	24.77	44.28	3.62
	35	26.09	43.25	3.60
	40	27.17	42.26	3.58
	45	28.17	41.45	3.56
	50	29.03	40.82	3.54

TABLE X (cont.)

Run No.	Time (Chart Spaces)	Ionization Currents (Chart Units)		
		Lower	Upper	Zero
90B	3	14.53	48.44	3.68
	6	16.45	47.26	3.68
	10	18.75	45.84	3.68
	15	21.13	44.25	3.68
	20	23.11	42.82	3.68
	25	24.81	41.65	3.68
	30	26.17	40.59	3.68
	33	26.92	40.06	3.68
91B	2	14.13	48.76	3.65
	4	15.86	47.57	3.65
	6	17.37	46.50	3.65
	10	20.06	44.54	3.65
	15	22.76	42.50	3.65
	20	24.87	40.78	3.65
	25	26.52	39.57	3.65
	30	27.92	38.63	3.65
	35	28.95	37.83	3.65
92B	3	14.24	46.93	3.69
	6	16.14	45.39	3.69
	10	18.39	43.65	3.70
	15	20.63	41.80	3.70
	20	22.49	40.33	3.71
	25	24.11	39.14	3.71
	30	25.42	38.11	3.72
	35	26.50	37.20	3.73
	40	27.40	36.59	3.74
93B	3	13.65	47.46	3.78
	6	15.33	46.27	3.78
	10	17.34	44.82	3.78
	15	19.47	43.14	3.78
	20	21.26	41.62	3.78
	25	22.76	40.36	3.78
	30	24.03	39.33	3.78
	35	25.12	38.41	3.78
	40	26.02	37.66	3.78

TABLE X (cont.)

Run No.	Time (Chart Spaces)	Ionization Currents (Chart Units) Lower	Upper	Zero
94B	3	12.13	47.97	3.71
	6	14.27	46.09	3.71
	9	16.16	44.47	3.71
	12	17.86	43.07	3.71
	15	19.28	41.78	3.71
	20	21.29	39.92	3.71
	25	23.01	38.46	3.71
	30	24.35	37.20	3.71
	35	25.41	36.25	3.71
95B	3	6.60	46.72	3.72
	6	8.44	45.02	3.72
	10	10.63	43.08	3.72
	15	13.05	41.02	3.72
	20	15.13	39.23	3.72
	25	16.88	37.66	3.72
	30	18.34	36.30	3.72
	35	19.55	35.19	3.72
	40	20.64	34.19	3.72
96B	3	6.89	46.63	3.75
	6	9.53	44.92	3.74
	9	11.83	43.24	3.73
	12	13.84	41.60	3.72
	15	15.57	40.15	3.71
	20	18.04	38.08	3.70
	25	20.00	36.37	3.69
	30	21.47	34.97	3.68
	35	26.68	33.75	3.67
97B	3	6.36	48.47	3.64
	6	8.27	46.95	3.64
	10	10.58	45.08	3.63
	15	13.13	43.05	3.62
	20	15.23	41.29	3.61
	25	17.04	39.83	3.60
	30	18.64	38.57	3.59
	35	20.00	37.46	3.58
	40	21.15	36.49	3.57

TABLE X (cont.)

Run No.	Time (Chart Spaces)	Ionization Currents (Chart Units)		
		Lower	Upper	Zero
98B	1	5.76	39.17	3.74
	3	7.48	37.92	3.74
	6	9.79	36.26	3.74
	9	11.75	34.75	3.73
	12	13.52	33.37	3.73
	15	14.96	32.20	3.73
	20	16.91	30.53	3.72
	25	18.40	29.33	3.72
	30	19.53	28.28	3.72
99B	2	5.36	45.00	3.75
	5	7.19	43.23	3.74
	10	9.84	40.66	3.73
	15	12.13	38.43	3.72
	20	14.03	36.55	3.71
	25	15.65	34.97	3.70
	30	17.04	33.60	3.69
	35	18.19	32.57	3.68
	40	19.20	31.75	3.66
100B	3	6.81	45.13	3.63
	6	9.54	42.74	3.63
	9	11.99	40.61	3.63
	12	14.01	38.68	3.63
	15	15.77	37.06	3.63
	18	17.23	35.66	3.63
	21	18.47	34.53	3.63
	24	19.49	33.49	3.63
	27	20.42	32.65	3.63
101B	1	7.80	48.22	3.74
	3	10.32	46.06	3.73
	6	13.60	43.33	3.72
	9	16.24	40.92	3.71
	12	18.46	38.97	3.70
	15	20.23	37.35	3.69
	18	21.71	35.95	3.68
	21	22.84	34.82	3.67
	24	23.77	33.87	3.67

TABLE X (cont.)

Run No.	Time (Chart Spaces)	Ionization Currents (Chart Units)		
		Lower	Upper	Zero
102B	3	7.38	46.91	3.67
	6	9.52	45.16	3.67
	10	12.08	43.18	3.67
	15	14.58	40.97	3.67
	20	16.80	39.18	3.67
	25	18.61	37.64	3.67
	30	20.05	36.35	3.67
	35	21.27	35.18	3.67
	40	22.38	34.25	3.67
103B	3	7.08	44.87	3.73
	6	9.28	43.13	3.73
	10	11.87	41.16	3.73
	15	14.58	39.02	3.73
	20	16.76	37.17	3.73
	25	18.57	35.63	3.73
	30	19.98	34.29	3.73
	35	21.14	33.28	3.73
	40	22.16	32.45	3.73
104B	3	7.16	47.67	3.67
	6	9.16	45.97	3.67
	10	11.53	43.88	3.67
	15	13.98	41.70	3.67
	20	16.08	39.89	3.67
	25	17.82	38.33	3.67
	30	19.42	36.94	3.67
	35	20.63	35.83	3.67
	40	21.64	34.85	3.67
105B	3	8.30	46.24	3.70
	6	10.41	44.41	3.70
	10	12.84	42.16	3.70
	15	15.35	39.84	3.70
	20	17.47	37.95	3.70
	25	19.16	36.33	3.70
	30	20.57	35.03	3.70
	35	21.72	33.93	3.70
	40	22.57	32.99	3.70

TABLE X (cont.)

Run No.	Time (Chart Spaces)	Ionization Current (Chart Units)		
		Lower	Upper	Zero
106B	1	8.26	49.34	3.83
	3	10.71	47.29	3.82
	6	13.94	44.43	3.81
	9	16.65	41.94	3.80
	12	18.71	39.97	3.79
	15	20.41	38.34	3.78
	20	22.74	36.24	3.77
	25	24.34	34.66	3.76
	30	25.53	33.57	3.75

APPENDIX B

SAMPLE CALCULATION FOR DIFFUSION RUN 84B

Data

Date: December 8, 1959

Major Components: H_2, A

Mole Fraction H_2: 0.624

Operating Pressure: Four readings at 763 PSIG

Operating Temperature:

Thermocouple 3: Four readings at 1.410 M.V.

Thermocouple 5: Four readings at 1.408 M.V.

Charging Data:

Cell pressurized to 422 PSIG with Sample G.

Cell pressurized to 455 PSIG with Sample 11.

Cell pressurized to 800 PSIG with Sample G.

Upper tubing entrance flushed to cell pressure of 763 PSIG.

Recorder Chart Speed: 6 inches per hour.

Voltage Range: 2.0 volts.

Ionization Currents Read From Figure 5, also in Table X.

Time	Uncorrected Ionization Currents (Chart Units)		
(Chart Spaces)	Upper	Lower	Zero
3	45.15	6.65	3.71
6	43.24	8.60	3.71
10	41.05	10.86	3.71
15	38.67	13.29	3.71
20	36.73	15.35	3.71
25	35.11	17.03	3.70
30	33.74	18.43	3.70
35	32.58	19.54	3.70
40	31.65	20.53	3.70

Background Currents (Chart Units)

Upper Chamber, 0.26 (50 space chart units)

Lower Chamber, 0.09 (50 space chart units)

CALCULATIONS:

Atmospheric Pressure = 14 PSIA

Gauge Correction = -8 PSIA

Absolute Run Pressure, P = 763 + 14 - 8 = 769 PSIA

Absolute Run Temperature

Upper Thermocouple (3) T = 308.3°K (35.1°C)

Lower Thermocouple (5) T = 308.2°K (35.0°C)

Compressibility Factor, $Z = PV/RT = 1.018$

$R = 1.2059$ (psia)(l)/(gram mole)(°K)

$$\text{Density, } \rho = \frac{P}{ZRT} = \frac{(769)}{(1.018)(1.2059)(308.2)}$$

$$= 2.033 \frac{\text{gm. moles}}{\text{liter}}$$

THE CONCENTRATION, C, AT CONSTANT DENSITY IS PROPORTIONAL TO THE CORRECTED IONIZATION CURRENT, I, FOR EACH CHAMBER.

$$C_{Upper} \alpha f \cdot I_{Upper}$$

$$C_{Lower} \alpha I_{Lower}$$

FOR THE TIME OF THREE CHART SPACES (ONE-SIXTH OF AN HOUR)

$$I_{Upper} = (I_{Chart})_{Upper} - (Background)_{Upper} - Zero$$

$$= 41.15 - 0.26 - 3.71 = 41.18$$

$$I_{Lower} = (I_{Chart})_{Lower} - (Background)_{Lower} - Zero$$

$$= 6.65 - 0.09 - 3.71 = 2.85$$

f = Ratio of ionization currents with same HT concentration in both chambers

f = 0.958 (for diffusion Path B in cell)

$$(f \cdot I_{Upper} - I_{Lower}) = (0.958)(41.18) - 2.85 = 36.600$$

TIME (Chart Spaces)	$f \cdot I_{Upper} - I_{Lower}$ (Chart Units)
3	36.600
6	32.821
10	28.463
15	23.753
20	19.834
25	16.602
30	13.889
35	11.668
40	9.787

FIGURE 7 IS THE SEMI-LOG PLOT OF THESE POINTS.

THE SLOPE OF THE RESULTING STRAIGHT LINE IS:

$$SLOPE = -0.01559 \frac{1}{\text{Time Chart Units}}$$

THE CELL CONSTANT WITH DIFFUSION PATH B IN PLACE

$$K = 0.01025 \text{ cm}^{-2}$$

$$\text{UNIT CONVERSION FACTOR} = \frac{\left(3 \frac{\text{Chart Spaces}}{\text{Inch}}\right)\left(2.303 \frac{\log_{10}}{\log_e}\right)}{3600 \text{ sec./hr.}} = \frac{2.303}{1200}$$

THE DIFFUSION COEFFICIENT, D:

$$D = \frac{(2.303)(\text{Slope})(\text{Chart Speed})}{(1200)(K)} = \frac{(2.303)(0.01559)(6)}{(1200)(0.01025)}$$

$$D = 0.0175 \text{ cm}^2/\text{sec}$$

$$D\rho = (0.0175)(2.033) = 0.0356 \frac{\text{cm}^2}{\text{sec}} \cdot \frac{\text{gm.moles}}{\text{liter}}$$

COMPUTED BY METHOD OF LEAST SQUARES:

$$D = 0.01753 \text{ cm}^2/\text{sec}$$

$$\rho = 2.033 \text{ gm. moles/liter}$$

$$D\rho = 0.03562 \frac{\text{cm}^2}{\text{sec}} \cdot \frac{\text{moles}}{\text{liter}}$$

$$y_{H_2} = 0.624$$

$$y_A = 0.376$$

$$T = 35.0°C$$

APPENDIX C

PREPARATION AND ANALYSIS OF GAS SAMPLES

For the diffusion investigation, it was necessary to prepare several samples of mixed gases of known concentrations.

NON-RADIOACTIVE GAS SAMPLES

Three samples of mixtures of hydrogen and carbon dioxide were prepared having approximately 19, 63, and 93 molecular percent of hydrogen respectively. Similarly, three samples of mixtures of hydrogen and argon were prepared having approximately 19, 62, and 93 molecular percent of hydrogen respectively. These samples were prepared from cylinders of nearly pure hydrogen, carbon dioxide, and argon having manufacturers stated purities of 99.8 percent, 99.9 percent, and 99.6 percent respectively. These gases were purchased from the Matheson Company, Incorporated.

The samples were prepared by adding either carbon dioxide or argon to an evacuated Number 3 gas cylinder to a pressure dictated by the desired molecular fraction, and then pressurizing with hydrogen to 1500 psia. The resulting samples were then equilibrated and analyzed to determine the exact molecular fractions. Mixtures of hydrogen and carbon dioxide were analyzed with an Orsat-type apparatus in which the carbon dioxide was absorbed in strong caustic. Mixtures of hydrogen and argon were analyzed by a mass spectrometer.

Table XI is a presentation of the sample analysis data taken before and after the diffusion runs for mixtures of hydrogen and carbon dioxide and after diffusion runs for hydrogen-argon mixtures.

TABLE XI

GAS SAMPLE ANALYSES

Sample	Date	Orsat Vol. Data Initial	Orsat Vol. Data Final	Percent H_2	Percent CO_2	Percent A	Analysis Method
A	7-9-59	82.88	77.31	93.28	6.72	-- --	Orsat CO_2 Absorption
A	7-12-59	87.48	81.66	93.35	6.65	-- --	" "
A	9-19-59	92.05	85.86	93.28	6.72	-- --	" "
A	9-19-59	86.74	80.93	93.30	6.70	-- --	" "
A	9-20-59	86.88	81.00	93.23	6.77	-- --	" "
C	7-7-59	81.30	51.08	62.83	37.17	-- --	" "
C	9-13-59	86.82	54.52	62.80	37.20	-- --	" "
C	9-14-59	87.13	54.65	62.72	37.28	-- --	" "
D	7-16-59	91.78	17.32	18.85	81.15	-- --	" "
D	7-16-59	87.97	16.66	18.94	81.06	-- --	" "
D	10-10-59	86.52	16.38	18.93	81.07	-- --	" "
D	10-12-59	89.96	16.98	18.88	81.12	-- --	" "
E	1- -60	-- --	-- --	92.55	-- --	7.45	Mass Spec. No. 5364
F	1- -60	-- --	-- --	19.47	-- --	80.53	Mass Spec. No. 5337
G	1- -60	-- --	-- --	63.36	-- --	37.64	Mass Spec. No. 5338

RADIOACTIVE SAMPLE PREPARATION

Radioactive samples were prepared from the samples of the above mixtures by addition of small measured amounts of tritiated hydrogen to separate portions of each gas mixture in smaller sample bottles. With the knowledge available at the time, it was necessary to prepare the radioactive samples accurately since the response of the equipment to tritium disintegrations was not known. The range of the equipment may not have extended into a region where the ratio of concentration of tritium to current produced was constant. In this event, the accurate calibrations afforded by accurate samples would be necessary for data analysis.

Gaseous tritium, T_2, is available for purchase from the United States Atomic Energy Commission in reasonably pure state, the chief impurity being traces of daughter compounds which are produced by its radioactive disintegration. The radioactive strength of pure tritium is about two and one-half curies per cubic centimeter of gas at one atmosphere of pressure and zero degrees centigrade temperature. Due to this relatively high strength for a small quantity of gas, it was found necessary to dilute the tritium to considerably lower concentrations, first with hydrogen and subsequently with the hydrogen-carbon dioxide and hydrogen-argon mixtures to be studied.

These dilutions were carried out in the gas dilution equipment schematically shown in Figure 24. Tritium was diluted to known molecular fractions with this equipment. The basic idea involves the

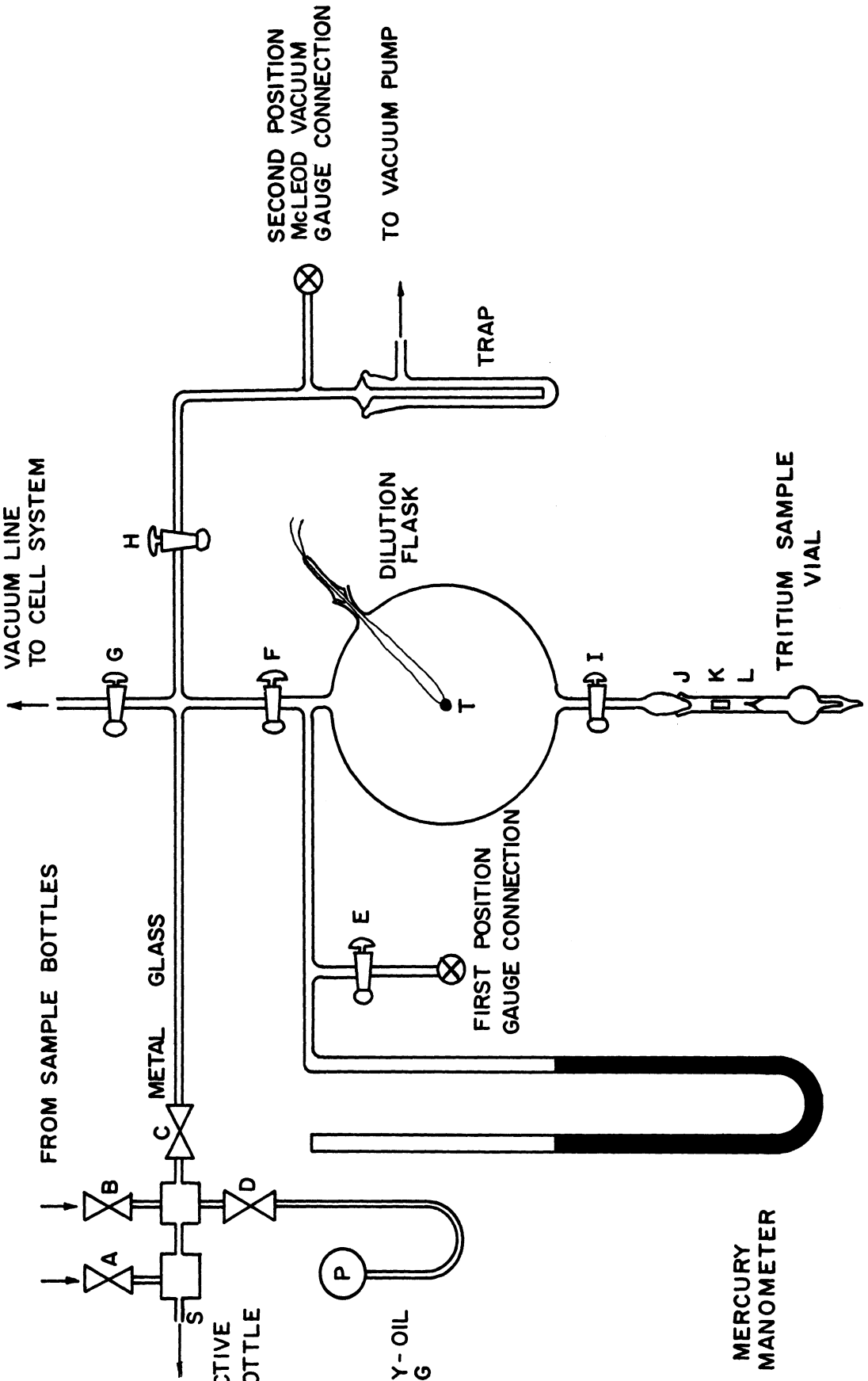

Figure 24. The Tritium Dilution System.

the measurement of the pressure and temperature of a known volume of gas and thereby determining its mass by a suitable relation of state.

The dilution equipment was made up of two sections, the low pressure section for dilutions below one atmosphere absolute pressure, and the high pressure section. The former section was constructed of steel high-pressure tubing and fittings. The two sections were connected by a short length of high vacuum rubber tubing. Pressures were measured in the low pressure section by means of a cathetometer and mercury manometer and by a McLeod vacuum gauge. In the high pressure section pressures were measured by a bourdon tube pressure gauge. Temperatures were measured by means of a thermocouple and portable potentiometer. Both sections were constructed in order that they be relatively leak-tight. The glass section was tested to retain a pressure of one micron of mercury without noticeable increase in pressure for one hour after being isolated from the vacuum pump. The high pressure section was tested to retain gaseous hydrogen at a pressure of 1000 pounds per square inch without noticeable decrease in pressure for a day after being isolated from the gas source.

The following description refers to Figure 24. The tritium was shipped in two small glass vials each with an easily broken finely drawn glass tip (L) inside of the exit neck. Upon receipt of the vials, a female ground glass tapered joint was fused to the exit neck of each vial. This joint matched the male joint (J) located below the dilution flask. When a tritium dilution was made, a vial was connected

to the low pressure dilution section by this ground-glass joint (J) with a small piece of iron (K) resting in the exit neck of the vial on the unbroken glass tip. The McLeod macuum gauge was placed in its first position as located in Figure 24 and with the connecting valve (C) between the high and low pressure sections closed, the glass section was evacuated to less than one micron of mercury absolute pressure.

With stopcock (F) closed and stopcock (I) open, the piece of iron (K) was elevated by a magnet and allowed to fall, breaking the glass tip (L) and causing the tritium to expand into the evacuated dilution flask, mercury manometer tube, and McLeod gauge. After a suitable waiting period, stopcock (I) was closed and the pressure and temperature in the dilution flask were measured using the McLeod gauge and the thermocouple (T), thus determining the total mass of tritium in the enclosed known volume.

After evacuation of the remainder of the low pressure section together with the high pressure section, throttling valve (C) and stopcocks (H) and (E) were closed, and with stopcock (F) open, hydrogen was carefully expanded into the glass system through valve (C) diluting the tritium and bringing the pressure in the dilution flask up to slightly less than one atmosphere. Pressure and temperature measurements were made using the mercury manometer and thermocouple and thereby the extent of dilution was determined quantitatively.

Further dilution was effected by allowing determined amounts of this hydrogen-diluted tritium to expand into evacuated steel sample bottles which were then pressurized with hydrogen or mixtures of hydrogen and carbon dioxide or hydrogen and argon. Since the amount of radioactive sample from the dilution flask was very small with respect to the amount of non-radioactive sample in the sample bottle, the resulting radioactive mixture was almost exactly the same concentration as the non-radioactive sample. The radioactive mixture was, however, slightly rich in hydrogen, the light component.

Table XII is a list of the radioactive samples prepared by dilution of the two vials of tritium with hydrogen, hydrogen-carbon dioxide mixtures and hydrogen-argon mixtures. Samples 2, 3 and 5 were prepared for use in the hydrogen-carbon dioxide diffusion runs. Samples 6-12 were prepared to be used without further dilution for calibration of the diffusion cell for ionization current-tritium concentration relationships. Samples 13-16 were prepared for use in the hydrogen and hydrogen-argon diffusion runs.

TABLE XII

RADIOACTIVE SAMPLES PREPARED
HYDROGEN-CARBON DIOXIDE, FIRST TRITIUM VIAL

Sample	Percent H_2	Total Moles	Moles HT X 10^7	Rad. Strength, $\frac{\text{Curies}}{\text{GM. Mole}}$
2	62.8	0.0948	5.27	.322
3	18.9	0.0955	4.99	.303
5	93.3	0.1334	5.51	.240
6	62.8	1.264	12.72	.0292
6A	62.8	1.242	7.74	.0181
7	62.8	1.311	0.568	.00126
8	93.3	1.196	0.602	.00146
9	62.8	1.324	2.85	.00624
11	18.9	0.832	0.577	.00201
12	62.8	0.773	0.419	.00157

HYDROGEN-ARGON, SECOND TRITIUM VIAL

13	100	1.015	142.8	.407
14	19.5	0.937	111.2	.344
15	62.4	0.978	67.6	.200
16	92.6	1.167	73.2	.182

APPENDIX D

CALIBRATION OF DIFFUSION CELL FOR HT CONCENTRATION

At the onset of the experimental work presented in this dissertation there was no information available concerning the ability of radiation caused by the radioactive disintegration of tritium to cause ionization in gases at high pressures. It was not known what concentrations were necessary to cause detectable ionization currents in an ionization chamber at these pressures. For this reason a study of concentration-ionization current relationships was made with the diffusion cell before any diffusion determinations were made. Information was desired concerning a molecular fraction of tritium, if there was one, below which there was a direct proportionality between tritium concentration and the ionization current produced in the diffusion cell within the desired experimental pressure range.

Radioactive samples 6-12 were prepared for use in these ionization current calibrations. These samples were of known varying radioactive strengths or known tritium molecular fraction. For a calibration run, the sample was compressed into the diffusion cell by means of the pressurizing equipment to an initial pressure of greater than 5000 pounds per square inch. Ionization currents from each cell chamber were

determined and recorded with the current measuring circuit and recording potentiometer. The pressure was decreased to about 500 pounds per square inch in about five equal steps, the ionization currents for each chamber being measured at each constant pressure step. The calibrations were carried out at 35° centigrade with samples of H_2-CO_2 containing 62.8 percent hydrogen of four different known tritium molecular fractions.

Three different results were derived from the ionization current calibration data of which two were actually used in the determination of diffusion coefficients. These three were: 1) the tritium concentration-ionization current relationships presented in Figure 25, 2) the ratio of chamber sensitivities with the chambers containing the same molecular fraction of tritium as presented in Figure 26, 3) the absolute ionization current for each chamber as a function of pressure as presented in Figure 27 for one calibration run.

In Figure 25 the ratio of concentration of tritium to ionization current produced in the lower chamber is plotted versus the cell pressure. If the concentration were proportional to the current for all four sample concentrations at all pressures within the range of the abcissa, the points for all four calibration molecular fractions would fall along the same line. This fact is true for the lower pressures, but as the pressure is increased, the lines representing the two higher

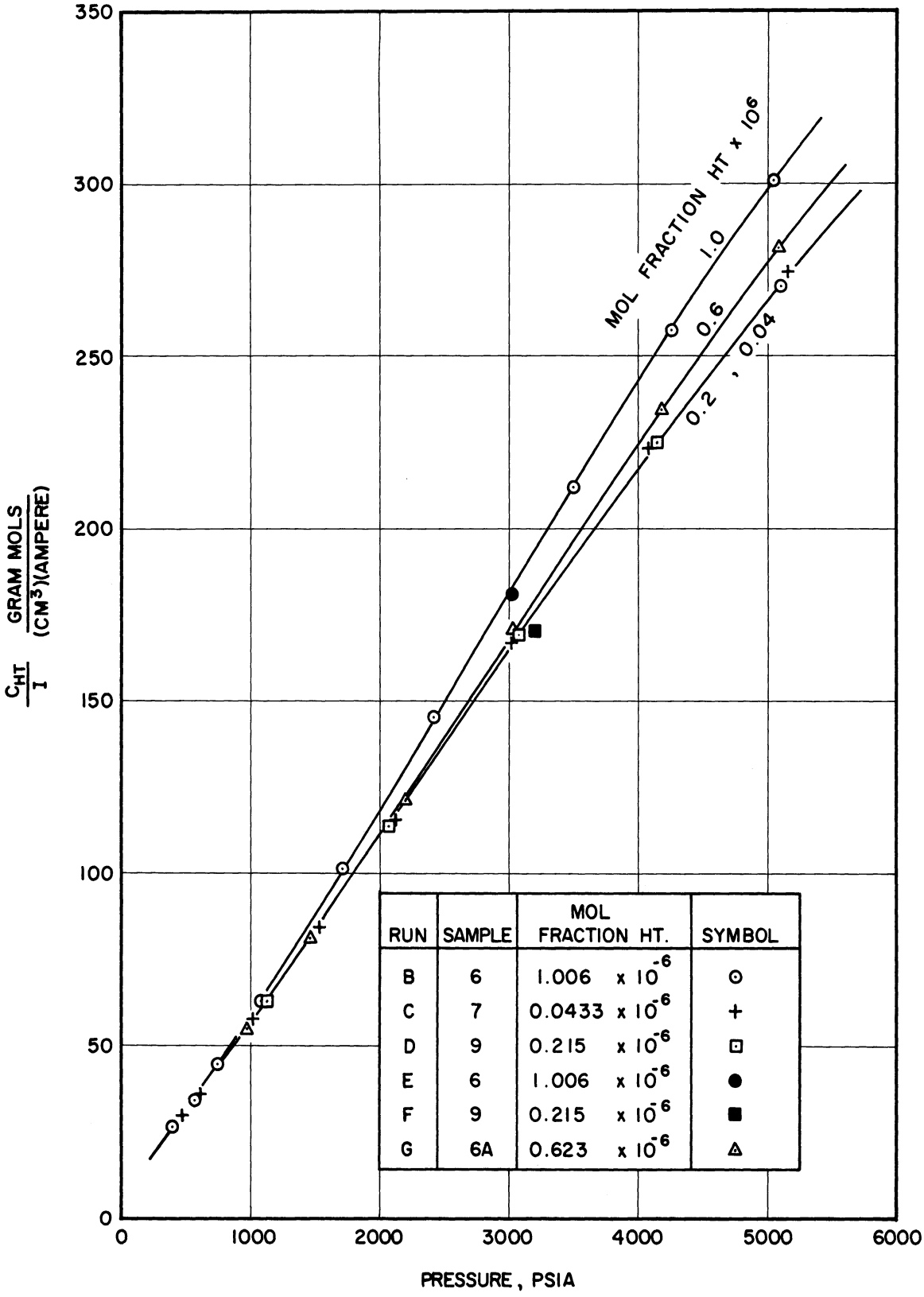

Figure 25. Concentration-Current Ratio HT-H_2-CO_2, 35°C.

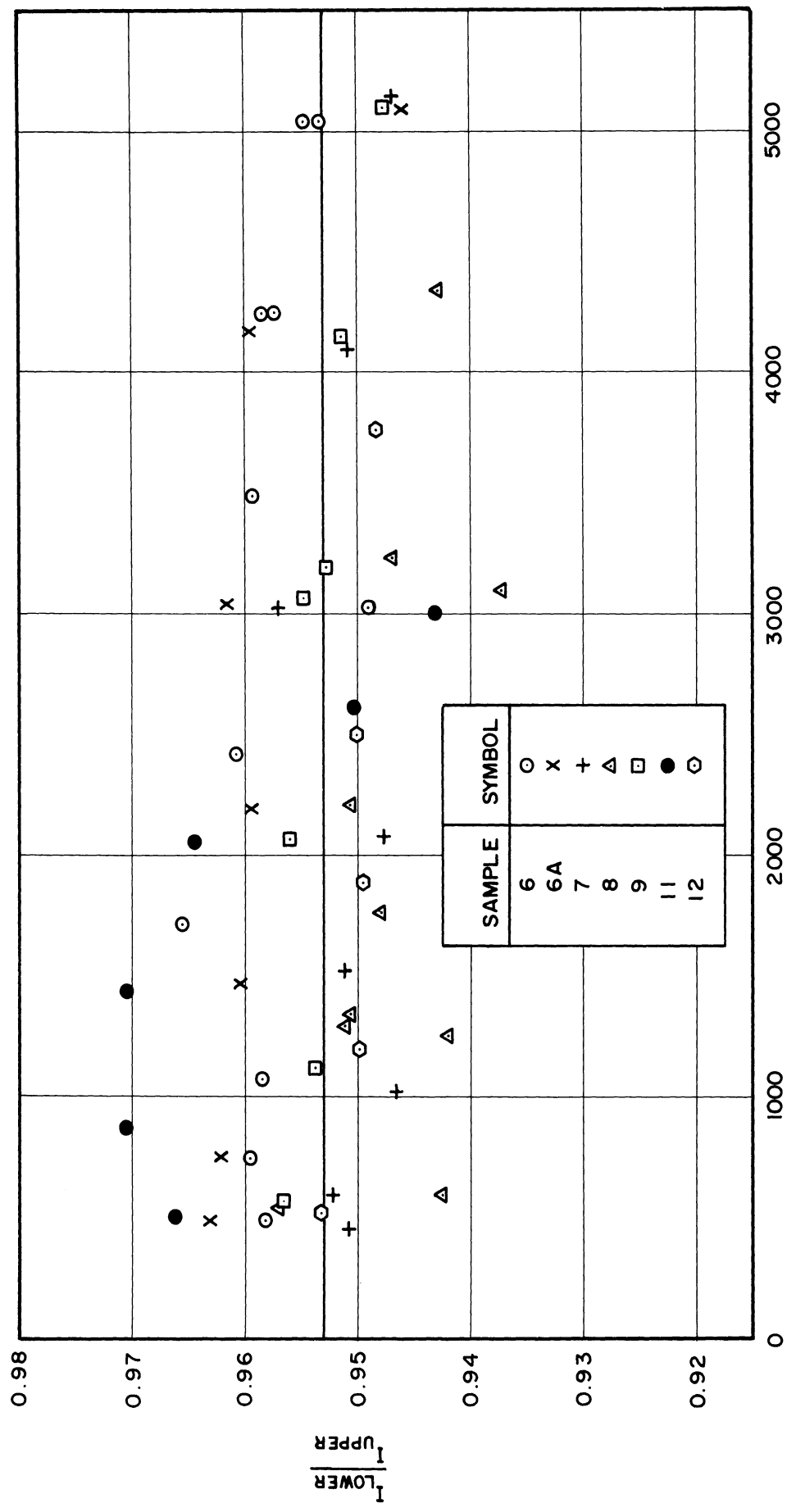

Figure 26. Ionization Current Ratio for Equal Concentration Both Chambers.
Diffusion Path A

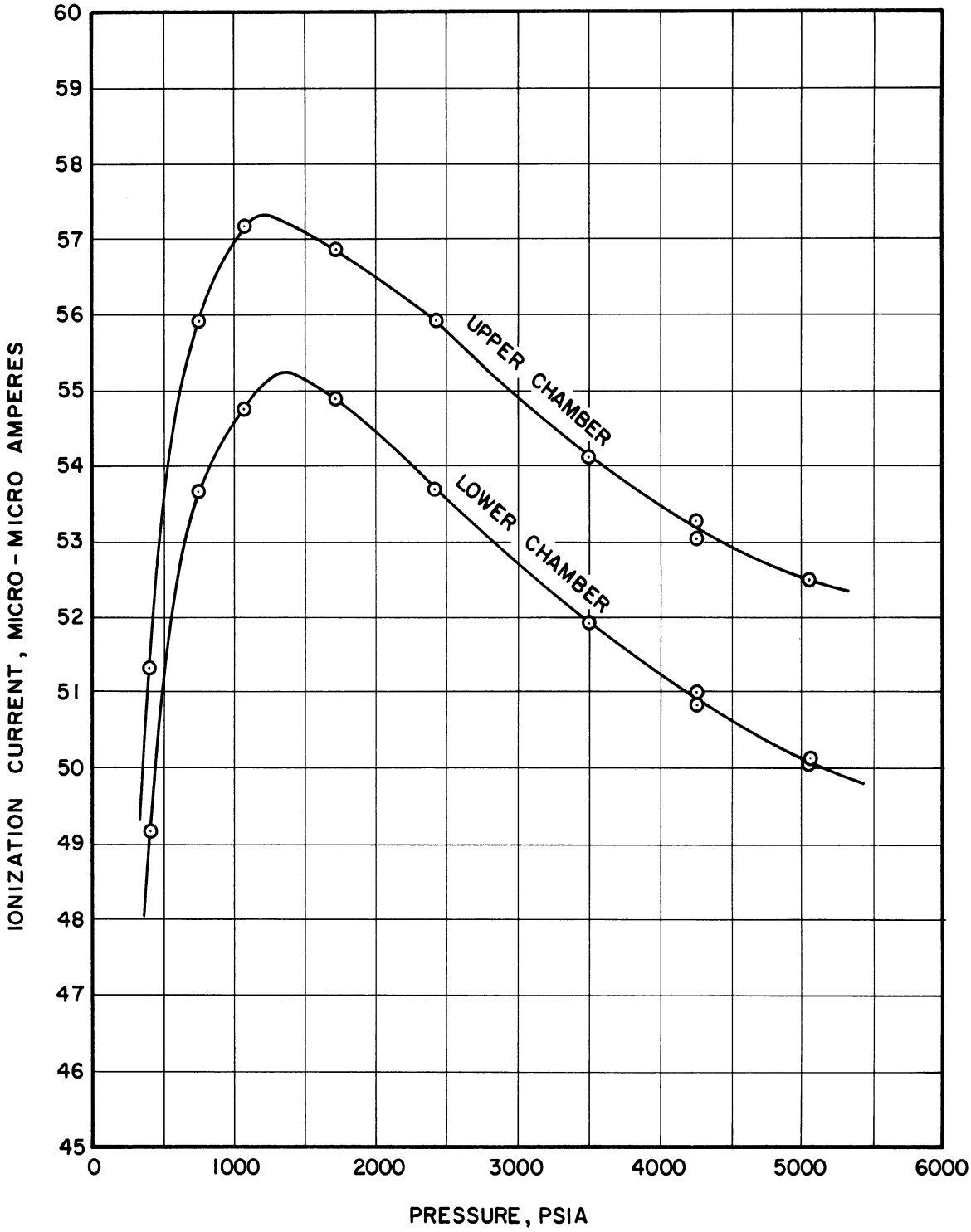

Figure 27. Ionization Current-Pressure Relation for Diffusion Cell HT-H_2-CO_2 at 35°C. HT Mol Fraction = 1.006×10^{-6}.

fraction samples split off from the line representing the proportionality, first the highest fraction and then the next highest fraction. The two lower molecular fraction tritium samples fall along the same line, the line of proportionality, for the entire pressure range studied. This indicates that as long as diffusion measurements were made using molecular fractions of tritium below the molecular fraction of Sample 9, the proportionality would hold between the concentration of tritium and the ionization current produced in the chambers. The currents in question quite fortunately were convenient to measure with the apparatus available. Had the measurements had to be made on more concentrated samples the calculations would have been greatly enhanced.

The ratio of sensitivities of the two cell ionization chambers was the second bit of information necessary from the ionization current calibrations in order to determine the diffusion coefficients. It was certainly conceivable that the two chambers would respond differently to the same concentration of tritium. Figure 26 is a plot of the ratio of the current from the lower chamber to the current from the upper chamber, when both chambers contained the same concentration of tritium, versus pressure. Although the scatter appears to be considerable, the actual variance is only about plus or minus about one and one-half percent of a mean value. Note that the mean value, about 0.953, is very close to

the ratio of the chamber volumes when diffusion path A is installed in the diffusion cell. Spot check values of the ratio of sensitivities of the two ionization chambers when diffusion path B is installed indicate that the ratio is 0.958 which is close to the ratio of the chamber volumes with this path in place. Chou [9] suggests that this sensitivity-volume ratio relationship occurs because for larger volume chambers there is less chance for ions to migrate to the chamber walls.

The third result derived from the ionization current calibrations is interesting although not essential to the diffusion determinations. It is included mainly for this reason and because the trends shown reflect upon the accuracy of the calibration determinations. Figure 27 is a plot of the absolute currents from the two chambers of the diffusion cell during one calibration run as pressure is reduced by steps with a constant molecular fraction of tritium sample in both chambers. As pressure is decreased, the current in each chamber increases and goes through a maximum at about 1500 pounds per square inch, the maximum for different samples occurring at different pressures that seem related to the molecular fractions of tritium in the samples. The currents then rapidly decrease toward zero for zero pressure of radioactive sample in the cell. This behavior might be explained due to two phenomena which occur simultaneously but to different extents at different gas densities.

At low pressures as the quantity of gas in a confined chamber is increased, also therefore the quantity of radioactive material is increased, the conductivity of the gas due to ions formed by radioactive disintegration might be expected to increase proportionately to the amount of radioactivity present. However, as the pressure increases and molecules are forced closer together, it becomes more difficult for ions to migrate to the walls and be collected before they are reunited. This phenomenon would tend to reduce the currents below the proportionality and pass them through a maximum as the effect becomes more important than the increasing radioactivity. That this maximum occurs at higher pressures for lower tritium fractions might be attributed to the fact that ion recombination is concentration dependent, the ion concentration being lower in lower tritium fraction samples.

APPENDIX E

COMPRESSIBILITY FUNCTIONS USED FOR DENSITY CALCULATIONS

Since the density of a substance is the macroscopic physical quantity which is proportional to the number of molecules in a given volume, this property is probably the best independent variable to use in conjunction with describing diffusion phenomena. Density, or compressibility data is very limited for the two systems studied in this investigation, especially in the pressure range between 2000 and 5500 pounds per square inch. For these reasons it was imperative that a generalized correlation be found which satisfactorily described the volumetric behavior. Chou [9] in his work with H_2-CO_2 mixtures found that the generalized compressibility factor chart presented by Dodge [12] predicted with good accuracy the limited data of Verschaffelt [45] and Krichevskii and Markov [23] if the pseudo critical properties of the mixtures were obtained by the following relations:

$$T_C = y_{CO_2} (T_C)_{CO_2} + y_{H_2} [(T_C)_{H_2} + 16] \qquad (40)$$

$$P_C = y_{CO_2} (P_C)_{CO_2} + y_{H_2} [(P_C)_{H_2} + 16] \qquad (41)$$

These relations differ slightly from the generally used equations predicting volumetric behavior of hydrogen from generalized compressibility charts in that the constant, 16, is used instead of the

constant, 8, for determining the pseudo-critical properties of hydrogen. The maximum pressure of the data used for this comparison is only 1800 pounds per square inch.

A recently published generalized compressibility relation by Pitzer and co-workers (32,33) which was adapted for use with mixtures by Prausnitz (35) is the relation chiefly used in this investigation. Prausnitz predicted the compressibilities of two mixtures of CO_2-H_2 in the temperature range of 273° to 473°K and the pressure range of 3000 to 7500 pounds per square inch with a maximum deviation of 2.2 percent and an average deviation of 1.3 percent. Pseudocritical properties of all of the mixtures of CO_2-H_2 and A-H_2 in this investigation were calculated by the Prausnitz method. The Pitzer compressibilities were used for the 19 and 62 percent hydrogen mixtures of both systems at both 35°C and 100°C. The measured compressibilities of pure hydrogen were used for 93 percent hydrogen mixtures of both systems and for the pure hydrogen diffusion runs. The 93 percent hydrogen mixtures of both systems were treated as if they were pure hydrogen at the pseudo reduced temperatures and pressures of the mixtures.

The Pitzer generalized gas compressibility correlations are based on the usual two reduced parameters, P_r and T_r, which in turn are based on the critical properties P_C and T_C, and a third property, ω, the acentric factor. The acentric factor is a measure of deviation

from a "simple fluid", for which the acentric factor is zero. Molecular potentials of such "simple fluids" (A, K_r, X_e, and CH_4)can be described accurately by the Lennard-Jones or 6-12 potential. Potentials of other molecules deviate somewhat from this form in a manner which can often be described mathematically. However, perhaps the best way to predict this deviation in order to facilitate its use is by an empirical method using an easily measured physical property, vapor pressure. The molecular potential has its greatest overall effect when molecules are clustered as in the liquid state. The vapor-liquid equilibrium, or vapor pressure for a pure component, should be a good manner of determining the molecular potential deviations.

The acentric factor, ω, for a certain pure component is defined by the equation:

$$\omega = -\log P_r - 1.00 \qquad (42)$$

where P_r is the reduced vapor pressure of the pure component at a reduced temperature of $T_r = 0.7$. This acentric factor is indicative of the slope of the vapor pressure curve of the component, which in turn is dependent on the entropy of vaporization of the material. The acentric factor is therefore related to the increase of the entropy of vaporization of the component in question over that of a "simple fluid".

The acentric factor, ω, is used as the factor of a correction which is added to the compressibility correlation of a "simple fluid". It is applied in the following manner:

$$Z = z^{(0)} + \omega z^{(1)} + \text{---} \tag{43}$$

where:

Z is the desired compressibility,

$z^{(0)}$ is the compressibility of a "simple fluid" with the same reduced properties.

$z^{(1)}$ is the correction to the "simple fluid" compressibility at the reduced properties.

Prausnitz has presented a method for calculation of pseudocritical properties of mixtures for use with the Pitzer compressibility relations by use of second virial coefficient relationships. Only the method of calculation of these properties will be presented here. The information necessary for the calculation of the pseudocritical properties for a binary mixture with mole fractions, y_i, are: the critical properties, T_C, V_C, Z_C, and the acentric factor, ω, for each component, the graphical tables of two variables, r and s, which are given by Prausnitz as tabular functions of T_r and ω, and the following relationships which are presented in five steps.

1) $$(T_C)_{12} = [(T_C)_1 (T_C)_2]^{1/2} \tag{44}$$

$$(\underline{V}_C)_{12} = 1/2 [(\underline{V}_C)_1 + (\underline{V}_C)_2] \tag{45}$$

2) $$\underline{V}_{Cm} = y_1^2 (\underline{V}_C)_1 + 2y_1y_2(\underline{V}_C)_{12} + y_2^2 (\underline{V}_C)_2 \tag{46}$$

$$\omega_m = y_1\omega_1 + y_2\omega_2 \tag{47}$$

3) $$\beta = y_1^2 (\underline{V}_C)_1 (T_C)_1 + 2y_1y_2(\underline{V}_C)_{12}(T_C)_{12} + y_2^2 (\underline{V}_C)_2(T_C)_2 \tag{48}$$

$$\gamma = y_1^2 (\underline{V}_C)_1 (T_C)_1^2 + 2y_1y_2(\underline{V}_C)_{12}(T_C)_{12}^2 + y_2^2 (\underline{V}_C)_2 (T_C)_2^2 \tag{49}$$

4) $$T_{Cm} = \frac{\beta + \sqrt{\beta^2 + r\underline{V}_{Cm}\gamma}}{2 s \underline{V}_{Cm}} \tag{50}$$

5) $$P_{Cm} = \frac{RT_{Cm}}{\underline{V}_{Cm}} [y_1(Z_C)_1 + y_2(Z_C)_2] \tag{51}$$

$\underline{V}_{Cm}$, P_{Cm}, ω_m are the pseudocritical constants necessary for use with the Pitzer compressibility relations. Before step 4 can be evaluated, a value for the reduced temperature must be determined in order to evaluate the variables, r and s. It can be approximated with sufficient accuracy by Equation (52).

$$T_r = \frac{T}{(\beta/\underline{V}_{Cm})} \tag{52}$$

Table XIII is a presentation of the values of the pseudo-critical properties and acentric factors calculated for the experimental mixtures used.

TABLE XIII

PSEUDOCRITICAL CONSTANTS FOR EXPERIMENTAL MIXTURES
H_2-CO_2 MIXTURES

Fraction H_2	T_{Cm}, °K	P_{Cm}, Psia	$\underline{V}_{Cm}$, cc/gm mole	ω_m	$(P_C)_K=\Sigma_i y_i (P_C)_i$
0.188	263	1035	87.1	0.183	928
0.629	144	768	67.0	0.084	590
0.933	58.8	406	53.1	0.015	357
H_2-A MIXTURES:					
0.195	129.8	656	70.4	0	627
0.624	82.0	498	59.8	0	456
0.926	49.3	350	51.9	0	336

For the calculations, pure component pseudocritical constants were used for hydrogen. These are the ones used by Prausnitz and are T_C = 43.4°K, $\underline{V}_C$ = 50 cc/gm. mole, and ω = 0.

APPENDIX F

MISCELLANEOUS CALIBRATIONS AND CALCULATIONS

1. Pressure Gauge Calibrations
2. Thermocouple Calibrations
3. Diffusion Path Hole Size Determinations
4. Cell Chamber Volume Determinations
5. Cell Constant Calculation
6. Background Calibration Data

1. PRESSURE GAUGE CALIBRATIONS

The two pressure gauges, No. C2-473 and No. C-2456, used for determining diffusion data run pressures and the gauge, No. C2-515, used for tritium dilutions were calibrated at the beginning and end of the investigation. Two different hydraulic gauge testers were used for the calibrations, American Gauge Tester No. 1315 at the beginning and Chandler Gauge Tester No. D3-13 at the finish. Table XIV is a listing of the calibrations made. All pressures listed are in pounds per square inch gauge.

TABLE XIV

PRESSURE GAUGE CALIBRATIONS

1500 PSI PRESSURE GAUGE NO. C2-473

Date: January 7, 1959

Tester	Gauge Up	Gauge Down	Add	Remarks
275	288	288	-13	
525	534	536	-10	
775	782	783	-8	
1025	1032	1034	-8	
1275	1285	1285	-10	
1475	1484		-9	
Date: December 30, 1959				Tested in Place
600	613		-13	
700	709		-9	
800	809		-9	
900	909		-9	
1000	1009		-9	

TABLE XIV (cont.)

Tester	Gauge Up	Down	Add	Remarks
1100	1110		-10	
1200	1211		-11	
1300	1311		-11	
1400	1411		-11	
1500	1510		-10	

10,000 PSI PRESSURE GAUGE NO. C-2456

Date: March 24, 1959

1750	1750	0	
2000	2000	0	
2250	2260	-10	
2500	2510	-10	
2750	2760	-10	
3000	3005	-5	
3250	3255	-5	
3500	3505	-5	
3750	3755	-5	
4000	4000	0	
4250	4250	0	
4500	4500	0	
4750	4740	+10	These points were taken
5000	4980	+20	at upper limit of tester, not used.

Date: December 30, 1959 Tested in Place

1500	1540	-40	
2000	2000	0	
2500	2500	0	
3000	3008	-8	
3500	3506	-6	
4000	4003	-3	
4500	4500	0	
5000	5000	0	
5500	5500	0	

TABLE XIV (cont.)

Tester	Gauge Up	Down	Add	Remarks
Date: January 7, 1949				
1000 PSI PRESSURE GAUGE NO. C2-515				
250	255	255	-5	
350	355	357	-6	
450	453	455	-4	
500	503	505	-4	
600	603	603	-3	
750	752	753	-3	
850	853	853	-3	
900	903	904	-4	
950	955	955	-5	
1000	1005		-5	

2. THERMOCOUPLE CALIBRATION

The two thermocouples imbedded in the diffusion cell body were calibrated at the start of the diffusion data runs by comparison with two National Bureau of Standards calibrated thermometers. For the calibration at approximately 35°C, the Princo No. 460641 thermometer was used which has a range from -5°C to 60°C with 0.1°C divisions. For the calibration at approximately 100°C, the Princo No. 253197 thermometer was used with a range from 48°C to 102°C with 0.1°C divisions. Calibrations were made using the same No. A12-64 Portable Potentiometer that was used during the diffusion runs for measurement of thermocouple E.M.F.'s.

TABLE XV

THERMOCOUPLE CALIBRATIONS
December 9, 1958

Thermometer °C	Thermocouples No.3	Thermocouples No.4	Corrected Temperature, °C
PRINCO NO. 460641			
34.5	1.386	1.385	34.5
34.7	1.395	1.394	34.7
34.9	1.402	1.402	34.9
35.0	1.408	1.407	35.0
35.1	1.410	1.410	35.1
35.3	1.418	1.418	35.3
35.5	1.427	1.426	35.5
PRINCO NO. 253197			
99.5	4.247	4.242	99.6
99.7	4.258	4.253	99.8
99.9	4.269	4.264	100.0
100.0	4.271	4.265	100.1
100.1	4.277	4.272	100.2
100.3	4.287	4.282	100.4
100.5	4.295	4.290	100.6

3. DIFFUSION PATH HOLE SIZE DETERMINATIONS

The holes in the diffusion paths A and B were determined by examining the ends of the tube bundles with calibrated microscope scales. Two different microscopes and eyepiece scales were used, the No. YB-595 Bausch and Lomb binocular microscope before installation of the paths into the diffusion cell, and the No. MeC3-1155 Unitron binocular microscope after completion of the diffusion runs. At no time were all of the hole sizes determined, but on both occasions, two diametrical passes were made at right angles to each other with measurement of all holes passing into view. The eyepiece micrometer located on the B and L microscope was calibrated against an ordinary machinists micrometer. The eyepiece micrometer used with the Unitron microscope was calibrated with a B and L stage micrometer having 0.01 mm small divisions. The eyepiece micrometer calibrations are located in Table XVI. The hole measurements for diffusion paths A and B are located in Table XVII.

TABLE XVI

EYEPIECE MICROMETER CALIBRATIONS

February 8, 1959
Bausch and Lomb Eyepiece with Machinists Micrometer

Eyepiece Scale	Micrometer Scale, inches	
Objective →	3.0x	7.5x
0.100	0.0977	0.0396
0.090	0.0877	0.0356
0.080	0.0778	0.0317
0.070	0.0682	0.0277
0.060	0.0582	0.0238
0.050	0.0487	0.0199
0.040	0.0389	0.0159
0.030	0.0289	0.0119
0.020	0.0192	0.0079
0.010	0.0095	0.0040
0.000	0.0000	0.0000

April 4, 1960

UNITRON MICROSCOPE, B AND L STAGE MICROMETER

Eyepiece: Ke 10x unitron micrometer

Objective: M 40x N.A. 0.65 T.L. 170

The following readings were made at two scale positions:

Two Scale Positions:

100 Eyepiece scale units = 0.02427 cm.
100 Eyepiece scale units = 0.02423 cm.
Average = 0.02425 cm.

Eyepiece: Ke 10x unitron micrometer

Objective: M 10x N.A. 0.30 T.L. 170

The following readings were made at two scale positions:

100 Eyepiece scale units = 0.0968 cm.
100 Eyepiece scale units = 0.0968 cm.
Average = 0.0968 cm.

TABLE XVII

DIFFUSION PATH HOLE SIZE DETERMINATION

PATH A, FEBRUARY 8, 1959
DIAMETER, B AND L EYEPIECE MICROMETER SCALE UNITS

Vertical Pass	Horizontal Pass
0.0392	0.0413
0.0402	0.0411
0.0442	0.0421
0.0429	0.0403
0.0426	0.0412
0.0420	0.0393
0.0405	0.0411

Average Diameter = 0.0413 S.U.
= 0.0420 cm.

PATH A, APRIL 4, 1960
UNITRON MICROSCOPE UNITS

Vertical Pass	Horizontal Pass
44.6	43.9
43.9	43.7
46.5	45.2
44.3	44.3
43.9	44.3
43.9	43.3
43.1	43.8
43.0	44.3
46.7	45.1
44.3	46.0
42.7	41.7

Average Diameter = 44.20 S.U.
= 0.04279 cm.

TABLE XVII (cont.)

PATH B, FEBRUARY 8, 1959
DIAMETER, B AND L EYEPIECE MICROMETER SCALE UNITS

Horizontal Pass		Vertical Pass	
0.0218	0.0226	0.0230	0.0227
0.0228	0.0216	0.0230	0.0231
0.0231	0.0227	0.0229	0.0228
0.0225	0.0240	0.0218	0.0230
0.0220	0.0252	0.0231	0.0229
0.0228	0.0225	0.0238	0.0220
0.0223	0.0220	0.0231	0.0222
0.0220	0.0226	0.0228	0.0220
0.0226	0.0224	0.0231	0.0224
0.0229	0.0221	0.0227	0.0222
0.0227	0.0229	0.0214	0.0232

Average Diameter = 0.02267 S.U.
= 0.02280 cm.

PATH B, APRIL 4, 1960
DIAMETER UNITRON EYEPIECE MICROMETER SCALE UNITS

Horizontal Pass		Vertical Pass	
91.8	93.2	97.0	94.0
91.1	94.7	94.7	95.2
93.9	93.8	90.3	95.4
94.0	94.0	94.6	95.3
94.0	92.0	92.2	94.3
94.7	94.7	96.1	93.2
94.8		93.9	

Average Diameter = 93.96 S.U.
= 0.02278 cm.

4. CELL CHAMBER VOLUME DETERMINATION

The volumes of the two cell chambers were determined by inserting a solid steel plug into the diffusion cell in place of the diffusion path plugs and weighing the amount of mercury which could be introduced into each of the chambers. The solid plug had nearly the same dimensions of the diffusion paths, however a small volume correction was necessary in order to determine the chamber volumes when the different diffusion paths were in place. Table XVIII is a list of the volumes determined with the solid plug in place.

TABLE XVIII

DIFFUSION CELL CHAMBER VOLUMES DETERMINED BY WEIGHT OF MERCURY

	Upper Chamber, cc	Lower Chamber, cc
	7.387	7.116
	7.394	7.120
	7.392	7.120
		7.101
Average Volume	7.391 cc	7.119 cc
Correction for Path A	0.0635 cc	0.0025 cc
Correction for Path B	-0.0224 cc	-0.0201 cc

5. CELL CONSTANT CALCULATION

Since the geometry of the diffusion cell is known, the cell constant can be calculated rather than be determined by a calibration. The cell constant as derived by the mathematical analysis of Section III is related to the cross sectional area of the diffusion path, A, the length of the diffusion path, L, and the volumes of the two chambers, V_U and V_L.

$$K = \frac{A}{L}\left(\frac{1}{V_U} + \frac{1}{V_L}\right) \qquad (53)$$

The respective lengths of paths A and B are 1.145 cm. and 1.397 cm. The methods for determination and values for the areas and volumes have been presented in previous sections of this appendix.

The value for the cell constant with diffusion path A installed is:

$A = 0.05899\ cm^2$ (41 tubes of 0.0428 cm diameter)

$L = 1.145\ cm$ $\qquad$ $V_U = 7.455\ cm^3$

$V_L = 7.122\ cm^3$ $\qquad$ $K = 0.01414\ cm^{-2}$

The value of the cell constant with path B installed is:

$A = 0.05176\ cm^2$ (127 tubes of 0.02278 cm diameter)

$L = 1.397\ cm$ $\qquad$ $V_U = 7.369\ cm^3$

$V_L = 7.099\ cm^3$ $\qquad$ $K = 0.01025\ cm^{-2}$

6. BACKGROUND CURRENT CALIBRATION DATA

There was a small measurable current detected by the ionization current measurement circuit for each electrode when the gas in the diffusion cell chambers contained no radioactive material. This background current was measured at intervals between the diffusion runs and was found to be relatively constant at a given temperature over a given series of runs. After each instance of electrode insulation repair the background currents for runs at 100°C differed from those detected at 100°C before the repair. Electrode insulation repair did not seem to effect the background currents noted at 35°C. Although the background was small with respect to the overall current measured during a diffusion run, less than one percent of average measurements at 35°C, the fact that it was different for the two electrodes would have introduced an error into the resulting diffusion coefficients had it not been corrected for in the calculations. Table XIX is a listing of background corrections made to ionization currents measured during the diffusion runs. The backgrounds are listed in chart units since calculations were made in chart units for convenience. The chamber backgrounds were subtracted from the respective ionization currents from the two chambers before further calculations were carried out. Diffusion runs made after December 5, 1959 were made on chart paper with 50 main divisions full scale rather

than 20 divisions full scale. As a result, chart units were smaller by a factor of 2/5 after that date. However, for comparison, values for the background are presented in Table XIX in 20 division chart units. These, of course, had to be in the proper units for their use in the calculations. The backgrounds, as given in chart units based on a voltage range of 2.0 and 20 spaces full scale can be converted to current in amperes by Equation (54) which is a specific case of Equation (39).

$$I = \frac{(\text{Background})(2.0)}{(10^{11})(17.37)} \qquad (54)$$

TABLE XIX

BACKGROUND CURRENT CALIBRATION DATA

Date	Temperature °C	Full Scale Chart Units	Voltage Range	Zero	Lower	Upper	Background* Lower Channel	Background* Upper Channel
BACKGROUNDS FOR RUNS 1A-5A, 10B-40B, 66B-88B								
6/29/59	35	20	0.02	1.3	5.0	10.0	0.04	0.09
8/29/59	35	20	0.02	1.5	6.0	13.1	0.05	0.12
11/16/59	35	20	0.02	1.5	5.5	12.8	0.05	0.11
12/7/59	35	50	0.02	3.4	10.6	25.7	0.03	0.09
BACKGROUND FOR RUNS 41B-65B								
8/17/59	100	20	0.10	1.5	11.7	15.3	0.51	0.69
9/25/59	100	20	0.10	1.5	13.7	15.5	0.61	0.70
10/12/59	100	20	0.10	1.5	11.3	13.5	0.49	0.60
BACKGROUND FOR RUNS 89B-100B								
12/10/59	100	50	0.05	3.7	9.7	28.9	0.06	0.25
12/21/59	100	50	0.05	3.7	9.4	29.6	0.06	0.26
BACKGROUND FOR RUNS 101B-106B								
1/6/60	100	50	0.05	4.3	14.1	22.0	0.10	0.18

* Based on V.R. = 2.0, 20 chart units full scale.

APPENDIX G

THE COMPUTER PROGRAM FOR DATA PROCESSING

The calculations necessary for the processing of raw experimental data were greatly expedited because of the generous availability of a high speed automatic computing machine, an IBM 704 which is located on the campus of the University of Michigan. It is believed that the techniques made accessible due to the use of this machine are slightly more objective in nature than the methods used previously in similar works.

The method of data analysis has been presented in the previous text, in Section III. In the analysis, values of the ionization currents from the two cell chambers were read at incremental values of the time from the chart traces prepared by the recording potentiometer. This data was fit to Equation (25) by the method of least squares and the coefficient of time was the desired diffusion coefficient.

$$-\frac{\ln (fI_1 - I_2)}{\frac{A}{L}\left(\frac{1}{V_1} + \frac{1}{V_2}\right)} = D\theta + \text{constant}_3 \qquad (25)$$

Equation (55) is the equation of a straight line with respect to the dependent variable, the left side of the equation, and the independent variable, time (θ). Since any set of data can be fit to a straight line

by the method of least squares, a check of the validity of the straight line representation for each data run was necessary to determine whether or not there was systematic deviation from this straight line representation. In order to give a qualitative indication of a tendency toward curvature, the same experimental data was first fit to a simple equation of a curved line, of the form:

$$y = A + Bx + Cx^2 \tag{55}$$

Since the data taken all were of the same relative size with respect to the variables fit, the constant, C, in Equation Form (55) was a fairly good indication of quantitative tendancy toward curvature. This constant was tested for size by the computer program and if it was less than an arbitrarily set maximum, the data was then fit to Equation (25) for evaluation of the diffusion coefficient.

In the event that the arbitrary limit of C was exceeded, a systematic procedure for further consideration of the data and curvature tendency was carried out by the program. In the data processing method previously used in which the left side of Equation (25) was plotted versus the time, if one or more points was bad, this would be immediately evident. If a suitable explanation could be presented as to the cause, the point or points in question could either be revised or eliminated.

Unless this function was also built into the data processing program, the former method would certainly have been superior.

It was felt that at least two such suitable explanations existed which should be allowed to cause elimination of one or more of the points which were incrementally read from the recorder traces. The first explanation involves one or more points which occur too close to the end of a run when the ratio of the HT concentrations present in the two cell chambers is too small for the resolution accuracy of the equipment. It was felt that such points could be safely eliminated if an adequate portion of straight line preceded these points. The second justifiable explanation concerns one or two points read from the beginning of a run which might deviate from the straight line representation because of mass transfer by mechanisms other than diffusion, such as convection caused by temperature inconsistencies. It was decided to allow the program to eliminate as many as two initial points for this reason.

The point eliminations were made in the following manner. The set of incremental recorder trace points from a given run was first fit by Equation Form (55) and the constant, C, was tested for curvature effect present in the fit. If the maximum was exceeded, the last point of the set was dropped and C was evaluated for the remaining data. This elimination was continued until C was within the desired limits or until

only four points remained. A large curvature effect in the first four points indicated that the excessive curvature was probably caused by bad points at the beginning of the run. A point from the beginning of the set was then dropped and the entire set including those previously eliminated from the end of the set were then fitted to Equation Form (55). If C was still excessive, points were eliminated from the latter part of the run as before. The program allowed a maximum of two points to be removed from the first part of the run and a total minimum of four points to be fit if the curvature limit was never conformed to.

The program furnished information in the output as to how many points were eliminated and from which extreme of the set before a successful fit was accomplished. For most runs, eight or ten points made up the entire set of points and normally all or all but one or two points satisfied the arbitrary curvature effect maximum. This maximum was determined by analyzing some of the runs graphically and setting the limiting constant to correspond with point eliminations which would have been made by critical inspection of the graphs. Only two runs, 13B and 21B, out of the 102 runs were found to be not acceptable due to not satisfying the curvature requirements. Both were calculated graphically and a definite curvature was noted for each. Since no slope could be determined graphically for these runs, no diffusion coefficient was evaluated.

TABLE XX

FORTRAN DATA PROCESSING PROGRAM

```
    1 FORMAT(F10.3,2F10.2,F10.5,F10.7)
    2 FORMAT(I10,F10.4,F10.0,F10.0,F10.3,F10.2,I5,F6.1)
    3 FORMAT(F10.0,3F10.2)
    4 FORMAT(I19,F19.3,F21.7,F20.5,I11,I3,I3,F10.2)
   13 FORMAT(37H1                CHAMBER FACTOR, F     = F10.3,/
     X37H                    CELL CONSTANT         = F12.5,/
     X37H                    ALLOWABLE CURVATURE   = F14.7,/
     X37H                    CHAMBER B BACKGROUND  = F9.2,/
     X37H                    CHAMBER R BACKGROUND  = F9.2,//
     X108H                    RUN NO.          DENSITY          DIFFUSIVITY
     X         DIFF. X DEN.      DATA POINTS      XH          /)
      DIMENSION Y(15),T(15),R(15),ZERO(15),B(15)
    5 READ INPUT TAPE 7,1,F,BB,RB,CONST,CMAX
      WRITE OUTPUT TAPE 6,13,F,CONST,CMAX,BB,RB
    6 READ INPUT TAPE 7,2,RUN,XH,CS,P,Z,BM,N,TEMP
      DO 7 I=1,N
    7 READ INPUT TAPE 7,3,T(I),B(I),R(I),ZERO(I)
      DO 9 I=1,N
      B(I)=B(I)-BB-ZERO(I)
      R(I)=F*(R(I)-RB-ZERO(I))
      Y(I)=LOGF(R(I)-B(I))
    9 T(I)=T(I)/CS
      J=1
   14 K=N
    8 SUMT=0.
      SUMT2=0.
      SUMT3=0.
      SUMT4=0.
      SUMY=0.
      SUMYT=0.
      SUMYT2=0.
      FK=(K-J+1)
      DO 10 I=J,K
      SUMT=SUMT+T(I)
      SUMT2=SUMT2+T(I)*T(I)
      SUMT3=SUMT3+T(I)*T(I)*T(I)
      SUMT4=SUMT4+T(I)*T(I)*T(I)*T(I)
      SUMY=SUMY+Y(I)
      SUMYT=SUMYT+Y(I)*T(I)
   10 SUMYT2=SUMYT2+Y(I)*T(I)*T(I)
      C=(FK*SUMT2*SUMYT2+SUMT*SUMYT*SUMT2+SUMY*SUMT*SUMT3-SUMT2*SUMY*SUM
     XT2-SUMYT2*SUMT*SUMT-FK*SUMYT*SUMT3)/(FK*SUMT2*SUMT4+SUMT*SUMT3*SUM
     XT2+SUMT2*SUMT*SUMT3-SUMT2*SUMT2*SUMT2-SUMT*SUMT*SUMT4-FK*SUMT3*SUM
     XT3)
      IF (ABSF(C)-CMAX) 11,11,12
   11 SLOPE=(FK*SUMYT-SUMT*SUMY)/(FK*SUMT2-SUMT*SUMT)
      D=SLOPE/(1200.*CONST)
      D=ABSF(D)
      DEN=P/(Z*TEMP*1.2059083)
      IF(BM) 16,17,16
   16 CM=XH*2.016+((1.0-XH)*44.01)
      D=D*SQRTF((4.01+BM)*CM/((4.01+CM)*BM))
   17 DDEN=D*DEN
      L=K-J+1
      WRITE OUTPUT TAPE 6,4,RUN,DEN,D,DDEN,L,N,J,XH
      GO TO 6
   12 K=K-1
      IF(K-J-2) 11,15,8
   15 J=J+1
      IF(J-3) 14,14,11
```

Table XX is the program used for data processing as listed in Fortran compiler language. The data was read into the computer on three types of IBM cards. The first type preceded the entire deck of data cards to be computed at a given time and furnished the chamber sensitivity factor, f, the upper and lower chamber background currents, B_R and B_B, the cell constant, K, and the maximum allowable curvature, C. Following this general information card, the remaining data cards were further subdivided into sets with a set of cards for each data run. Each run set was made up of a general information card followed by cards furnishing data for each increment of time from the recorder trace. The run general information card provided the program with the run number, the sample mole fraction of hydrogen, the chart speed, the run pressure, the run compressibility, the average molecular weight of all runs from the sample bottle used, the number of time incremental points to be read by the program, and the run temperature. Each incremental data card furnished the values of time in chart units, the ionization currents in chart units, and the zero value of the trace when the Ultrohmeter input was shorted. The results of the computations for one run were printed out on the equivalent of a single IBM card giving the run number, the run density, the computed Fick diffusion coefficient, the diffusivity-density product, three numbers indicating the locations and numbers of any eliminated data points, and the mole fraction of hydrogen in the run sample.

NOMENCLATURE

Symbol	
A	Area, cm^2.
$B(T)$	Second virial coefficient for real gases, cm^3 per gram mole.
b_o	Second virial coefficient for solid spherical molecules.
C_i	Concentration, gram moles per liter, of i^{th} component.
D_i	Diffusion coefficient, cm^2 per second, of one component of a multicomponent mixture.
D_{ij}	Binary diffusion coefficient, cm^2 per second, of i^{th} component through j^{th} component.
D_o	Diffusion coefficient, cm^2 per second, evaluated by dilute gas theory.
D_L	Liquid diffusion coefficient, cm^2 per second.
D_{FS}	Diffusion coefficient, cm^2 per second, in free space.
d	Diameter of capillary tube, cm.
E	Energy constant associated with exponential form of liquid diffusivity temperature dependence.
f	Ratio of ionization currents of lower to upper chambers containing same HT concentration.
$f_C^{(2)}$	Theoretically derived factor of the diffusivity which accounts for the concentration, resulting in the second approximation of the diffusion coefficient.
I_i	Ionization current from upper or lower chambers, $i = U, L$.
i	Index, represents number or letter denoting specific entity.
j	Index, represents number or letter denoting specific entity.

Symbol	
J_i	Diffusion flux, gram moles per second per cm^2.
K	Cell constant, differs for paths A or B installed in diffusion cell.
L	Length of tube bundle, cm.
M_{AVG}	Weighted average molecular weight of components.
M_i	Molecular weight of component i, computed on the basis of the following atomic weights: A, 39.944; H, 1.008; T, 3.017; C, 12.011; O, 16.000.
N_i	Total flux past stationary coordinates, gm moles per second per cm^2.
n	Number of molecules per unit volume.
P	Pressure, psia.
P_C	Critical pressure, psia, of a pure component.
P_{Cm}	Pseudocritical pressure, psia, of a mixture.
P_r	Reduced pressure, $P/P_{C(m)}$.
R	Gas constant, $10.7315 \frac{(psia)(ft^3)}{(lb.\ mols)(°R)} \approx 1.20591 \frac{(psia)(liter)}{(gm\ mols)(°K)}$.
r	Derived constant, listed as function of the acentric factor, ω, and T_R.
s	Derived constant, listed as function of the acentric factor, ω, and T_R.
T	Absolute temperature, °K, t°C + 273.2.
t	Temperature, °C.
T_C	Critical temperature of pure component, °K.
T_{Cm}	Pseudocritical temperature of a mixture, °K.
T_r	Reduced temperature, $T/T_{C(m)}$.

NOMENCLATURE (cont.)

$\underline{U}$	Internal energy, Calories per mol.
$\underline{V}$	Specific volume, cm^3 per gram mole.
$\underline{V}_C$	Critical specific volume, cm^3 per gram mole, of pure component.
$\underline{V}_{Cm}$	Critical specific volume, cm^3 per gram mole, of a mixture.
V_i	Volume of chamber i, cm^3, i = U, L.
x	Distance parallel to diffusion flux, cm.
Y_i	Dense gas correction to pure component diffusion coefficient. (Enskog[13]).
Y_{ij}	Dense gas correction to binary diffusion coefficient. (Thorne[42]).
$y = \frac{PV}{RT} - 1$	for rigid spheres; the basis of the Enskog relations between the state variables and diffusion theory for dense gases.
y_i	Mol fraction of component i in the gaseous state.
Z, $Z_{(T,V)}$	Compressibility factor.
Z_C	Critical compressibility factor.
$z^{(0)}$	Compressibility for gas for which the acentric factor, ω, is equal to zero.
$z^{(1)}$	Additive compressibility correction for gases having appreciable acentric factor.

Greek Symbols

α	Sign indicating proportionality.
Δ	Operator denoting macroscopic difference with respect to distance or time.
∇	Space gradient operator, $\frac{\partial}{\partial x} + \frac{\partial}{\partial y} + \frac{\partial}{\partial z}$ in three dimensional space.

NOMENCLATURE (cont.)

ϵ_i	Characteristic parameter of a molecule, i, which describes the attractive force between molecules.
ϵ_{ij}	Equals $(\epsilon_i \cdot \epsilon_j)^{1/2}$ for molecules i, j of a binary mixture.
θ	Time, seconds.
k	Boltzmann's constant.
λ	Mean free path of a molecule, cm.
ρ	Density, gram moles per liter.
σ_i	Parameter of Lennard-Jones potential for a single component, i, known as the "collision diamerter", values from reference (17), $\sigma_{H_2} = 2.915\text{Å}$ $\sigma_{CO_2} = 3.897\text{Å}$, $\sigma_A = 3.465\text{Å}$.
σ_{ij}	"Collision diameter" for collisions between unlike molecules, i and j, cm, $= \frac{\sigma_i + \sigma_j}{2}$.
$\Omega^{(1,1)*}$	"Collision integral", function of $\frac{kT}{\epsilon}$, describing diffusional collisions. Tabular values in Reference (17).
ω_i	Acentric factor parameter of Pitzer (32) correlation for compressibility of component i. Equals - log P_R - 1.00 at $T_r = 0.7$.
ω_m	Mean acentric factor for a mixture.

Singular subscripts.

U	Denotes upper chamber of the diffusion cell.
L	Denotes lower chamber of the diffusion cell.
0	Denotes value predicted by dilute gas theory.

BIBLIOGRAPHY

1. Becker, E. W., Vogell, W. and Zigen, F., Z. Naturforsch., 8a: 686 1953.

2. Bennett, C. O., "Diffusion in Binary Mixtures," Chemical Engineering Science, 9: 45 1958.

3. Berry, V. J., Koeller, R. C., "Diffusion in Compressed Binary Gaseous Systems," A.I.Ch.E. Journal 6: 274 1960.

4. Bird, R. B., Advances in Chemical Engineering, Vol. 1, pp. 156-239, Academic Press, New York, 1956.

5. Boardman, L. E. and Wild, N. E., Proceedings of the Royal Society of London, A162: 511 1937.

6. Boyd, C. A., Stein, N., Steingrimsson, V. and Rumpel, W. F., J. Chem. Phys., 19: 548 1951.

7. Chang, C. S. W., Ph.D. Thesis, University of Michigan, 1944.

8. Chapman, S. and Cowling, T. G., The Mathematical Theory of Non-Uniform Gases, Cambridge Press, 1939.

9. Chou, C., Ph.D. Thesis, University of Michigan, 1954.

10. Chou, C. and Martin, J. J., "Diffusion of $C^{14}O_2$ in Mixtures of $C^{12}O_2$-H_2 and $C^{12}O_2$-C_3H_8," Ind. Eng. Chem. 49: 758 1957.

11. Crank, J., "The Mathematics of Diffusion," Oxford U. Clarendon Press, London, 1956.

12. Dodge, B., Chemical Engineering Thermodynamics, McGraw-Hill Book Company, Inc., New York, 1944.

13. Enskog, D., Dissertation, Upsala, 1917.

14. Groth, W. and Harteck, P., Z. Physik, Chem., 199: 114 1952.

15. Harteck, P. and Schmidt, H. W., Z. Physik Chem., B21: 447 1933.

16. Heath, H., Ibbs, T. and Wild, N., Proc. Roy. Soc. (London) A178: 380 1941.

BIBLIOGRAPHY (cont.)

17. Hirschfelder, J. O., Curtiss, C. F. and Bird, R. B., Molecular Theory of Gases and Liquids, Wiley, New York, 1954.

18. International Critical Tables, McGraw-Hill, New York, 1929.

19. Jefferies, Q. R. and Drickamer, H. G., J. Chem. Phys., 16: 968 1948.

20. Jefferies, Q. R. and Drickamer, H. G., J. Chem. Phys., 22: 436 1954.

21. Jost, W., Diffusion in Solids, Liquids and Gases, New York Academic Press, 1952.

22. Kihara, T., Imperfect Gases, Asakusa Bookstore, Tokyo, 1949.

23. Krichevskii, I. and Markov, V., Acta Physicochim., U.R.S.S., 12: 59 1940.

24. Lonius, A., Ann. Physik, 29: 664 1909.

25. Loschmidt, J., Sitzungsber. Akad. Wien, 61: 367 1870.

26. Mason, E. A., J. Chem. Phys., 23: 49 1955.

27. Mattraw, H. C., Pachucki, C. F. and Dorfman, L., J. Chem. Phys., 20: 926 1952.

28. Mifflin, T. R., Ph.D. Thesis, Purdue University, 1959.

29. Mifflin, T. R. and Bennett, C. O., "Self-Diffusion in Argon to 300 Atmospheres," J. Chem., Phys., 29: 975 1958.

30. O'Hern, H. A., Ph.D. Thesis, University of Michigan, 1952.

31. O'Hern, H. A. and Martin, J. J., Ind. Eng. Chem., 47: 2081 1955.

32. Pitzer, K. S., J. Am. Chem. Soc., 77: 3427 1955.

33. Pitzer, K. S., J. Am. Chem. Soc., 79: 2369 1957.

34. Pollard, W. and Present, R., Phys. Rev., 73: 762 1948.

BIBLIOGRAPHY (cont.)

35. Prausnitz, J. M. and Gunn, R., A.I.Ch.E. Journal, 4: 430 1958.

36. Prausnitz, J. M., A.I.Ch.E. Journal, 5: 3 1959.

37. Reid, R. C. and Sherwood, T. K., The Properties of Gases and Liquids, McGraw Hill, New York, 1958.

38. Robb, W. L. and Drickamer, H. G., J. Chem. Phys., 19: 1504 1951.

39. Roth, W., Arch. Eisenhuttenw., 8: 401 1935.

40. Schafer, K., Corte, H., and Moesta, H., Z. Elektrochem., 19: 662 1951.

41. Slattery, J. C., M.S. Thesis, Univ. of Wisconsin, Department of Chemical Engineering, 1955.

42. Thorne, H. H., c.f. Chapman and Cowling (8), p. 292.

43. Timmerhaus, K. D. and Drickamer, H. G., J. Chem. Phys., 19: 1242 1951.

44. Timmerhaus, K. D. and Drickamer, H. G., J. Chem. Phys., 20: 981 1952.

45. Verschaffelt, J. E., Arch. Neerland. Sci. Exact. Nat., 11: 403 1906.

46. Waldmann, L., Naturwissenschaften, 32: 222 1944.

47. Wilke, C. R., "Diffusional Properties of Multicomponent Gases," Ch. Eng. Prog., 46: 95 1950.

48. Woolley, H. W., Scott, R. B. and Brickwedde, F. G., J. Res. Nat'l. Bur. Stds., 41: 379 1948.